Nanocolorants for Hot-melt Inks

by
Ahmed Al-Aeeb

Dissertation presented for the degree of PhD (Polymer Science) in the Faculty of Science at Stellenbosch University

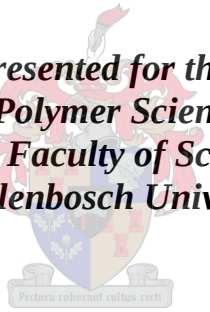

Supervisor: Prof. Bert Klumperman

March 2013

Declaration

By submitting this thesis/dissertation electronically, I declare that the entirety of the work contained therein is my own, original work, that I am the sole author thereof (save to the extent explicitly otherwise stated), that reproduction and publication thereof by Stellenbosch University will not infringe any third party rights and that I have not previously in its entirety or in part submitted it for obtaining any qualification.

Ahmed Al-Aeeb

Stellenbosch, March 2013

To my parents,
Zayied andHalima,
And my wife Saadiqa

Abstract

A new class of nanocolorants is described for the use as a colorant in hot-melt ink application for ink-jet printing technology. An inverse miniemulsion polymerization process was utilized successfully as a one-step encapsulation process to encapsulate the highly hydrophilic water-soluble fluorescent Rhodamine B dye (RhB) by the hydrophilic water-soluble poly(acrylamide) (PAAm). Three types of Rhodamine B-based nanocolorants, PAAm/RhB, crosslinked-PAAm/RhB and poly(AAm-co-Sty)/RhB, were synthesized using inverse miniemulsion polymerization. The PAAm/RhB nanocolorants exhibited solid dark nanoparticles morphology, while crosslinked-PAAm/RhB and poly(AAm-co-Sty)/RhB showed a core-shell type of morphology. The nanocolorants showed improved light and dye migration fastness as well as high thermal stability, especially, nanocolorants with core-shell morphology.

The synthesis of polymerizable RhB-based nanocolorants is described. Poly(AAm-*co*-RhB) nanocolorants were successfully synthesized for the first time via inverse miniemulsion polymerization. RhB dye was first functionalized by esterification reaction to introduce an acrylate polymerizable group. The RhB-acrylate dye was copolymerized with AAm monomer in an inverse miniemulsion polymerization to produce nanocolorants with superior light and migration fastness. Crosslinked-poly(AAm-*co*-RhB) nanocolorants could be obtained based on the incorporation of a crosslinking agent. Poly(AAm-*co*-RhB) and crosslinked-poly(AAm-*co*-RhB) nanocolorants exhibited a morphology of dark solid and core-shell particles, respectively. In both nanocolorants, the RhB-acrylate dye was completely integrated by copolymerization into the polymer matrix, and by that, the dye migration was completely

supressed. Both poly(AAm-*co*-RhB) and crosslinked-poly(AAm-*co*-RhB) nanocolorants showed high thermal stability as well as high T_g values.

The syntheses of PAAm/RhB nanocolorants-based solid inks were carried out successfully via inverse miniemulsion polymerization. An *in situ* inverse miniemulsion polymerization, with the paraffin wax as the organic phase, was utilized in making a crosslinked-PAAm/RhB nanocolorants-based solid ink. A crosslinked-poly(AAm-*co*-RhB) nanocolorants-based solid ink was prepared by the direct mixing of the readymade crosslinked-PAAm/RhB nanocolorants (suspended in cyclohexane) with paraffin wax at temperature above the melting temperature of the wax until all the cyclohexane evaporated. The obtained solid inks appeared as a solid homogenous waxy material with a deep bright colour reflecting that the nanocolorants were well dispersed in the wax. DSC thermograms showed that the solid inks have one sharp melting transition indicating the applicability of our nanocolorants for hot-melt ink applications.

Opsomming

'n Nuwe reeks nonokleursels word beskryf vir die gebruik in ink-smelt drukker tegnologie. Inverse minie-emulsie polymerisasie was suksesvol gebruik om die kleurstof Rhodamine B (RhB) in die water oplosbare poly(akrielamied) (PAAm) te enkapsuleer. Die roete is gebruik om drie tipes kleurstof te produseer. Elk van die kleurstowwe was gebaseer op Rhodamine B en 'n PAAm, naamlik PAAm/RhB, kruisgebonde PAAm/RhB en poli(akrielamied-ko-stireen)/RhB. PAAm/RhB nanokleursel was in die vorm van soliede donker nanopartikels. Die kruisgebonde PAAm/RhB en poli(akrielamied-ko-stireen) het bestaan uit nanoparikels met 'n kern en skil morfologie. Die nanokleursels het 'n verbetering in terme van lig en hitte stabiliteit getoon. Die migrasie van kleursel uit die nanopartikels, veral die met kern en skil morfologie, was baie minder.

Die sintese van 'n polimeeriseerbare nanokleursel gebaseer op RhB word beskryf. Poly(AAm-ko-RhB) nanokleursels was vir die eerste keer suksesvol gesintetiseer met behulp van 'n inverse minie-emulsie polimerisasie. RhB kleursel was eers gefunksionaliseer deur middel van 'n esterifikasie reaksie om 'n polimeeriseerbare akrilaat groep te verkry. Die RhB-akrilaat kleursel was gekopolimeeriseer met AAm monomeer in 'n inverse minie-emulsie polimerisasie om nanokleursels met verbeterde lig en migrasie stabiliteit te verkry. Kruisgebonde poli(AAm-ko-RhB) nanokleursels was verkry deur 'n geskikte verbinding in die reaksie mengsel by te voeg. Beide poli(AAm-ko-RhB) and kruisgebonde poly(AAm-ko-RhB) nanokleursels was verkry as donker partikels met 'n kern en skil morfologie. In beide gevalle was die RhB-akrilaat kleursel deeglik geintegreer in die matriks en sodoende was die migrasie van die kleursel heeltemal onderdruk. In albei gevalle het poli(AAm-ko-RhB) en kruisgebonde poli(AAm-ko-RhB) nanokleursels hoë hitte stabiliteit en hoë T_g waardes getoon. Die sintese van

nanokleursels gebaseer op PAAm/RhB was sukselvol uit gevoer via inverse minie-emulsie polimerisasie. ‘n In situ inverse minie-emulsie polimerisasie met paraffin waks as die organiese fase was gebruik om soliede ink te produseer wat opgemaak is uit kruisgebonde PAAm/RhB nanokleursel. Die kruisgebonde poli(AAm-ko-RhB) soliede ink was voorberei deur die kruisgebonde PAAm/RhB nanokleursels (in suspensie met sikloheksaan) direk met die paraffin waks te meng by ‘n temperatuur hoër as die smeltpunt van die waks todat al die sikloheksaan verdamp het. Die soliede ink was verkry as ‘n homogene waksagtige materiaal met ‘n diep en helder kleur wat ‘n aanduiding was dat die nanokleursels goed versprei was in die waks. DSC termogramme het bewys dat die ink slegs een skerp smelt punt oorgang het wat beteken dat die materiaal geskik is om te gebruik in ink-smelt drukkers.

Acknowledgements

First and foremost, all praise be to ALLAH who has guided me to be who I am, and all thanks to HIM for his guidance and mercy that he bestowed on me so I had the strength to complete this study successfully.

My sincere appreciation and gratitude go to my promoter, Bert Klumperman for allowing me to be a member of his group and to work under his supervision. Thank you Bert for all your efforts, advices and time spent to make this study successful.

It was a wonderful and great opportunity for me to study here in Stellenbosch, and for that I would like to acknowledge Prof. R. Sanderson who was the reason for me being here.

Thanks to all my friends and colleagues in the department of polymer science, especially the free radical group, and to all the staff and people who supported and helped me during my study.

For all the unconditional love and support and patience, for all the encouragement and sacrifices, I would like to thank my parents Zayied and Halima, my wife Saadiqa and my in-laws Mogamat Sedick and Kashiefa Jappie, may ALLAH bless you and reward you abundantly here and in the hereafter.

Ahmed
March 2013

Contents

Chapter 1: Introduction and objectives 1

1.1 Introduction 1
1.2 Nanocolorants 2
1.3 Objectives 4
1.4 References 6

Chapter 2: Historical and theoretical background 12

2.1 Miniemulsion polymerization 12
2.1.1 Introduction 12
2.1.2 Formulation and composition contents 13
2.1.2.1 Surfactants 14
2.1.2.2 Co-stabilizers 18
2.1.2.3 Initiators 19
2.1.3 Preparation and homogenization techniques 20
2.1.4 Miniemulsion Stability 22
2.1.5 Kinetics and mechanism in miniemulsion polymerization 26
2.2 Encapsulation via miniemulsion polymerization 31
2.3 Nanocolorants via miniemulsion polymerization 36

Chapter 3: Synthesis and characterization of nanocolorants via inverse miniemulsion polymerization 46

Abstract 46
3.1 Inverse miniemulsion polymerization 47
3.1.1 Introduction 47
3.1.2 Encapsulation via inverse miniemulsion polymerization 49
3.2 Experimental 52
3.2.1 Materials 52
3.2.2 Synthesis of PAAm/RhB and core-shell crosslinked-PAAm/RhB based nanocolorants in inverse miniemulsion polymerization 52
3.2.2 Preparation of poly(AAm-*co*-Sty)/RhB core-shell nanocolorants in inverse miniemulsion polymerization 53
3.2.3 Characterization and analytical techniques 54

3.2.3.1 Dynamic light scattering (DLS) 54
3.2.3.2 Transmission electron microscopy (TEM) 54
3.2.3.3 Scanning electron microscope (SEM) 54
3.2.3.4 UV-vis spectroscopy 55
3.2.3.5 Thermogravimetric analysis (TGA) 55
3.3 Results and discussion 56
3.3.1 Stability and choice of the surfactants 58
3.3.2 Particle size and size distribution of nanocolorants 59
3.3.3 Morphology of the nanocolorants 60
3.3.4 Colour and migration fastness of nanocolorants 65
3.3.5 Thermal stability of nanocolorants 72
3.4 Conclusions 74
3.5 References 76

Chapter 4: Synthesis and characterization of modified acrylate-Rhodamine B-based nanocolorants 80

Abstract 80
4.1. Introduction 81
4.2. Experimental 84
4.2.1 Materials 84
4.2.2 Synthesis of Rhodamine B acrylate derivative. 85
4.2.2 Synthesis of poly(PAAm-*co*-RhB) and crosslinked-poly(PAAm-*co*-RhB) nanocolorants in inverse miniemulsion polymerization 85
4.2.3 Characterization and analytical techniques 86
4.3. Results and discussion 86
4.3.1 Characterization of RhB-acrylate 86
4.3.2 Characterization of poly(PAAm-*co*-RhB) and crosslinked-poly(PAAm-*co*-RhB) nanocolorants 88
4.3.2.1 Size distribution and morphology of the nanocolorants 89
4.3.2.2 Colour and migration fastness of the nanocolorants 92
4.3.2.3 Thermal properties and stability of Poly(AAm-*co*-RhB) nanocolorants 95
4.3.2.3.1 Thermal properties and glass transition temperature of poly(AAm-*co*-RhB) nanocolorants as determined by DSC 95
4.3.2.3.2 Thermal stability of RhB-acrylate and poly(AAm-*co*-RhB) nanocolorants as determined by TGA 96
4.4 Conclusions 98

4.5 References 100

Chapter 5: Synthesis and characterization of PAAm/RhB nanocolorants-based solid inks... 104

Abstract 104

5.1 Introduction 105

5.2. Experimental 108

5.2.1 Materials 108

5.2.2 Synthesis of (PAAm/RhB) and Poly(AAm-*co*-RhB) nanocolorants-based solid inks in inverse miniemulsion polymerization 109

5.2.3 Characterization and analytical techniques 109

5.3 Results and discussion 110

5.3.1 Size distribution and morphology of the solid ink 112

5.3.2 Fluorescence microscopy 114

5.3.3 Thermal properties of the crosslinked-PAAm/RhB and crosslinked-Poly(AAm-*co*-RhB) nanocolorants-based solid inks as determined by DSC 115

5.4 Conclusions 116

5.5 References 118

Chapter 6: Summary and recommendations 121

6.1 Summary 121

6.2 Recommendations 123

List of figures

Figure 2.1: Approach of the steady state as revealed by surface tension and turbidity measurements.[5, 34] 22

Figure 2.2: : Calorimetric curve of a typical miniemulsion.[50] 30

Figure 3.1: Nanocolorants loaded with 5% (a), 10% (b) and 20% (c) RhB, respectively. 58

Figure 3.2: PAM/RhB nanocolorants stabilized with Hypermer B246 (A) and Span 80 (B). 59

Figure 3.3: SEM images of (A) PAAm/RhB, (B) crosslinked-PAAm/RhB and (C) Poly(AAm-co-Sty)/RhB nanocolorants 61

Figure 3.4:TEM images of PAAm/RhB nanocolorants with 10 wt% RhB. 62

Figure 3.5: TEM images of crosslinked-PAAm/RhB nanocolorants with 10 wt % RhB. 63

Figure 3.6: TEM images of poly(AAm-*co*-Sty)/RhB nanocolorants with 10 wt % RhB. 64

Figure 3.7: Absorption spectra of PAAm/RhB, crosslinked-PAAm/RhB and poly(AAm-co-Sty)/RhB nanocolorants loaded with 10 wt % RhB. 65

Figure 3.8: Absorption spectra of poly(AAm-co-Sty)/RhB nanocolorants loaded with 10, 15 and 20 wt % RhB. 68

Figure 3.9: Dye migration properties of PAAm/RhB and crosslinked-PAAm/RhB nanocolorants loaded with 5 and 15 wt % RhB (with regard to monomer). 71

Figure 3.10: TGA thermograms of PAAm/RhB, crosslinked-PAAm/RhB and poly(AAm-co-Sty)/RhB nanocolorants prepared with 15 wt % RhB (relative to monomer). 73

Figure 3.11: TGA thermograms of crosslinked-PAAm/RhB nanocolorants prepared with different amounts of RhB. 74

List of figures

Figure 4.1: Molecular structures of Rhodamine dyes (A) and Rhodamine B dye (B)[25]. 82

Figure 4.2: ^{1}H NMR spectrum of RhB-acrylate in $(CD_3)_2CO$. 87

Figure 4.3: UV-vis absorption spectra of RhB and RhB-acrylate. 88

Figure 4.4: SEM images of (A) poly(PAAm-*co*-RhB) and (B) crosslinked-poly(PAAm-*co*-RhB) nanocolorants 90

Figure 4.5: TEM images of poly(PAAm-*co*-RhB) nanocolorants 91

Figure 4.6: TEM images of crosslinked-poly(PAAm-*co*-RhB) nanocolorants 92

Figure 4.7: UV-vis absorption spectra of RhB-acrylate, poly(PAAm-*co*-RhB) and crosslinked-poly(PAAm-*co*-RhB). 93

Figure 4.8: Dialysis of (A) poly(PAAm-*co*-RhB) nanocolorants and (B) PAAm/RhB nanocolorants 94

Figure 4.9: DSC thermograms of poly(AAm-*co*-RhB) and crosslinked-poly(AAm-*co*-RhB) nanocolorants and their corresponding reference experiments. 95

Figure 4.10: TGA thermograms of RhB and RhB-acrylate dyes 97

Figure 4.11: TGA thermograms of RhB-acrylate dye, PAAm and poly(AAm-co-RhB) and poly(PAAm-co-RhB) nanocolorants. 98

Figure 5.1: Printing process using solid ink printer with offset printing[5]. 105

Figure 5.2: (a) the synthesized crosslinked-PAAm/RhB and crosslinked-Poly(AAm-*co*-RhB) nanocolorants-based solid inks and (b) commercial solid inks. 112

List of figures

Figure 5.3: SEM images of (a) the crosslinked-PAAm/RhB nanocolorants-based solid ink and (b) the crosslinked-Poly(AAm-*co*-RhB) nanocolorants-based solid ink. 113

Figure 5.4: TEM images of (a) the crosslinked-PAAm/RhB nanocolorants-based solid ink and (b) the crosslinked-Poly(AAm-*co*-RhB) nanocolorants-based solid ink. 114

Figure 5.5: Fluorescence microscope images of (a) the crosslinked-PAAm/RhB nanocolorants-based solid ink and (b) the crosslinked-Poly(AAm-*co*-RhB) nanocolorants-based solid ink (The scale bar in the images represents 2 µm). 115

Figure 5.6: DSC thermograms of the crosslinked-PAAm/RhB and crosslinked-Poly(AAm-co-RhB) nanocolorants-based solid inks. 116

List of schemes

Scheme 2.1: Concept of miniemulsion polymerization 13

Scheme 2.2: HLB range[22]. 15

Scheme 2.3: various types of stabilizer molecules: (a) non-ionic surfactant; (b) random coil polymers; (c) linear block copolymer; (d) comb or brush copolymer; (e) grafted polymer chains; (f) globular molecules 18

Scheme 2.4: Formation of miniemulsion by sonication process. 21

Scheme 2.5: Emulsion polymerization mechanism versus miniemulsion polymerization mechanism. 28

Scheme 2.6: The encapsulation process of materials soluble in the dispersed phase and the possible morphological structures. 33

Scheme 2.7: : possible equilibrium morphologies with the relevant spreading coefficients. . 35

Scheme 3.1: : Encapsulation of Rhodamine B dye via an inverse miniemulsion process 51

Scheme 3.2: The decomposition mechanism of CHP/TEPA and The chemical structure of Rhodamine B dye. 67

Scheme 3.3: Hydrogen-bonded and electron-conjugated complexes of amines and hydroperoxides. 69

Scheme 4.1: Synthesis of a Rhodamine B acrylate derivative[34] 83

List of tables

Table 2.1: choices of HLB values 16

Table 3.1: Table 3.1 Formulations used in the inverse miniemulsion polymerizations for the preparation of Rhd-B based nanocolorants 57

Table 3.2: Average particle size of nanocolorants made with different RhB dye loadings. 60

Table 4.1: Formulations used in the inverse miniemulsion polymerizations for the preparation of poly(PAAm-*co*-RhB) and crosslinked-poly(PAAm-*co*-RhB) nanocolorants. 89

Table 4.2: Average particle size of poly(PAAm-*co*-RhB) and crosslinked-poly(PAAm-*co*-RhB) nanocolorants. 90

Table 4.3: T_g of poly(AAm-*co*-RhB) and crosslinked-poly(AAm-*co*-RhB) nanocolorants and their corresponding reference experiments. 96

Table 5.1:1 Formulations used in the *in situ* inverse miniemulsion polymerizations for the preparation of crosslinked-PAAm/RhB and crosslinked-Poly(AAm-*co*-RhB) nanocolorants-based inks. 111

List of acronyms

AA	**Acrylic acid**
AAm	**Acrylamide**
AIBN	**2,2'-azobisisobutyronitrile**
BA	**Butyl acrylate**
BPO	**Benzoyl peroxide**
CMC	**Critical Micelle Concentration**
CHP	**Cumene hydroproxide**
CH	**Cyclohexane**
DMAP	**4-Dimethylamino pyridine**
DCC	**1,3-Dicyclohexyl carbodiimide**
DSC	**Dynamic scanning calorimetry**
HBA	**4-Hydroxy butyl acrylate**
HEMA	**2-Hydroxyethyl methacrylate**
HLB	**Hydrophile Lipophile Balance**
MBA	**N,N'-methylene bis acrylamide**
MMA	**Methyl methacrylate**
NIPAM	**N-isopropylacrylamide**
NMR	**Nuclear magnetic resonance**
PNIPAAm	**poly(*N*-isopropylacrylamide)**
RhB	**Rhodamine B**
PSty	**Polystyrene**
SDS	**Dodecyl sulphate**
SEM	**Scanning electron microscope**
TEPA	**Tetraethylenepentamine**
TEM	**Transmission electron microscopy**
TGA	**Thermogravimetric analysis**
V-50	**2,2´-azobis(2-methylpropionamidine) dihydrochloride**
VAc	**Vinyl acetate**
O/W	**Oil-in-water**
W/O	**Water-in-oil**
W/O/W	**Water-in-oil-in-water**

List of symbols

$\prod_{osm}$	**osmotic pressure (kPa)**
$\prod_{L}$	**Laplace pressure (kPa)**
R	**radius of droplets (m)**
σ_{ow}	**interfacial tension (N/m)**
k_B	**Boltzmann constant (1.38×10^{-23} J/K)**
T	**absolute temperature (k)**
η	**number of ultrahydrophobe molecules**
λ_{max}	**maximum wavelength of absorption (nm)**

Chapter 1: Introduction and objectives

1.1 Introduction

The production and development of materials composed of polymer nano/microparticles has been a field of interest to many polymer scientists. Working as small containers, the nano/microparticles are desirable for a variety of applications. They can be used to encapsulate dyes and pigments for paints and inks, drugs and enzymes for new intracellular delivery systems such as drug delivery and gene therapy, catalysis, cosmetics, or to encapsulate any other organic and inorganic materials as desired.

The preparation of polymer nano/microparticles has been extensively investigated over the past two decades. Approaches include colloidal or liquid-core templating methods [1-4], suspension polymerization[5], phase separation of block copolymers[6-8], lipid/liposome or vesicle templates [9-11], cored dendrimers[12], layer-by-layer (LBL) methods[6, 13-15], utilization of covalent bonds and hydrogen bonds [7, 16], electrochemical oxidation of pyrrole [17], *in-situ* interfacial polymerization[18-25], emulsion polymerization[20, 25-30], W/O/W emulsion polymerization[31], and miniemulsion processes[32-44] have been developed recently. However, with the exception of emulsion and miniemulsion techniques, most of these technologies are unsuitable for large-scale production, as they are of low efficiency and usually involve complicated multi-step procedures.

Emulsion and miniemulsion polymerization techniques have shown to be attractive approaches to obtain polymeric nanoparticles and to achieve efficient encapsulation.

Encapsulation of organic and inorganic particles has been reported. Particles such as, pigments and dyes [39, 41, 45-53], colloidal silica[40], and other organic and inorganic compounds[33, 36, 38, 39], were successfully encapsulated using various polymeric materials. However, it has been found that it is often difficult to achieve high encapsulation efficiency by emulsion polymerization due to the complexity of the particle nucleation and polymerization mechanism. Contrarily, and thanks to its characteristic features, the miniemulsion polymerization technique offers several advantages over emulsion polymerization. In the miniemulsion system, the monomer droplets are numerous and sufficiently small (approximately 50-500 nm), and the polymerization only takes place in those monomer droplets.[54] The mini-droplets act as independent nano-reactors, in which they can be used as encapsulating containers for compounds that are satisfactorily suspended into the monomer phase.[33, 44, 55, 56]

1.2 Nanocolorants

Nanocolorants[57] are a new class of materials that have received great attention in both academia and industry. Nanocolorants have been used in many digital and colored printing, biological and pharmaceutical applications. Moreover, they have been also used as a replacement of dyes and pigments in a wide variety of applications. The need to develop these nanocolorants was a result of the prospective inherent disadvantages of dyestuffs and pigments. In applications such as coating, printing and paint, dyestuffs exhibit excellent chromatic properties (*e.g.* brilliant color and good image), but they suffer from poor durability (*e.g.* poor light stability, weak solvent resistance and insufficient thermal stability), whereas the pigments exhibit good durability, but they suffer from poor chromatic properties and processability. For these reasons, an

innovated material that integrates the excellent properties of both dyes and pigments and overcome their drawbacks had to be found.[51, 58]

In principle, nanocolorants are nanocomposites that combine a suitable polymeric matrix and dyes or pigments acting as the essential ingredient, providing the desired color. Methods for the preparation of nanocolorants, which include emulsion polymerization[59], microemulsion polymerization[60, 61] and miniemulsion polymerizations have been well reported in the literature.[44] Although conventional emulsion polymerization is regarded as a suitable method to prepare nanocolorants, some drawbacks have been observed. As the emulsion polymerization proceeds, the dye must travel along with the monomer from the monomer droplets through the continuous aqueous phase to the monomer-swollen polymerization particles, this will result in an undesirable situation where the dye aggregates and where the dye content in the particles is not high enough for practical use. Contrarily, miniemulsion polymerization provides an ideal situation for the preparation of nanocolorants. The molecules involved in the polymerization do not have to diffuse into the polymerization loci through the continuous phase, as the miniemulsion will provide a large number of tiny monomer droplets that act as small reactors, where the polymerization mainly occurs.[62]

In our study we aim to investigate the synthesis and characterization of nanocolorants and their application as a toner for hot-melt ink (also known as phase-change ink). The main idea in this project is to improve the way of implementing the coloured polymer latex that is used in the preparation of the hot-melt ink. In the conventional way, the colorant that is used is either a hydrophobic dye/pigment or coloured latex that is

made of a hydrophobic dye encapsulated by a polymeric matrix.[63-65] In the case where coloured latex is used, the dye tends to diffuse out of the particles into the favoured hydrophobic wax, which is an undesirable situation. Our approach to improve this situation is to make optimum use of the polarities of the two different phases. Polymerizations are carried out to synthesize particles that contain a polar dye and a slightly less polar polymer, dispersed in a non-polar wax. This leads to a reduction of process steps and ensures minimization of particle coalescence or clustering as well as of diffusion of the dye from the particles.

In view of all possible approaches, inverse miniemulsion polymerizations seem to have the best potential to achieve our goal. As it will be discussed in chapters 2 and 3 in more detail, the inverse miniemulsion is a reversed formula of the regular miniemulsion system, but has the same characteristics. It can be defined as organic dispersions of surfactant stabilized water droplets within a size range 50-500 nm prepared by shearing a system containing oil, water, a surfactant, and an osmotic pressure agent. Surfactants with low HLB values are required and a very hydrophilic substance (Ionic compounds, e.g., simple salts or sugars) working as the osmotic pressure agent must be added to stabilize the dispersed droplets.[66]

1.3 Objectives

The objectives of this study were:

1) The synthesis and characterization of well-defined structured nanocolorants via an inverse miniemulsion polymerization process. The nanocolorants particles are made of a hydrophilic water-soluble fluorescent dye (*e.g*. Rhodamine B)

encapsulated by a hydrophilic water-soluble polymer (*e.g*. polyacrylamide). The formulation of the inverse miniemulsion will be tuned to incorporate a crosslinking agent and hydrophobic monomers, so various nanocolorant particles morphologies can be obtained. The obtained nanocolorants will be investigated in terms of their nanostructure and morphology, their light and migration fastness and their thermal behaviour and stability.

2) The synthesis and characterization of nanocolorants made of a polymerizable fluorescent dye incorporated as a comonomer in inverse miniemulsion polymerization. Typically, the polymerizable dye is a modified version of the dye used in the first step. The nanocolorants will be investigated in terms of their nanostructure and morphology, light and migration fastness and thermal stability.

3) The applicability of the nanocolorants as a colouring agent in solid ink will be tested. The solid ink will be synthesized either via *in situ* inverse miniemulsion polymerization, where the ink vehicle is employed as the organic continuous phase, or by directly mixing the readymade nanocolorants miniemulsion with a melted ink vehicle (*e.g*. paraffin wax). The obtained solid ink will be investigated in terms of morphology and thermal stability.

1.4 References

1. Marinakos, S. M.; Novak, J. P.; Brousseau, L. C.; House, A. B.; Edeki, E. M.; Feldhaus, J. C.; Feldheim, D. L. *J. Am. Chem. Soc.* **1999,** 121, 8518-8522.

2. Marinakos, S. M.; Anderson, M. F.; Ryan, J. A.; Martin, L. D.; Feldheim, D. L. *J. Phys. Chem. B* **2001,** 105, 8872-8876.

3. Jang, J.; Oh, J. H.; Li, X. L. *J. Mater. Chem.* **2004,** 14, 2872-2880.

4. Yuan, L.; Liang, G.; Xie, J.; Li, L.; Guo, J. *Polymer* **2006,** 47, 5338-5349.

5. Okubo, M.; Konishi, Y.; Minami, H. *Colloid. Polym. Sci.* **1998,** 276, 638-642.

6. Donath, E.; Sukhorukov, G. B.; Caruso, F.; Davis, S. A.; Möhwald, H. *Angew. Chem. Int. Ed.* **1998,** 37, 2201-2205.

7. Wang, M.; Jiang, M.; Ning, F.; Chen, D.; Liu, S.; Duan, H. *Macromolecules* **2002,** 35, 5980-5989.

8. Thurmond, K. B.; Kowalewski, T.; Wooley, K. L. *J. Am. Chem. Soc.* **1997,** 119, 6656-6665.

9. Ruysschaert, T.; Germain, M.; Gomes, J. F. P. d. S.; Fournier, D.; Sukhorukov, G. B.; Meier, W.; Winterhalter, M. *IEEE Trans Nanobiosci* **2004,** 3, 49-55.

10. Meier, W.; Hotz, J.; Gnther-Ausborn, S. *Langmuir* **1996,** 12, 5028-5032.

11. Du, J.; Chen, Y. *Macromolecules* **2004,** 37, 5710-5716.

12. Wendland, M. S.; Zimmerman, S. C. *J. Am. Chem. Soc.* **1999** 121, 1389-1390.

13. Decher, G. *Science* **1997,** 277, 1232-1237.

14. Schneider, G.; Decher, G. *Nano Lett.* **2004,** 4, 1833-1839.

15. Caruso, F.; Caruso, R. A.; Möhwald, H. *Science* **1998,** 282, 1111-1114.

16. Wang, M.; Zhang, G.; Chen, D.; Jiang, M.; Liu, S. *Macromolecules* **2001,** 34, 7172-7177.

17. Qu, L.; Shi, G. *J. Polym. Sci., Part A: Polym. Chem.* **2004,** 42, 3170-3177.

18. Sun, Q.; Deng, Y. *J. Am. Chem. Soc.* **2005,** 127, 8274-8275.

19. McFarland, B.; Popwell, S.; Pojman, J. A. *Macromolecules* **2006,** 39, 55-63.

20. Jiang, B.; Gao, C.; Shen, J. *Colloid. Polym. Sci.* **2006,** 284, 513-519.

21. Chang, C. P.; Chang, J. C.; Ichikawa, K.; Dobashi, T. *Colloids Surf., B: Biointerfaces* **2005,** 44, 187-190.

22. Kang, M.; Myung, S. J.; Jin, H.-J. *Polymer* **2006,** 47, 3961-3966.

23. Gao, H.; Jiang, T.; Han, B.; Wang, Y.; Du, J.; Liu, Z.; Zhang, J. *Polymer* **2004,** 45, 3017-3019.

24. Liu, W.-J.; He, W.-D.; Wang, Y.-M.; Wang, D.; Zhang, Z.-C. *Polymer* **2005,** 46, 8366-8372.

25. Lamb, D. J.; Anstey, J. F.; Fellows, C. M.; Monteiro, M. J.; Gilbert, R. G. *Biomacromolecules* **2001,** 2, 518-525.

26. McDonald, C. J.; Bouck, K. J.; Chaput, A. B.; Stevens, C. J. *Macromolecules* **2000,** 33, 1593-1605.

27. Kim, J.-W.; Joe, Y.-G.; Suh, K.-D. *Colloid. Polym. Sci.* **1999,** 277, 252-256.

28. Luo, Y.; Rong, M. Z.; Zhang, M. Q.; Friedrich, K. *J. Polym. Sci., Part A: Polym. Chem.* **2004,** 42, 3842-3852.

29. RL, T.-K. *Chem. Ind.* **1990,** 16, 512.

30. Soula, R.; Saillard, B.; Spitz, R.; Claverie, J.; Llaurro, M. F.; Monnet, C. *Macromolecules* **2002,** 35, 1513-1523.

31. Harada, A.; Kataoka, K. *Science* **1999,** 283, 65-67.

32. Landfester, K. *Adv. Mater.* **2001,** 13, 765-768.

33. Luo, Y.; Zhou, X. *J. Polym. Sci., Part A: Polym. Chem.* **2004,** 42, 2145-2154.

34. Tiarks, F.; Landfester, K.; Antonietti, M. *Langmuir* **2001,** 17, 908-918.

35. Landfester, K.; Rothe, R.; Antonietti, M. *Macromolecules* **2002,** 35, 1658-1662.

36. Paiphansiri, U.; Tangboriboonrat, P.; Landfester, K. *Macromol. Biosci.* **2006,** 6, 33-40.

37. Landfester, K. *Macromol. Rapid Commun.* **2001,** 22, 896-936.

38. Tiarks, F.; Landfester, K.; Antonietti, M. *Macromol. Chem. Phys.* **2001,** 202, 51-60.

39. Bechthold, N.; Tiarks, F.; Willert, M.; Landfester, K.; Antonietti, M. *Macromol. Symp.* **2000,** 151, 549-555.

40. Tiarks, F.; Landfester, K.; Antonietti, M. *Langmuir* **2001,** 17, 5775-5780.

41. Erdem, B.; Sudol, E. D.; Dimoni, V. L.; El-Aasser, M. S. *J. Polym. Sci., Part A: Polym. Chem.* **2000,** 38, 4419-4430.

42. Erdem, B.; Sudol, E. D.; Dimoni, V. L.; El-Aasser, M. S. *J. Polym. Sci., Part A: Polym. Chem.* **2000,** 38, 4431-4440.

43. Erdem, B.; Sudol, E. D.; Dimoni, V. L.; El-Aasser, M. S. *J. Polym. Sci., Part A: Polym. Chem.* **2000,** 38, 4441–4450.

44. Weiss, C.; Landfester, K. *Adv Polym Sci* **2010,** 233, 185-236.

45. Lelu, S.; Novat, C.; Graillat, C.; Guyot, A.; Bourgeat-Lami, E. *Polym. Int.* **2003,** 52, 542–547.

46. Templeton-Knight, R. L. *Chem. Ind.* **1990,** 16, 512.

47. Haga, Y.; Watanabe, T.; Yosomiya, R. *Angew. Makromol. Chem.* **2003,** 189, 23 - 34.

48. Lorimer, J. P.; Mason, T. J.; Livsey, D. K.; Templeton-Knight, R. L. *Colloid. Polym. Sci.* **1991,** 269, 392-397.

49. Oliveira, A. M.; Silva, M. L. C. P.; Alves, G. M.; Santos, A. M. *Polimeros: Ciencia Tecnol.* **2002,** 12, 123-129.

50. Oliveira, A. M. d.; Silva, M. L. C. P. d.; Alves, G. M.; Oliveira, P. C. d.; Santos, A. M. d. *Polym. Bull.* **2005,** 55, 477–484.

51. Barashkov, N. N.; Liu, R. In *Fluorescent Nanocolorants Based on Dye-Packaging Technology for Ink Jet Application*, IS&T NIP16: International Conference on Digital Printing Technologies, Fort Lauderdale, Florida, 2001; Fort Lauderdale, Florida, 2001; pp 878-880.

52. Viala, P.; Bourgeat-Lamy, E.; Guyot, A.; Legrand, P.; Lefebvre, D. *Macromol. Symp.* **2002,** 187, 651-661.

53. Ganschow, M.; Metz, H. J.; Rohr, U.; Schweikart, K.-H.; Landfester, K. Method for Production of Polymer-Encapsulated Pigments. PCT/EP05/04258, 2007.

54. Sudol, E.; El-Aasser, M., Miniemulsion Polymerization. In *Emulsion Polymerization and Emulsion Polymers*, Lovell, P.; El-Aasser, M., Eds. John Wiley & Sons Ltd: New York, 1997; pp 699-722.

55. Chern, C.-S.; Lin, C.-H. *Polymer* **1998,** 40, 139-147.

56. Chern, C. S.; Chen, T. J.; Liou, Y. C. *Polymer* **1998,** 39, 3767-3777.

57. Böhm, A.; Kielhorn-Bayer, S. *Prog. Colloid Polym. Sci.* **1999,** 113, 121-128.

58. Boehm, A. J.; Glaser, A.; Koch, O., Nanocolorants-more than colored nanoparticles. In *ANTEC 2003 Plastics: 61st Annual technical conference*, Society of Plastics Engineers: Nashville, USA, 2003; Vol. 2, pp 2419-2422.

59. TRONC, F. D. R.; LI, M.; LU, J.; WINNIK, M. A.; KAUL, B. L.; GRACIET, J.-C. *J. Polym. Sci., Part A: Polym. Chem.* **2003,** 41, 766-778.

60. Zhao, L.; Lei, Z.; Li, X.; Li, S.; Xu, J.; Peng, B.; Huang, W. *Chem. Phys. Lett.* **2006,** 420, 480-483.

61. Yao, G.; Wang, L.; Wu, Y.; Smith, J.; Xu, J.; Zhao, W.; Lee, E.; Tan, W. *Anal. Bioanal. Chem.* **2006,** 385, 518-524.

62. Takasu, M.; Shiroya, T.; Takeshita, K.; Sakamoto, M.; Kawaguchi, H. *Colloid Polym Sci* **2003,** 282, 119-126.

63. BIRAU, M. M.; IFTIME, G.; VANBESIEN, D. W.; WOSNICK, J. H.; WAGNER, C. A.; ALLEN, C. G. FLUORESCENT SOLID INK MADE WITH FLUORESCENT NANOPARTICLES. US 2010/0086683 Al, 2010.

64. Chovancova-Lovel, V.; Pekarovicova, A.; Fleming, P. D. *J. Imaging Sci. Technol.* **2006,** 50, 550-555.

65. Pekarovicova, A.; Bhide, H.; Paul D, F.; Pekarovic, J. *J. Coating. Technol.* **2003,** 75, 65-72.

66. Landfester, K.; Willert, M.; Antonietti, M. *Macromolecules* **2000,** 33, 2370-2376.

Chapter 2: Historical and theoretical background

2.1 Miniemulsion polymerization

2.1.1 Introduction

Since its first introduction as a new heterogeneous aqueous polymerization technique by Ugelstad *et al*.[1] in 1973, miniemulsion polymerization has been regarded as one of the most important techniques for the production of polymer latex. Miniemulsion polymerization is a simple, convenient and uncomplicated method that has been widely used for the polymerization of numerous monomers and for the encapsulation of organic and inorganic materials.[2] This simple procedure has proved to be beneficial in comparison to other dispersion polymerization methods. The significance of this particular technique can be attributed to: the small particle size of the latex produced, the low amount of surfactant used, the production of latices with high solid content, and final particles that are a 1:1 replica of the original miniemulsion droplets. This formation of the polymer particles as exact duplicates of the original monomer droplets is the main factor that sets miniemulsion polymerization apart from all other known dispersion techniques.[3]

Miniemulsion is known for its nanoscale monomer droplets size in the range between 50-500 nm.[4] Monomer droplets in a miniemulsion system are the outcome of shearing two pre-mixed immiscible phases: a continuous phase and a dispersed phase, in the presence of a surfactant and cosurfactant. The dispersed phase is normally the monomer phase, while the continuous phase is the carrier media of the

whole miniemulsion. Two types of miniemulsions are normally recognized: a conventional miniemulsion (known as oil-in-water miniemulsions O/W), in which the monomer phase is dispersed in an aqueous continuous phase, and an inverse miniemulsion (known as water-in-oil miniemulsions W/O) where the monomer phase is dispersed in an organic continuous phase (*e.g*. heptane, toluene, cyclohexane, etc.). [5, 6] Scheme 2.1 shows a simple illustration of the concept of a miniemulsion.

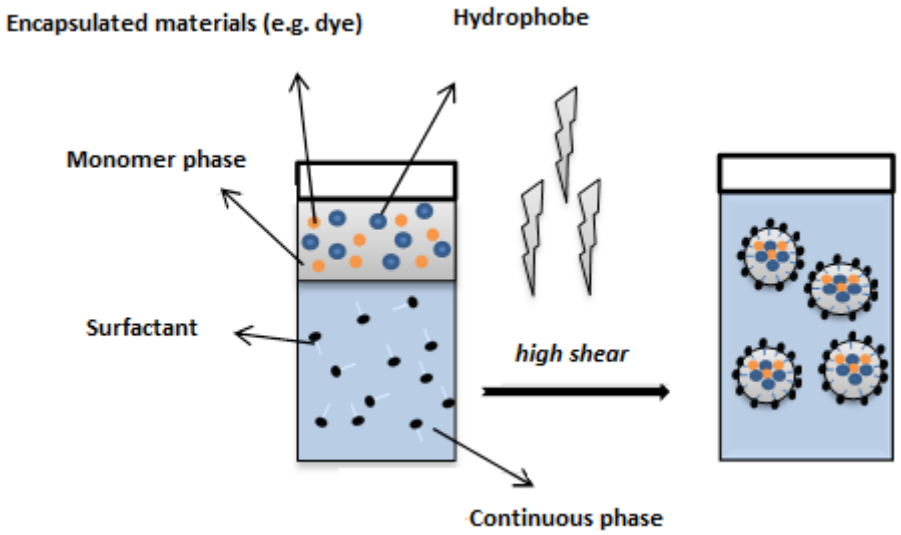

Scheme 2.1: Concept of miniemulsion polymerization

2.1.2 Formulation and composition contents

A miniemulsion formulation usually consists of water or organic media (whether it is O/W or W/O) as a carrier media, a monomer or a monomer mixture, a surfactant (also called emulsifier), a co-stabilizer (also called hydrophobe for O/W type and lipophobe for W/O type) and a compatible initiator system. Miniemulsion polymerization of monomers such as styrene (Sty),[1, 7, 8] methyl methacrylate (MMA),[9-12] butyl acrylate (BA)[9, 13] and vinyl acetate (VAc),[14] have been extensively studied. Successful synthesis of homopolymers as well as copolymers of these

monomers via O/W miniemulsion polymerization have been widely reported.[9] Moreover, very water-soluble monomers such as: acrylic acid (AA)[5] and methacrylic acid (MAA),[15] have been polymerized successfully in the miniemulsion polymerization. Water-soluble polymers are prepared via W/O miniemulsion polymerization. Monomers such as: acrylamide (AAm), hydroxymethyl methacrylate (HEMA) and N-isopropylacrylamide (NIPAAm) have been reported.[5, 16-18]

2.1.2.1 Surfactants

For a successful (mini) emulsion polymerization, the selection of a suitable surfactant is very crucial. Surfactants provide colloidal stability to the monomer droplets, the growing polymer particles and the end product by mainly preventing coalescence. Factors such as particle size and particle size distribution rely pretty much on the choice of the surfactant.[6, 19]

Surfactants are chemical substances that possess an amphiphilic nature, which means that they contain within their chemical structure two different segments, a hydrophilic (water-loving or polar) segment and a lipophilic (oil-loving or non-polar) segment. Due to this general structure, surfactants are mostly situated at the oil-water interface. As a result, the surface energy is reduced, phase separation is prevented and micelles are formed.[19, 20] These micelles provide sites for the formation of monomer droplets, which develop into polymer particles at a later stage. In order to form micelles, the surfactant concentration must be above a certain value called “Critical Micelle Concentration” (CMC). Another important value that must be considered when choosing a suitable surfactant is the HLB value. The

HLB value was first introduced in 1948 by William C. Griffin.[21] It is identified as "Hydrophile Lipophile Balance" and calculated mathematically as the ratio of molecular weight of the hydrophilic portion to the molecular weight of the hydrophobic portion of the surfactant. The HLB value is also a reflection of the solubility of the surfactant in the continuous phase, and an indication for its end use.[22] (Scheme 2.2).

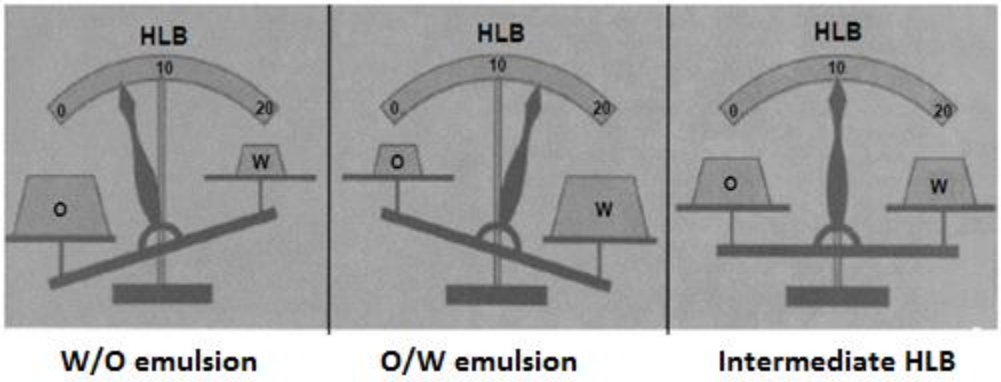

Scheme 2.2: HLB range[22].

O/W emulsions require water-soluble surfactants with higher HLB value while oil soluble surfactants with lower HLB value are required for W/O emulsions. Some other applications may need surfactants with different HLB value. Table.2.1 shows some of HLB values and their correlated applications.[22]

Table 2. 1: choices of HLB values

HLB range	Use
4-6	**W/O emulsifiers**
7-9	**Wetting agents**
8-18	**O/W emulsifiers**
13-15	**Detergents**
10-18	**Solubilizers**

There are many types of surfactants that have been used and described in literature, but the most important classes are known as ionic, non-ionic and zwitterionic (amphoteric). This classification is based mainly on the nature of their hydrophilic groups.

***Ionic**:* ionic surfactants are featured with a charged hydrophilic head-group, which stabilizes emulsions electrostatically by creating repulsion between the particles.[23, 24] These types of surfactants are divided into two main groups: anionic and cationic. Anionic surfactants are the most widely used and favored over cationic surfactants since the cationic surfactants are (in many cases) incompatible with the negatively charged latex particles (that could result from using initiators such as persulfates and common comonomers such as acrylic acid).[25]However, the cationic surfactants can also be used successfully in emulsion and miniemulsion polymerizations.[26, 27] The best examples of anionic surfactants include sodium dodecyl sulphate (SDS) and the Aerosol series (sodium dialkyl sulphosuccinates). Cationic surfactants include polyamines and their salts, polyoxyethylenated amines and their quaternized

derivatives, and amine oxides. The ionic surfactants are generally known for producing mondisperse latexes.[25]

Non-ionic: non-ionic surfactants have no ionic charges and normally consist of long chain molecules such as polyols, sugar derivatives or ethylene oxide.[19, 28] The use of these surfactants provides steric stability only and can result in latexes with large particles and broad particle size distributions. [28]Nevertheless, they help producing particles with better morphology and provide great stability against freeze-thawing, mechanical shearing and any added electrolytes.[25] Examples of non-ionic surfactants include the Brij series (polyoxyethylenated alkyl ethers) and the Span and the Tween series (polysorbates). Some polymeric surfactants are also included in this type of surfactants. Pluronic and Tetronic series from BASF are the best examples of the polymeric surfactants. They consist of block copolymer of poly(ethylene oxide) (PEO) and poly(propylene oxide) (PPO) in which the PEO block can vary from 10-80% of the copolymer.[25] There is evidence from various studies that polymeric surfactants are the most suitable choice for stabilization of W/O emulsions.[6] Surfactants such as KLE3729 (poly(ethylene-*co*-butylene)-*b*-poly(ethylene oxide))[5, 29] and Hypermer B246 (polyhydroxystearic acid-polyethylene glycol-polyhydroxystearic acid)[16, 30] have been utilized successfully in W/O emulsion and miniemulsion polymerizations. As shown in Scheme 2.3, the architecture of the surfactant and the chemical composition (polymer blocks) control the way the surfactant sterically stabilizes the emulsion.[23]

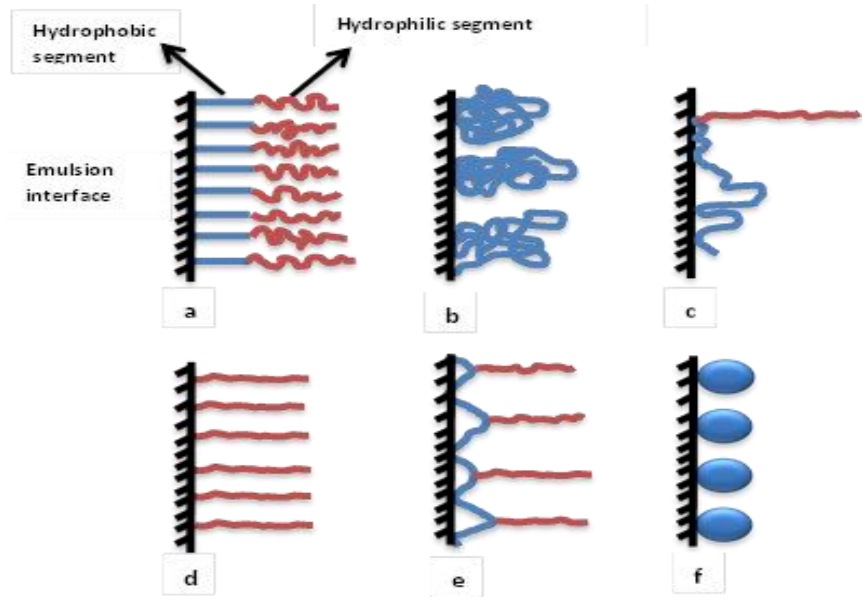

Scheme 2.3: various types of stabilizer molecules: (a) non-ionic surfactant; (b) random coil polymers; (c) linear block copolymer; (d) comb or brush copolymer; (e) grafted polymer chains; (f) globular molecules

Amphoteric: Although they are not commonly used in emulsions, amphoteric surfactants are the best choice for an emulsion formulation when the pH is a major concern. The ionic functionality within the hydrophilic part exhibits anionic properties at high pH and cationic properties at low pH, and some of them such as sulfobetaines show amphoteric properties at all pH values. Examples of this type of surfactants include imidazoline carboxylates, amine oxides and *N*-alkylbetaines.[25]

2.1.2.2 Co-stabilizers

Co-stabilizers had are also been known in literature as co-surfactants. Recently they have become known as hydrophobe (for O/W miniemulsion) or lipophobe (for W/O miniemulsion).[31, 32] A co-stabilizer is defined as "a surface-active agent which acts in addition to the surfactant by further lowering the interfacial energy, but which

cannot form micellar aggregates by itself"[31]. Various compounds have been reported as co-stabilizer, especially in O/W miniemulsion systems. Hexadecane is probably the most famous one that has been extensively used. However, any hydrophobic compound (including hydrophobic polymers) can be used as a hydrophobe, and the more hydrophobic the hydrophobe is, the more suitable it is. On the other hand, the lipophobe that is used in W/O miniemulsion systems must be highly hydrophilic and water-soluble. Therefore, any electrolyte salt such as sodium chloride or sodium sulfate[5, 16], sugars, or any other ionic compound would be a suitable lipophobe[31].

2.1.2.3 Initiators

As in any other polymerization process, an initiation system is needed to start the polymerization in a miniemulsion process. The generations of free radicals by thermal decomposition of initiators such as peroxy compounds, by redox reactions, or by γ-radiation are the most common methods. Whether they are thermally decomposing initiators or redox initiators, the free radical initiators can be classified into two classes, *i.e.* water-soluble initiators and oil-soluble initiators.[25]

Thermal initiators: Water-soluble thermal initiators decompose at a temperature in the range of 50-90 °C to generate two radicals. The most common initiators of this category are the salts of persulfates, especially: sodium, potassium and ammonium persulfate. Other important water-soluble initiators are some ionic azo-compounds such as 2,2´-azobis(2-methylpropionamidine) dihydrochloride (known also as V-50) and 4,4'-azobis(4-cyanopentanoic acid). On the other hand the oil-soluble initiators are mostly non-ionic and decompose to produce two radicals. The best known

examples of this type of initiators are benzoyl peroxide (BPO) and 2,2´-azobis(isobutyronitrile) (AIBN). It should be mentioned that, although the oil-soluble initiators decompose into two radicals, they still kinetically behave similar to the water-soluble initiators in which only single radicals enter the particles.[8]

Redox initiators: this type of initiators is advantageous when the polymerization is performed at low temperature (<50 °C), especially when a polymer with high molar mass and low levels of branching and crosslinking is desired. In a redox initiation system, an oxidation-reduction reaction takes place between an oil-soluble/water-soluble pair of oxidizing and reducing agents to generate the radicals required for starting the polymerization. Some common redox systems that have been used include; persulfate/bisulfite, sodium formaldehyde sulfoxylate/ *tert*-butyl hydroperoxide and persulfate/iron(II).[25] In redox initiation, only one radical per initiator molecule is generated.

2.1.3 Preparation and homogenization techniques

The homogenization process (also called emulsification) is one of the most important and crucial steps in the preparation of a miniemulsion. In the presence of a co-stabilizer, emulsification results in uniform monomer droplets, which at a later stage lead to predominance of droplet nucleation.[32] The starting point is the premixing of the different components by the means of simple stirring to produce an emulsion (sometimes called pre-emulsion or macroemulsion). The next step is emulsification with a high shear device, where the pre-emulsion droplets break up and subsequently produce the final monomer droplets in which the polymerization

eventually takes place.[31] Various emulsification techniques and devices have been described and used, including rotor-stator systems (*e.g*. Omni Mixer, Ultra Turrax), sonication (ultrasonicator) and high-pressure homogenization (*e.g*. microfluidizer and Manton-Gaulin). The sonication method has been proven to be the most effective, particularly for small-scale production or laboratory investigations.[31-33]

The ultrasonicator supplies powerful ultrasound waves that break up the initial pre-emulsion droplets in a fission and fusion manner to smaller droplets. This emulsification process is carried out until a pseudo steady-state is reached where a stable miniemulsion with smaller and narrow size distribution droplets is obtained. Scheme 2.5 [6] gives a simple illustration of what happens during emulsification process.[28, 31]

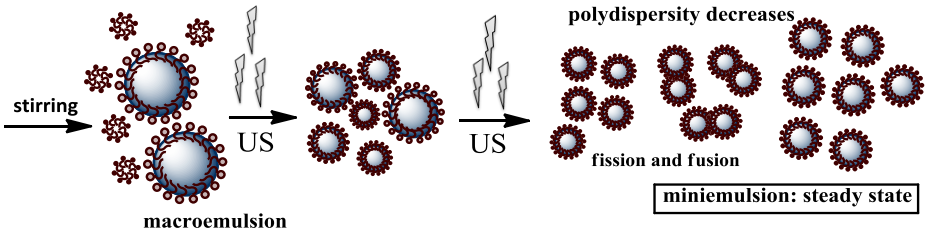

Scheme 2.4: **Formation of miniemulsion by sonication process.**

Landfester *et al*.[5, 31, 34] measured the turbidity and surface tension as a function of sonication time and found that the steady state is reached only when there is a dynamic equilibrium reached between fission and fusion of the droplets. Figure 2.1 shows the turbidity and surface tension measurements against sonication time for both O/W and W/O miniemulsion systems.[5, 34]

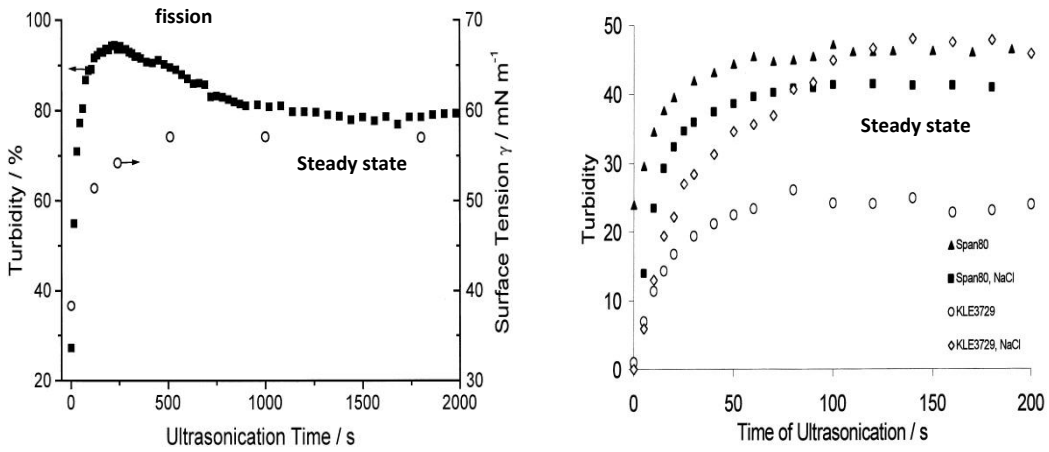

Figure 2.1: Approach of the steady state as revealed by surface tension and turbidity measurements.[5, 34]

It was concluded that the miniemulsion process produces nanodroplets with the minimum possible size by efficiently making use of the amount of surfactant available. This means that these nanodroplets are at the borderline between stability and instability, and that is why miniemulsions are considered to be 'critically stabilized'.[34, 35]

2.1.4 Miniemulsion Stability

Emulsions in general are thermodynamically unstable, and over time they undergo many physical changes until they return back to their preferred stable state where they become completely phase-separated. Destabilization of emulsion results from the lack of energy required to maintain the large surface area of the formed droplets. Accordingly, the droplet size is the main factor when the stability of the emulsion is concerned. The destabilization of emulsions can take place in two manners: reversibly and irreversibly. The reversible destabilization is observed when

creaming or sedimentation takes place, while the destabilization becomes irreversible when coalescence or molecular diffusion (well known as Ostwald ripening) occurs. [36, 37]

Creaming and sedimentation are usually followed by flocculation, which involves the collision of two monomer droplets without forming a larger droplet. In contrast, coalescence and Ostwald repining cause deformation to the monomer droplets to form new larger droplets, usually at the expense of the smaller droplets. Therefore, in order to form a stable miniemulsion system, coalescence and Ostwald ripening must be suppressed, which can be achieved by an efficient emulsification procedure and by suitable types and amounts of surfactant and cosurfactant.

Coalescence and the surfactant role: As in any other emulsion system, the colloidal stability of the droplets is very crucial to carry out a miniemulsion polymerization process. Coalescence occurs when two or more droplets collide and form a new larger droplet. The addition of a surfactant provides that colloidal stability against coalescence. However, surfactant-free emulsion and miniemulsion polymerizations have been reported[38-40].

The way surfactants stabilize emulsions varies according to their chemical structure and functionalities. Anionic and cationic surfactants provide electrostatic stabilization, while the non-ionic surfactants provide steric stabilization. It was reported that ionic surfactants are more capable of producing smaller size particles than non-ionic surfactants.[26, 28] However, that cannot be true for W/O miniemulsions

as it is believed that W/O miniemulsions are best stabilized with non-ionic polymeric surfactants.[5, 6] Polymeric surfactants provide steric stabilization, which is considered to be the main stabilization mechanism in inverse systems.

It should be also mentioned that the amount of the surfactant deployed plays a big role in controlling the particle size. The larger the amount of the surfactant is, the smaller the size of the particles. An increase in the amount of surfactant (*e.g*. up to 50 wt% with respect to monomer) results in a very small particle size (*e.g*. 30 nm or less) that is comparable to the particle size produced in microemulsion. In contrast to the microemulsion system, most of the surfactant molecules used in miniemulsion participate in covering the surface area and only a small amount of free surfactant exists that is below the CMC, which means that there are no free micelles present.[31]

Ostwald ripening and the role of co-stabilizer: The phenomenon called Ostwald ripening is an explanation of a certain behavior that exists in a two-phase system, where one of the phases is dispersed in the other. Such a system is thermodynamically unstable and needs high energy to maintain its large surface area. In this situation, a decrease in the total interfacial area by increasing the size of the dispersed phase will bring relief to the stressed system. This process can be illustrated in emulsion systems by the size reduction of small droplets and the growth of large ones via the diffusion of monomer from the shrinking small droplets to the growing larger droplets. This behavior is known as 'Ostwald ripening or coarsening'[41] and is the main cause for destabilization in systems such as emulsions, suspensions and dispersions.

This phenomenon was first introduced by Ostwald in 1901 and only studied kinetically 60 years later by Lifshitz and Slyozov[42], and Wagner[41, 43], when the growth of the particles was modeled and a distinguish between normal coagulation and Ostwald ripening was made.[42] Since then, the literature has witnessed a dramatic increase in the number of studies investigating in detail the effect of Ostwald ripening and possible ways to suppress it.[37, 41, 43-47]

Davis *et al*.[44] and Webster and Cates[47] reported that the addition of a low vapor pressure component that is completely soluble in the dispersed phase will significantly enhance the stability in emulsion systems. The presence of this soluble compound effectively creates an osmotic pressure inside the droplets, which will prevent the monomer diffusion from smaller to bigger droplets. The osmotic pressure (Π_{osm}) works against the droplet pressure (Laplace pressure; Π_L) to establish the required stability. Theoretically, an absolute stability can be achieved when; $\Pi_{osm} > \Pi_L$.[47] However, studies by Landfester and workers[34, 35] have shown that after reaching steady state by miniemulsification, the Laplace pressure is much higher than the osmotic pressure. This indicates that the stability of the droplets is not a result of a real zero droplet pressure ($\Pi_{osm} = \Pi_L$) but rather a state of equal pressure in all the droplets. On the contrary, it is believed that the zero droplet pressure exists in inverse miniemulsion, as Laplace pressure counterbalances the osmotic pressure, and that is why the inverse miniemulsion is considered to be a very stable system rather than a critically stable system.[31]

If it is taken in consideration that the osmotic pressure and the Laplace pressure are giving by $\Pi_L = \frac{2\sigma_{ow}}{R}$ and $\Pi_{osm} = \frac{k_B T\eta}{(4\pi/3)R^3}$ respectively, where R is the radius of the droplet, $2\sigma_{ow}$ the interfacial tension, k_B the Boltzmann constant, T the absolute temperature and η is the number of ultrahydrophobe molecules. It can be seen that both the osmotic pressure and the Laplace pressure are function of the droplet radius R. However, since the osmotic pressure scales with R^{-3} and Laplace only scales with R^{-1}, any small decrease in droplet size (due to monomer diffusion) will have a great effect on osmotic pressure.

2.1.5 Kinetics and mechanism in miniemulsion polymerization

Miniemulsion polymerization shares some aspects with other heterophase polymerization systems in terms of mechanism and kinetics involved, particularly with emulsion polymerization. In actual fact, the mechanism of miniemulsion polymerization is based mainly on the theory that describes the mechanism and kinetics of conventional emulsion polymerization. Therefore, it is necessary to first review the mechanism of conventional emulsion polymerization.

An emulsion in its initial state contains large monomer droplets (1-10 µm in diameter) and monomer-swollen surfactant micelles (Scheme 2.5). All the suggested mechanisms are based on the existence of these elements. The theory that was developed by Harkins (1947)[48] and Smith and Ewart (1948)[49] have inspired all the studies that discuss the emulsion polymerization mechanism. This theory suggests that emulsion polymerization progresses in three different intervals (I, II and III).

Interval I is considered to be the stage of particle formation. After initiation, one or more of three nucleation mechanisms take place, namely, micellar, homogeneous and droplet nucleation. Droplet nucleation is normally considered insignificant and has very limited effect. Interval I is marked with increasing the particle number and rate of polymerization. The micellar nucleation occurs when the generated radicals from the continuous phase enter the monomer swollen micelles and initiate polymerization to form monomer swollen polymeric particles. Homogeneous nucleation occurs when the radicals react with monomer units in the continuous phase to form oligo-radicals. Eventually, the oligo-radicals precipitate and adsorb surfactant molecules to form primary particles that continue growing throughout the polymerization process. In the droplet nucleation the radicals from the continuous phase enter directly to monomer droplets that contain 100% monomer and propagate to form polymeric particles.

Interval II is the particle growth period and it begins upon the disappearance of the micelles. This interval is characterized by a constant number of particles and a concomittant constant rate of polymerization.

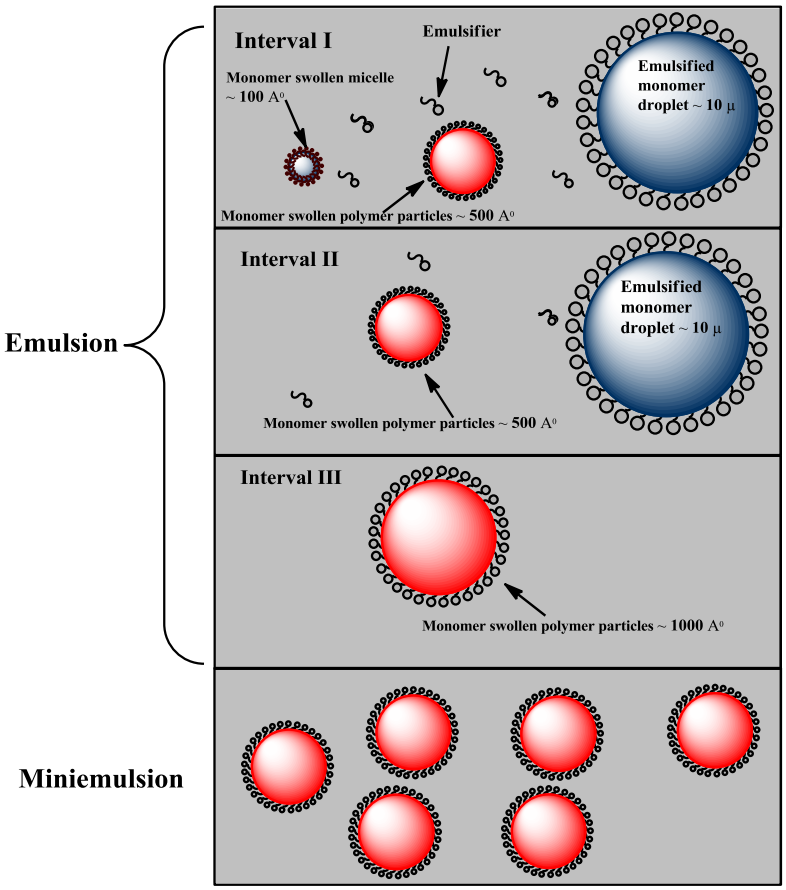

Scheme 2.5: Emulsion polymerization mechanism versus miniemulsion polymerization mechanism.

In interval III, the rate of polymerization starts to decrease due to the exhaustion of the monomer. Also, the number of particles stays constant as all monomer droplets have disappeared and only monomer swollen polymer particles exist where the polymerization continues until high conversion is obtained.

It was the idea of an emulsion system in which droplet nucleation is the dominant particle nucleation process that has led to the discovery of the miniemulsion polymerization process.[1] The formation of a system (that later has become known as miniemulsion) with small, homogeneous and stable droplets can restrict the formation of particles greatly to the droplet nucleation mechanism only. The

presence of only monomer droplets before polymerization (Scheme 2.5), as well as an unchanged number of particles after polymerization suggested that droplet nucleation is the predominant mechanism. As a result of this mechanism all the droplets can be converted into polymer particles in a one-to-one manner leading (ideally) to the same number of polymer particles after polymerization as monomer droplets before polymerization. Accordingly, the kinetics of droplet nucleation, polymer growth and overall reaction rate should be discussed with regards to the particle size and initiator concentration.

Bechthold *et al.*[50] used calorimetry measurements to follow the kinetics involved in styrene miniemulsion polymerization. Similar to conventional emulsion polymerization, three intervals were observed. However, although interval I and III exist in miniemulsion polymerization, interval II was not observed. Instead a new interval referred as interval IV is present (see Figure 2.2). Interval I is the period when the nucleation process takes place. It ends very quickly and carries on until the conversion is about 10%. This period of time allows the establishment of an equilibrium radical concentration inside each droplet where the average number of radicals (n) per particle should be in the range between $0<n<0.5$. In this interval also, the rate of polymerization increases until it reaches a maximum value, which marks the beginning of interval III.

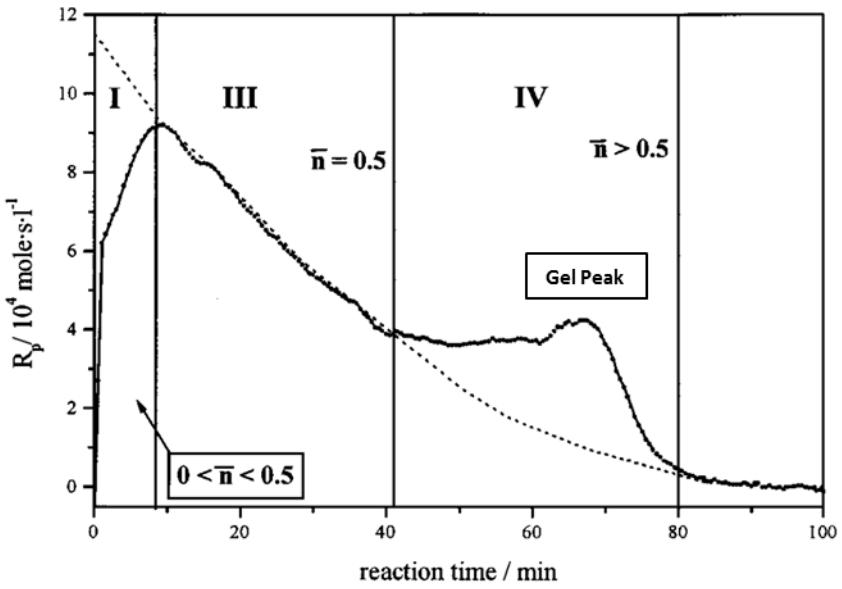

Figure 2.2: : Calorimetric curve of a typical miniemulsion.[50]

Interval III witnesses a decrease in the rate of polymerization as the monomer inside the particles is consumed while the number of radicals per particle stays constant at a value of 0.5 (Figure 2.2). The presence of this number of radicals inside the particles is an indication of the zero-one condition, where it is believed that only zero or one radicals exist within the particle at any time. This means that the presence of two radicals inside a particle is highly unlikely and if it happens, termination would take place at a rate that is much faster than propagation. The zero-one system is normally observed when $n \leq 0.5$.

On the other hand, the third interval (interval IV) is marked by an increased number of radicals as well as the increase of viscosity inside the particles as a result of the autoacceleration effect, which is also recognized in suspension polymerization. The typical gel-peak shown in Figure 2.2 is a clear indication of the increased viscosity inside the particles and the coupled kinetic hindrance of radical recombination.

In conclusion, it has been shown that droplet nucleation is the predominant nucleation mechanism in miniemulsion as there are only monomer droplets available as nucleation loci. This is in fact gives a great advantage to miniemulsion polymerization over the other heterogeneous polymerization techniques, conventional emulsion polymerization in particular, as these droplets can work individually as nano-reactors, which can be utilized for making hybrid and advanced materials that possess distinctive and improved properties. For example, miniemulsion polymerization has been shown to be a very unique and versatile method for encapsulating various organic and inorganic materials. In the way that miniemulsion polymerization proceeds, the material that needs to be encapsulated is already situated at the locus of polymerization along with the monomer(s) and it will be encapsulated with a polymer shell that is formed during polymerization. Therefore, the concept and the application of encapsulation via miniemulsion polymerization will be discussed in the following section.

2.2 Encapsulation via miniemulsion polymerization

The utilization of miniemulsion polymerization in encapsulating chemical substances and materials has been of great interest to polymer scientists. In their latest and comprehensive review, Weiss and Landfester[2] have discussed what miniemulsion polymerization has to offer for the encapsulation of organic and inorganic materials. It was obvious from the large number of studies that this technique is a great tool for producing functional nanostructures. The preparation of novel materials by the encapsulation of small molecules, liquids and solids, in polymeric matrices has been

proven to be simple and effective. Encapsulation can be achieved using different approaches based on the nature of the materials to be encapsulated and the final products. Although the concept is similar but the details and way of encapsulation can be different.

Encapsulation via miniemulsion polymerization can be classified into three main categories. First category is the encapsulation of material that is soluble in the dispersed phase (monomer droplets) as well as in the polymeric phase (polymer particles) (*e.g*. dyes, metal complexes and functional organic molecules). Second category is the encapsulation of materials that is soluble in the dispersed phase but not in the polymeric phase. In this category, capsules of a core/shell structured particles are usually formed, and that includes capsule formation by phase separation, capsule formation by polymerization from or at the interface and polymer precipitation on preformed nanodroplets. The third category is the encapsulation of material insoluble in the dispersed phase. In this category, the encapsulated material is normally surface modified so it can be dispersed in the monomer phase. Typical examples are the inorganic structures such as iron oxide or titania, silica and organic pigments such as carbon black or insoluble dyes. Their hydrophilicity makes it difficult to disperse them in a typical hydrophobic monomer phases. In this study we will consider the approaches of both the encapsulation of material soluble in the dispersed phase and the capsule formation by phase separation. The study involves the encapsulation of a dye that is soluble in the dispersed phase and also involves some aspects of capsule formation.

Generally, it is required for the encapsulated compound to be completely soluble in the monomer phase. This allows a homogeneous distribution of the material within the droplets formed during the homogenization process. The solubility of the encapsulated compound in the polymer formed during the course of the polymerization is very crucial in determining the final morphology of the particles. If the encapsulated compound stays soluble and fully miscible with the formed polymer, then solid particles of a polymer matrix with the encapsulated compound that is homogenously integrated are obtained. On the other hand, if the encapsulated compound becomes immiscible with the polymer, then phase separation occurs, which can result in either particles with core/shell structure or particles that contain microdomains of the encapsulated compound.[2]

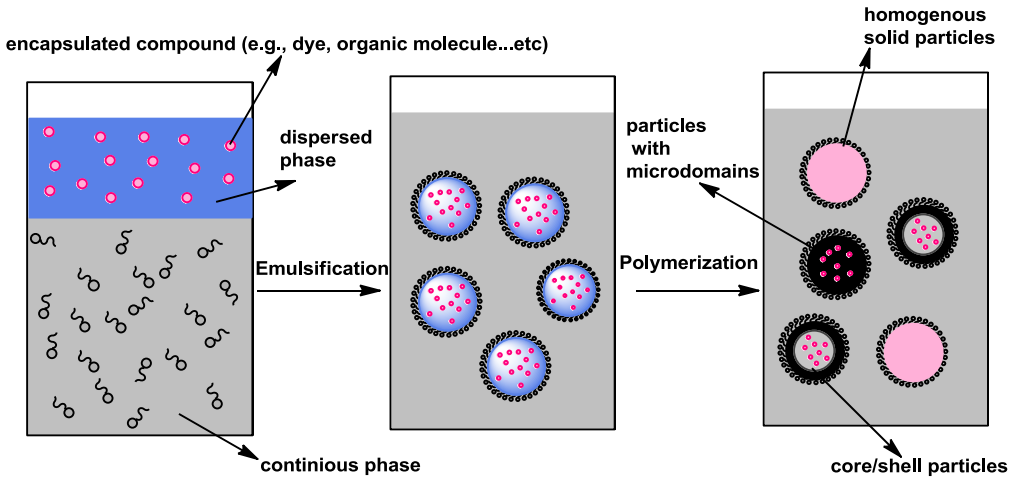

Scheme 2.6: The encapsulation process of materials soluble in the dispersed phase and the possible morphological structures.

In the approach where capsules are formed by phase separation, the encapsulated material is normally a liquid that is a solvent for the monomer(s) but a nonsolvent for the formed polymer. As the polymerization proceeds and the polymer chains grow, the polymer becomes insoluble in the encapsulated liquid and phase

separation takes place. It is essential that the polymer is highly insoluble in the encapsulated liquid for the phase separation to take place, resulting in the formation of core/shell type of capsules.

If the polymer becomes insoluble in the core liquid then the system can be regarded as a three immiscible phases system. According to Torza and Mason,[51] the equilibrium morphology in such system can be predicted thermodynamically. The resulting morphology of the interactions of two immiscible organic liquids (phases 1 and 3) suspended in water as the third immiscible phase (phase 2) can be predicted via surface tension measurements. If equilibrium is considered between phases 1 and 3 then the interfacial tensions γ_{ij} ($i \neq j \neq$ k = *1, 2, 3*) and the spreading coefficient S_i can be defined as:

$$S_i = \gamma_{jk} - (\gamma_{ij} + \gamma_{ik}) \qquad (2.1)$$

If the phases are chosen in such a way that $\gamma_{12} > \gamma_{23}$, it follows from equation 2.1 that $S_1 < 0$. This implies that three possible sets of S_i with different equilibrium morphologies can be predicted. A complete engulfment of phase 1 by phase 3 is obtained when $S_1 < 0$, $S_2 < 0$ and $S_3 > 0$, which means that a core/shell type of morphology is obtained. Second possible set is when $S_1 < 0$, $S_2 > 0$ and $S_3 < 0$, and here no engulfment occurs. The third possibility is when $S_1 < 0$, $S_2 < 0$ and $S_3 < 0$ and that results in a partial engulfment and the formation of two-phase droplets with three interfaces. Scheme 2.7 shows all three different equilibrium morphologies that could exist in a three-phase system.

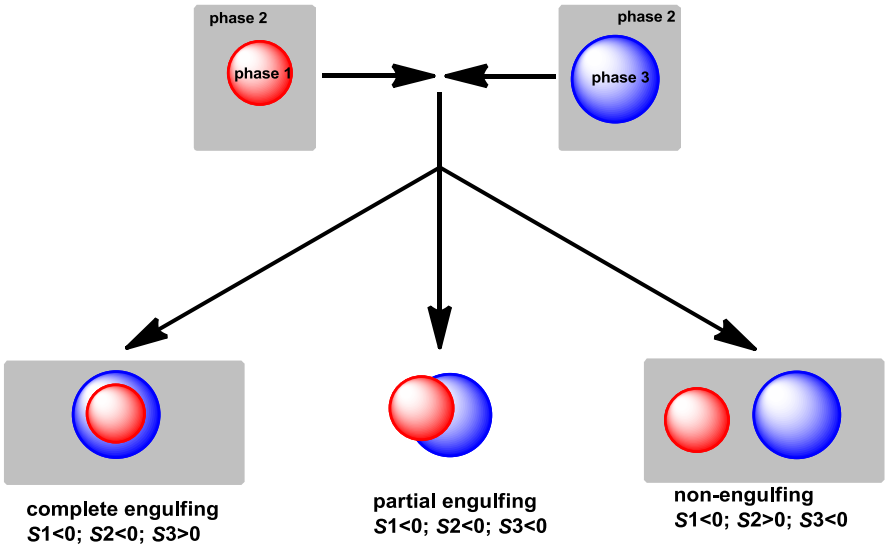

Scheme 2.7: : possible equilibrium morphologies with the relevant spreading coefficients.

Although the work of Torza and Mason was applied to a system consisting of three drops of immiscible liquids, their model can still be applied on systems consisting of a polymer phase or even two polymer phases such as in the case of emulsion systems. However, other studies, like the one published by Berg *et al.*[52], have shown that in such cases, other variables including formulation and process, have a significant effect on the resultant morphological structure. Berg *et al*. associated the resulting morphology of the encapsulation of oil (n-decane or hexadecane) via emulsion polymerization of methyl methacrylate, with the type of emulsifier and initiator used. Sundberg *et al.*[53, 54] studied the effect of the viscosity of the polymeric phase on the particle morphology. He was concluded that the restriction on the polymer chain mobility, due to the high viscosity, can lead to non-thermodynamically stable morphologies, but rather to a number of states of phase separation that may exist. Chen *et al.*[55, 56] also related some other different morphologies to the internal viscosity, the influence of surfactant and the initiating system. Furthermore, Waters[57] extended the work of Torza and Mason and quantified the interfacial

energies in an emulsion system and by that he could predict the thermodynamically-favored surface morphology. He could define the interfacial energy equations for engulfment of both a non-deforming and deformable spheres, which allowed him to predict the degree of engulfment in relation to the interfacial energy.

2.3 Nanocolorants via miniemulsion polymerization

The utilization of miniemulsion polymerization for the encapsulation of dyes has been a field of interest. Miniemulsion polymerization provides nanoscale particles, thus, encapsulation of dyes via this method results in colored particles that can be regarded as "nanocolorants". However, the synthesis of nanocolorants via miniemulsion polymerization has only been recently done. One of the early studies that involved making nanocolorants is the work that was done in 1998 by Chern *et al.*[58, 59] Their main objective was to study the effect of the dye as a low molecular weight cosurfactant and the use of the dye as a potential probe to propose a mechanism for the particle nucleation during the miniemulsion polymerization. Surprisingly, their work resulted in nanocolorants of a polystyrene encapsulating water-insoluble blue dye. This study has shown that in the encapsulation of materials such as highly water-insoluble dyes, these compounds can be used as a hydrophobe that will work as an osmotic pressure agent, thus retarding Ostwald ripening.

In similar work by Bourgeat-Lami *et al*.[60], the miniemulsion polymerization technique was utilized to encapsulate an organic phthalocyanine blue pigment into polystyrene

latex. Besides the satisfactory embedding into the polystyrene latex particles, the pigment contributed towards the stabilization of the miniemulsion. By carrying out the miniemulsion without introduction of any other hydrophobe, the organic pigment could play the role of a hydrophobe and stabilize the miniemulsion. It was therefore assumed that the solubilized blue pigment contributes to retardation of Ostwald ripening by increasing the osmotic pressure in the monomer droplets. However, the addition of a hydrophobe such as hexadecane, hexadecanol or a polystyrene prepolymer could enhance the stability of the miniemulsion droplets even further.

Landfester and co-workers[61] also studied the encapsulation of different organic pigment particles into polystyrene and polyacrylates or their corresponding copolymers. Miniemulsion polymerizations were carried out by the cosonicating of the corresponding pigment dispersion and a monomer miniemulsion which resulted in polymers efficiently encapsulating organic yellow, magenta, and blue pigment nanoparticles. A weight ratio of pigment to polymer of about 80:20 was sufficient to obtain hybrid structured nanocomposites. It was found that the molecular structure of the pigments influences the morphology of the resulting nanoparticles as well as the kinetics of the miniemulsion polymerization.

As the use of the nanocolorants is becoming more important in many applications such as ink-jet inks and electrographic toners, many studies have been carried out in order to improve some of the essential properties of the nanocolorants. Issues like the improvement of migration fastness and the preserving fastness of dyes as well as

the architecture and morphology control of the nanocolorants have been the focus of many studies. Some of the studies concluded that the morphology and the amount of the dye loaded into the particles have major effects on the properties of the nanocolorants. Kawaguchi *et al.*[62-64] reported the preparation of colored latex containing a high load of oil-soluble dye via the miniemulsion polymerization process. They show that polystyrene and methyl methacrylate colored latex loaded with phthalocyanine dye (30 wt %) and styryl dye (40 wt %) with particle size around 100 nm could be obtained. UV measurements were applied to investigate dye contents inside latex particles as well as the dye migration properties. It was observed that, although the dyes are oil-soluble, the migration of dyes from latex particles to the aqueous phase occurred over time. Results showed that the dye migration depends on the diffusion rate of the dye molecules which varies according to the dye used. Dyes that form aggregates or have bulky molecular structure such as phthalocyanine showed low diffusion rates as they tend to be retained inside the particles.

Liu *et al.*[65, 66] reported the preparation of nanocolorants via a modified miniemulsion polymerization process. Three anthraquinone-based solvent dyes were encapsulated within crosslinked polystyrene (PS)/polymethyl methacrylate (PMMA) particles. The hydrophilicity of polar monomers like MMA and the crosslinker ethylene glycol dimethacrylate (EGDMA) will cause them to locate at the interface and form the outer layer of the nanoparticles. The dyes will be encouraged to locate themselves in the core of the nanoparticles due to their high hydrophobicity. In this way, the formation of nanocolorants with good migration fastness, light fastness, thermal

stability and processibility was claimed. In 2010, Liu *et al.*[67] investigated the synthesis of nanocolorants by miniemulsion polymerization stabilized with waterborne polyurethane surfactant. The use of such surfactant resulted in nanocolorants with small particle sizes (less than 100 nm), having superior migration fastness and good thermal stability.

In conclusion, it has been shown throughout this chapter that the miniemulsion polymerization technique has much to offer in the field of making nanocolorants. However, to our knowledge no serious effort has been made to investigate the synthesis of nanocolorants in an inverse miniemulsion system. The inverse miniemulsion can be manipulated to introduce a new type of nanocolorants with a hydrophilic nature. As with nanocolorants prepared with conventional miniemulsion polymerization, properties of nanocolorants prepared with inverse miniemulsion such as light fastness, migration fastness, and thermal stability need to be investigated. In the following chapters, the synthesis and characterization of nanocolorants via inverse miniemulsion will be discussed. Also their possible use in the field of hot-melt ink application will be addressed.

2.4 References

1. Ugelstad, J.; El-Asser, M. S.; Vanderhoff, J. W. *J. Polym. Sci.:Polym. Lett.* **1973,** 11, 503 - 513.

2. Weiss, C.; Landfester, K. *Adv Polym Sci* **2010,** 233, 185-236.

3. Landfester, K.; Bechthold, N.; Förster, S.; Antonietti, M. *Macromol. Rapid Commun.* **1999,** 20, 81-84.

4. Sudol, E.; El-Aasser, M., Miniemulsion Polymerization. In *Emulsion Polymerization and Emulsion Polymers*, Lovell, P.; El-Aasser, M., Eds. John Wiley & Sons Ltd: New York, 1997; pp 699-722.

5. Landfester, K.; Willert, M.; Antonietti, M. *Macromolecules* **2000,** 33, 2370-2376.

6. Landfester, K.; Antonietti, M. *Top. Curr. Chem.* **2003,** 227, 75-123.

7. Choi, Y.; El-Asser, M.; Sudol, E.; Vanderhoff, J. *J. Polym. Sci., Part A: Polym. Chem.* **1985,** 23, 2973-2987.

8. Alduncin, J. A.; Forcada, J.; Asua, J. M. *Macromolecules* **1994,** 27, 2256-2261.

9. Unzué, M. J.; Asua, J. M. *J. Appl. Polym. Sci.* **1993,** 49, 81-90.

10. Fontenot, K.; Schork, F. J. *J. Appl. Polym. Sci.* **1993,** 49, 633-655.

11. Reimers, J.; Schork, F. J. *J. Polym. Sci., Part A: Polym. Chem.* **1996,** 59, 1833-1841.

12. Mouran, D.; Reimers, J.; Joseph, F. *J. Polym. Sci., Part A: Polym. Chem* **1996,** 34, 1073-1081.

13. Tang, P. L.; Sudol, E. D.; Adams, M.; El-Aasser, M. S.; Asua, J. M. *J. Appl. Polym. Sci.* **1991,** 42, 2019-2028.

14. Wang, S.; Schork, F. J. *J. Appl. Polym. Sci.* **1994,** 54, 2157-2164.

15. Masa, J. A.; Arbina, L. L. D.; Asua, J. M. *J. Appl. Polym. Sci.* **1993,** 48, 205-213.

16. Qi, G.; Eleazer, B.; Jones, C. W.; Schork, F. J. *Macromolecules* **2009,** 42, 3906-3916.

17. Willert, M.; Landfester, K. *Macromol. Chem. Phys.* **2002,** 203, 825-836.

18. Ganschow, M.; Metz, H. J.; Rohr, U.; Schweikart, K.-H.; Landfester, K. Method for Production of Polymer-Encapsulated Pigments. PCT/EP05/04258, 2007.

19. van Herk. A . M, *Chemistry and Technology of Emulsion Polymerisation*. Blackwell Publishing Ltd: Oxford, UK, 2005; p 1-324.

20. Anderson, C. D.; Daniels, E. S., *Emulsion Polymerisation and Latex Applications*. Rapra Technology Limited: Shawbury, United Kingdom, 2003; Vol. 14, p 146.

21. Griffin, W. C. *J. Soc. Cosmet. Chem.* **1949,** 1, 311-326.

22. Anonymous, *The HLB System- A Time-Saving Guide to Emulsifier Selection*. ICI Americas Inc: Wilmington, Delaware 19897, USA, 1976; p 22.

23. Ottewill, R. H., Stabilization of Polymer Colloid Dispersions. In *Emulsion Polymerization and Emulsion Polymers*, Lovell, P.; El-Aasser, M., Eds. John Wiley & Sons Ltd: New York, 1997; pp 59-121.

24. Verwey, E. J. W.; Overbeek, J. T. G., *Theory of the Stability of Lyophobic Colloids*. Dover Publications Inc: New York, 1999; p 218.

25. Klein, A.; Daniels, E. S., Formulation Components. In *Emulsion Polymerization and Emulsion Polymers*, Lovell, P.; El-Aasser, M., Eds. John Wiley & Sons Ltd: New York, 1997; pp 207-237.

26. Landfester, K.; Bechthold, N.; Tiarks, F.; Antonietti, M. *Macromolecules* **1999,** 32, 2679-2683.

27. Bechthold, N.; Tiarks, F.; Willert, M.; Landfester, K.; Antonietti, M. *Macromol. Symp.* **2000,** 151, 549-555.

28. Landfester, K. *Macromol. Rapid Commun.* **2001,** 22, 896-936.

29. Jagielski, N.; Sharma, S.; Hombach, V.; Mailänder, V.; Rasche, V.; Landfester, K. *Macromol. Chem. Phys.* **2007,** 208, 2229-2241.

30. Qi, G.; Jones, C. W.; Schork, F. J. *Macromol. Rapid Commun.* **2007,** 28, 1010-1016.

31. Antonietti, M.; Landfester, K. *Prog. Polym. Sci.* **2002,** 27, 689-757.

32. Schork, F. J.; Luo, Y.; Smulders, W.; Russum, J. P.; Butté, A.; Fontenot, K. *Adv. Polym. Sci.* **2005,** 175, 129–255.

33. Asua, J. M. *Prog. Polym. Sci.* **2002,** 27, 1283-1346.

34. Landfester, K.; Bechthold, N.; Tiarks, F.; Antonietti, M. *Macromolecules* **1999,** 32, 5222-5228.

35. Landfester, K. *Macromol. Symp.* **2000,** 150, 171-178.

36. Abismail, B.; Canselier, J. P.; Wilhelm, A. M.; Delmas, H.; Gourdon, C. *Ultrason. Sonochem.* **1999,** 6, 75-83.

37. Fontenot, K.; Schork, F. J. *Ind. Eng. Chem. Res.* **1993,** 32, 373-385.

38. Faridi-Majidi, R.; Sharifi-Sanjani, N.; Agend, F. *Thin Solid Films* **2006,** 515, 368-374.

39. Jhaveri, S. B.; Koylu, D.; Maschke, D.; Carter, K. R. *J. Polym. Sci., Part A: Polym. Chem.* **2007,** 45, 1575-1584.

40. Meng, Q.; Li, Z.; Li, G.; Zhu, X. X. *Macromol. Rapid Commun.* **2007,** 28, 1613-1618.

41. Voorhees, P. W. *J. Stat. Phys.* **1985,** 38, 231-252.

42. Lifshitz, I. M.; Slyozov, V. V. *J. Phys. Chem. Solids* **1961,** 19, 35-50.

43. Kuehmann, C.; Voorhees, P. *Metall. Mater. Trans. A* **1996,** 27, 937-943.

44. DAVIS, S. S.; ROUND, H. P.; PUREWAL, T. S. *J. Colloid Interface Sci.* **1981,** 80, 508-511.

45. Kabalnov, A. S.; Pertzov, A. V.; Shchukin, E. D. *J. Colloid Interface Sci.* **1987,** 118, 590-597.

46. Kabal'nov, A. S.; Pertzov, A. V.; Shchukin, E. D. *Colloids and Surfaces* **1987,** 24, 19-32.

47. Webster, A. J.; Cates, M. E. *Langmuir* **1998,** 14, 2068-2079.

48. Harkins, W. D. *J. Am. Chem. Soc.* **1947,** 69, 1428-1444.

49. Smith, W. V.; Ewart, R. H., *Kinetics of Emulsion Polymerization*. 1948; Vol. 16, p 592-599.

50. Bechthold, N.; Landfester, K. *Macromolecules* **2000,** 33, 4682-4689.

51. Torza, S.; Mason, S. G. *J. Colloid Interface Sci.* **1970,** 33, 67-83.

52. Berg, J.; Sundberg, D.; Kronberg, B. *J. Microencaps.* **1989,** 6, 327-337.

53. Sundberg, D. C.; Casassa, A. P.; Pantazopoulos, J.; Muscato, M. R.; Kronberg, B.; Berg, J. *J. Appl. Polym. Sci.* **1990,** 41, 1425-1442.

54. Sundberg, E. J.; Sundberg, D. C. *J. Appl. Polym. Sci.* **1993,** 47, 1277-1294.

55. Chen, Y.-C.; Dimonie, V.; El-Aasser, M. S. *J. Appl. Polym. Sci.* **1991,** 42, 1049-1063.

56. Chen, Y.-C.; Dimonie, V.; El-Aasser, M. S. *J. Appl. Polym. Sci.* **1992,** 45, 487-499.

57. Waters, J. A. *Collloids Surf., A: Physiochem. Eng. Aspects* **1994,** 83, 167-174.

58. Chern, C. S.; Chen, T. J.; Liou, Y. C. *Polymer* **1998,** 39, 3767-3777.

59. Chern, C.-S.; Lin, C.-H. *Polymer* **1998,** 40, 139-147.

60. Lelu, S.; Novat, C.; Graillat, C.; Guyot, A.; Bourgeat-Lami, E. *Polym. Int.* **2003,** 52, 542–547.

61. Steiert, N.; Landfester, K. *Macromol. Mater. Eng.* **2007,** 292, 1111-1125.

62. Takasu, M.; Kawaguchi, H. *Colloid Polym Sci* **2005,** 283, 805–811.

63. Takasu, M.; Shiroya, T.; Takeshita, K.; Sakamoto, M.; Kawaguchi, H. *Colloid Polym Sci* **2003,** 282, 119-126.

64. Takasu, M.; Shiroya, T.; Takeshita, K.; Sakamoto, M.; Kawaguchi, H. *Colloid Polym Sci* **2004,** 282, 740-746.

65. Hu, Z.; Xue, M.; Zhang, Q.; Sheng, Q.; Liu, Y. *Dyes Pigm.* **2008,** 76, 173-178.

66. Hu, Z. K.; Xue, M. Z.; Zhang, Q.; Sheng, Q. R.; Liu, Y. G. *J. Appl. Polym. Sci.* **2007,** 104, 3036–3041.

67. Liu, T.; Li, Z.; Wu, Q.; Ma, X. *Polym. Bull.* **2010,** 64, 511-521.

Chapter 3: Synthesis and characterization of nanocolorants via inverse miniemulsion polymerization

Abstract

This chapter discusses the synthesis and characterization of well-defined structured nanocolorants. An inverse miniemulsion polymerization process was manipulated to tune the formulation and the final structure of the nanocolorants. The nanocolorant particles were made of the highly hydrophilic water-soluble fluorescent Rhodamine B dye encapsulated by the hydrophilic water-soluble poly(acrylamide). By incorporating crosslinking agent and hydrophobic monomers, various nanocolorant particles morphologies could be obtained. TEM and SEM images confirmed the structure of the nanocolorants as varied from solid particles of polyacrylamide with Rhodamine B dye that is homogenously integrated, to a core-shell type of particles where the Rhodamine B dye is confined to the core of the particles. The colour strength and thermal behaviour of the nanocolorants were also studied by UV-vis absorption and TGA methods respectively.

3.1 Inverse miniemulsion polymerization

3.1.1 Introduction

Inverse miniemulsion polymerization was first reported in 2000 by Landfester *et al*.[1, 2]. The inverse miniemulsion polymerization may systematically differ from the conventional miniemulsion polymerization but it has the same concept and characteristics. In inverse miniemulsions, hydrophilic monomers, such as acrylic acid, acrylamide, hydroxyethyl acrylate can be emulsified in a non-polar continuous phase, for example, cyclohexane or heptane. The stabilization of inverse miniemulsions is achieved by using an osmotic pressure agent that is highly soluble in the dispersed polar phase, known as 'lipophobe', as well as surfactants with a low hydrophilic/lipophilic balance (HLB) value.

Lipophobes: alkaline or earth-alkaline salts (*e.g*. NaCl[1, 3] and $MgSO_4$[4]) or any organic compounds that are insoluble in the organic continuous phase[3, 5], can be used as a lipophobe. Similar to the role of the hydrophobe in conventional miniemulsion, the presence of the lipophobe causes the build-up of the osmotic pressure inside the droplets, which counterbalances the Laplace pressure. Although, the type of the lipophobe has no effect on the stability of the droplets of the inverse miniemulsion, the amount of the lipophobe greatly influences the droplet size[5, 6]. It has been reported, as it will also be discussed later in this chapter, that the size of the droplets increases with increasing amount of the lipophobe. In comparison to the conventional miniemulsion, the inverse miniemulsion is considered to be a completely stable system rather than a critically stable system. This can be

interpreted as the result of reaching a pressure equilibration state, where the osmotic pressure inside the droplets is in an equilibrium with the outer Laplace pressure, "a real zero-effective pressure situation"[5].

Surfactants: inverse miniemulsions require surfactants with a low HLB value, generally, lower than 9[7], and preferably in the range between 4 and 6[2, 8]. Moreover, an inverse miniemulsion is sterically stabilized and requires a surfactant with a steric demanding nature[5]. Many surfactant systems that can be used are found in the literature, but the most commonly used surfactants are the non-ionic sorbitan fatty acid esters such as sorbitane monooleate (Span 80)[1, 2, 9-12] and non-ionic block copolymers. However, the non-ionic block copolymers are more favourable as they provide maximum stability due to their polymeric and steric nature[5, 6]. Landfester *et al*.[1] have shown that the non-ionic block copolymer of poly(ethylene-*co*-butylene)-*b*-poly(ethylene oxide), known as KLE3729, to be a very efficient polymeric surfactant. In this study, a polymeric surfactant known commercially as Hypermer B246 with an HLB value of 6 was used to stabilize the inverse miniemulsion. This polymeric surfactant[13] is an ABA triblock copolymer of poly(hydroxystearicacid-*b*-ethylene glycol-*b*-hydroxystearic acid) and one of the polymeric surfactants that have been widely used in inverse emulsion systems[14-16], and recently, in inverse miniemulsions[4, 17].

In inverse miniemulsion also, the droplet size decreases with an increasing amount of surfactant. Accordingly, the surface coverage with surfactant will be higher as the particle size decreases. However, the incomplete coverage of the surface of the

droplets with the surfactant is still expected regardless of the increasing amount of surfactant, as this will result in a micelle-free miniemulsion, which is important so that the nucleation mechanism is restricted only to particle nucleation[5].

3.1.2 Encapsulation via inverse miniemulsion polymerization

The encapsulation of hydrophilic materials into polymer nanoparticles has been a field of interest for various applications. Due to its efficiency and simplicity, inverse miniemulsion polymerization has been shown to be a great tool to encapsulate any organic or inorganic hydrophilic materials (Figure 3.2). The capability of producing well defined nanocapsules with aqueous/polar-liquid core in an one-step process makes the inverse miniemulsion very advantageous over other techniques, especially, in the field of biomedical applications[18]. The formation of the polymeric shell can be performed by different polymerization processes such as radical polymerization/copolymerization[10, 12, 18-20] and interfacial polyaddition reactions[3, 21-23], or by polymer precipitation on preformed nanodroplets[24, 25].

Matyjaszewski *et al*.[9, 10, 12, 20] have reported the synthesis of a series of biodegradable nanogels via inverse miniemulsion polymerization for biomedical applications as drug carriers. Water-soluble materials such as Rhodamine dye, doxorubicin (an anticancer drug), bovine serum albumin and gold nanoparticles could be encapsulated within the nanogels and then released upon biodegradation. Landfester *et al*. have utilized the inverse miniemulsion for the encapsulation of various materials for use as biocarriers[22, 23], antiseptic nanocapsules [24, 25], contrast agents for medical imaging[3] and the synthesis of polyvinylpyrrolidone/silver

nanoparticles hybrid latex[26]. Under normal circumstances the encapsulated molecule can be utilized as the osmotic pressure agent. This is important and desirable as it can reduce the number of ingredients involved as well as lowering the amount of impurities in the end product, especially, if these materials are difficult to remove. Examples include, compounds such as Magnevist and Gadovist[3] and iron oxide (Fe_3O_4)[19, 27] were used as lipophobes in the encapsulation process via inverse miniemulsion.

In this study, an inverse miniemulsion polymerization process has been successfully utilized for the encapsulation of the hydrophilic fluorescent Rhodamine B dye for the purpose of making nanocolorants that can be potentially used in hot-melt ink applications. Rhodamine B dye was chosen because of its high hydrophilicity, high solubility in aqueous phase and large absorption coefficient in most of the polar solvents. This allowed the use of Rhodamine B furthermore as a lipophobe to prevent Ostwald ripening. A simple illustration of the process is shown in Scheme 3.1.

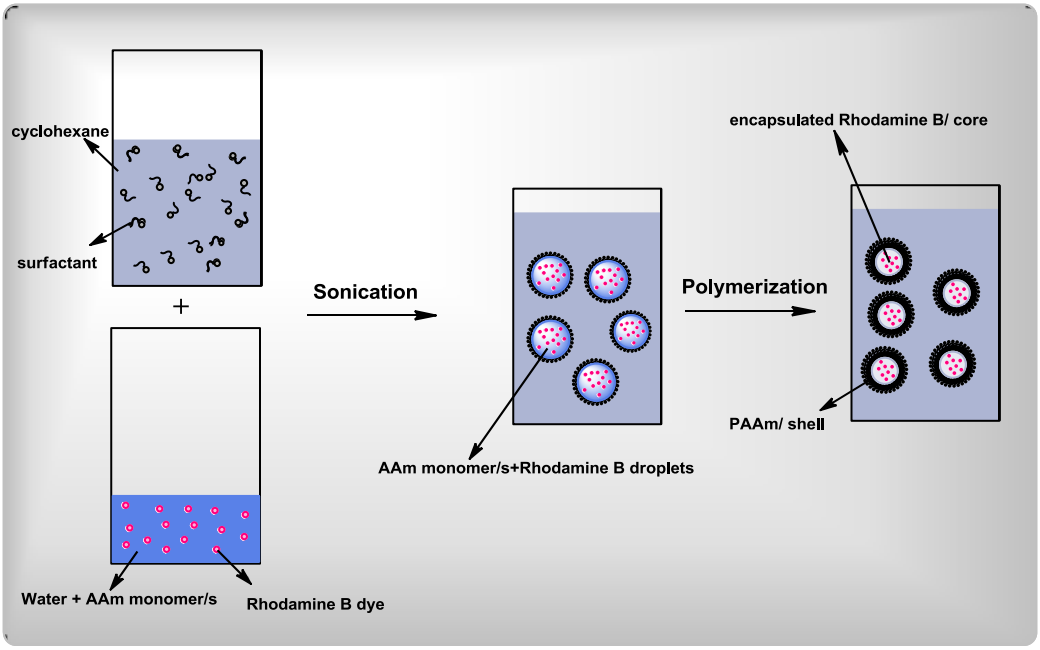

Scheme 3.1: : Encapsulation of Rhodamine B dye via an inverse miniemulsion process

The aqueous solution of the hydrophilic fluorescent dye Rhodamine B (RhB) and acrylamide (AAm) monomer is added to a surfactant/cyclohexane solution under stirring. Subsequently, the formed emulsion is treated by sonication to form the miniemulsion, and with the presence of an oil-soluble initiator the polymerization could be started. Depending on the type of monomer/s, the particle morphology and the location of the dye can be tuned. When only AAm monomer is used, solid particle nanocolorants consisting of PAAm with the dye homogeneously distributed within the polymeric texture are obtained. While core/shell type of particles are obtained when the polymerization occurs in the presence of the hydrophilic crosslinking monomer *N,N'*-methylene bis acrylamide (MBA) and/or styrene (Sty) monomer.

In this chapter, the synthesis and characterization of RhB based nanocolorants via inverse miniemulsion is discussed. The focus is on investigating the formation of a

stable inverse miniemulsion in terms of the type and amount of surfactant, the amount of dye, the type of monomer used, the formed particles morphology and the encapsulation efficiency.

3.2 Experimental

3.2.1 Materials

Acrylamide (AAm) (≥ 99%), *N,N'*-methylenebisacrylamide (MBA) (≥ 99.5%,) and Span 80 were all obtained from Fluka and used as received. Styrene (Sty) (99%, Aldrich) was purified by distillation at 40 °C under reduced pressure. The thermal initiator 2,2'-azo bis(isobutyronitrile) (AIBN) (98%, Aldrich) was recrystallized from methanol. Rhodamine B (RhB) (dye content ~95 %) was obtained from Sigma. The polymeric surfactant Hypermer B246 was a gift from Croda. Cumene hydroperoxide (CHP) (tech, 80%) and tetraethylenepentamine (TEPA) were obtained from Aldrich. Cyclohexane (CH) (tech) was obtained from Sigma-Aldrich and used as received.

3.2.2 Synthesis of PAAm/RhB and core-shell crosslinked-PAAm/RhB based nanocolorants in inverse miniemulsion polymerization

The nanocolorants were prepared with various formulations according to the following procedure. RhB fluorescent dye, AAm monomer and MBA crosslinker (when applicable) were dissolved in water and stirred until a homogenous aqueous solution is obtained. The aqueous solution then was added to the organic solution of cyclohexane containing a surfactant (Span80 or Hypermer B246) and AIBN initiator, and the mixture was stirred at room temperature for 30 minutes. The resultant pre-

emulsion was then emulsified by an ultrasonicator, Vibracell VCX 750, operated at 70% amplitude for 3 minutes under ice cooling to avoid polymerization due to heating. The resulting miniemulsion was then transferred to a three-neck 250 mL flask equipped with a nitrogen tube, a reflux condenser and magnetic stirrer. The system was purged with nitrogen while stirring for 30 minutes then heated to 65 °C under nitrogen flowing. Stirring at 300 rpm, the polymerization was carried out for 6 hours.

3.2.2 Preparation of poly(AAm-*co*-Sty)/RhB core-shell nanocolorants in inverse miniemulsion polymerization

An interfacial polymerization was carried out to prepare poly(AAm-*co*-Sty)/RhB nanocolorants. A similar procedure as above was followed except for the addition of Sty monomer to the organic phase prior to emulsification as well as the use of a redox initiating system. The initiator system in this case comprised of cumene hydroperoxides (CHP) as the hydrophobic oil-soluble part and Tetraethylenepentamine (TEPA) as the hydrophilic water-soluble part. TEPA was dissolved in water along with RhB and AAm monomer to form the aqueous solution prior to the emulsification process. After the emulsification process, CHP/cyclohexane was injected via a syringe (under nitrogen environment) to the reaction vessel to start the polymerization and the temperature was kept at 40 °C.

3.2.3 Characterization and analytical techniques

3.2.3.1 Dynamic light scattering (DLS)

DLS technique was used to investigate the particle size of the nanocolorants. A Zetasizer ZS 90 (Malvern Instruments, United Kingdom) instrument fitted with a 4 mW He-Ne laser, operating at a wavelength of 633.0 nm was used. The measurements are based on the detection of the scattered light from the particles at an angle of 90°. All the samples were diluted with cyclohexane prior to the analysis. The particle sized is presented as the Z-average particle size (Z-avg) and was calculated via a CONTIN analysis.

3.2.3.2 Transmission electron microscopy (TEM)

TEM analysis was used to visually inspect the size and the morphology of the nanocolorants particles at the nanometer level. High-resolution TEM images were taken using a LEO 912 Omega TEM instrument (Zeiss, Germany), at an accelerating voltage of 120 kV. Samples of the nanocolorants were prepared for TEM analysis by first dilution with cyclohexane, and then deposited on 300-mesh copper grids, which were then inserted in the TEM instrument and placed under the electron microscope. ImageJ (NIH, USA), computer software was used to analyse the TEM images and determine the average particle size.

3.2.3.3 Scanning electron microscope (SEM)

SEM was used to visualize the microstructure of dried nanocolorants samples. SEM images were taken by a field emission gun SEM instrument (FEI Nova NanoSEM),

equipped with an Oxford X-Max EDS detector (University of Cape Town). The nanocolorant samples were deposited on the top of the SEM stub and then left to dry. The next step was to make the sample surface electrically conducting, which was done by coating the samples with a thin layer of gold. Images with magnification ranging between 10,000× and 100,000× magnifications were recorded at 2-5 keV voltages, with a working distance of ~ 13 mm.

3.2.3.4 UV-vis spectroscopy

UV-vis absorption was used to evaluate the colour strength of the nanocolorants with respect to the UV-vis absorption spectra of RhB dye. Samples of both dried nanocolorants and RhB dye were prepared in water prior to analysis. In order to get homogeneous samples, all nanocolorant samples were first filtered through 450 nm PTFE filters to remove any dye molecule clusters or aggregates as well as any extremely nanocolorant's large particles. The nanocolorant samples were then dried and re-dispersed in deionized water (0.1 mg/mL). UV-vis absorption measurements were conducted using a UV-vis spectrometer (SPECORD 210 PLUS).

3.2.3.5 Thermogravimetric analysis (TGA)

TGA was carried out to study the thermal behaviour of the nanocolorants using a Q500 thermogravimetric analyzer (TA Instruments, USA). Samples of a size less than 15 mg were heated up under a nitrogen atmosphere (nitrogen flow was at a rate of 50 mL/min), at a heating rate of 20 °C/min, from room temperature to 600 °C. The results were analysed with TA Instruments Advantage Software (release 4.2.1).

3.3 Results and discussion

The syntheses of RhB-based nanocolorants were carried out successfully via an inverse miniemulsion polymerization process. Stable nanocolorants were prepared with different concentrations of RhB dye (5, 10, 15, 20 wt % relative to monomer) (Table. 3.1).

The RhB dye was completely soluble in the monomer aqueous phase and exhibited a very strong colour, ranging from pink to dark magenta, depending on the concentration of the dye (Figure 3.1). No aggregates or precipitates of RhB were observed during the polymerization, and the resulting latexes displayed a homogenous deep colour.

Table 3.1: Formulations used in the inverse miniemulsion polymerizations for the preparation of Rhd-B based nanocolorants

No	RhB (g)	AAm (g)	MBA (g)	Sty (g)	B246 (g)	Span80 (g)	AIBN (g)	CHP(g)/5g CH	TEPA (g)	H_2O (g)	CH (g)
AM-1	—	6.05	—	—	—	1.01	0.12	—	—	8.02	64.55
AM-2	—	6.07	—	—	1.08	—	0.098	—	—	8.02	64.62
FAM1	0.61	6.08	0.610	—	1.01	—	0.10	—	—	8.00	64.10
FAM2	0.60	6.02	0.630	—	—	1.05	0.11	—	—	8.01	64.50
FAM3	0.29	6.02	—	—	1.06	—	0.110	—	—	8.00	64.20
FAM4	0.60	6.00	—	—	1.03	—	0.101	—	—	8.00	64.40
FAM5	0.90	6.06	—	—	1.06	—	0.104	—	—	8.10	64.50
FAM6	1.20	6.03	—	—	1.02	—	0.101	—	—	8.2	64.03
FAM7	0.31	6.02	0.600	—	1.02	—	0.103	—	—	8.00	64.20
FAM8	0.61	6.03	0.605	—	1.01	—	0.100	—	—	8.00	64.00
FAM9	0.91	6.03	0.610	—	1.00	—	0.102	—	—	8.06	64.30
FAM10	1.23	6.02	0.680	—	1.07	—	0.105	—	—	8.05	64.00
FAM11	0.31	3.02	0.610	3.06	1.07	—	—	0.20	0.11	8.01	60.11
FAM12	0.60	3.00	0.600	3.00	1.03	—	—	0.21	0.10	8.00	60.00
FAM13	0.90	3.00	0.650	3.01	1.07	—	—	0.20	0.13	8.01	60.15
FAM14	1.20	3.00	0.600	3.04	1.08	—	—	0.22	0.12	8.03	60.05

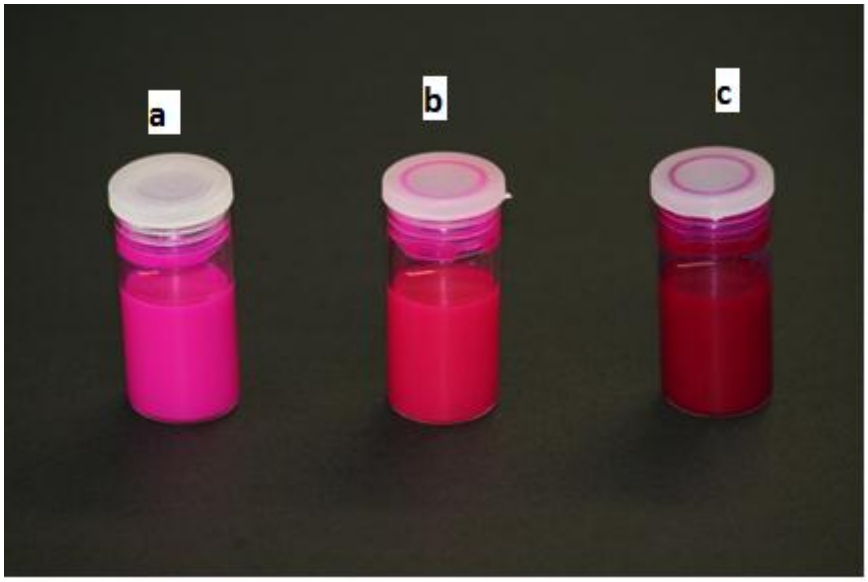

Figure 3.1: Nanocolorants loaded with 5% (a), 10% (b) and 20% (c) RhB, respectively.

3.3.1 Stability and choice of the surfactants

One of the requirements for the formation of an inverse miniemulsion is a surfactant with a low HLB value (lower than 7). Stabilized nanocolorants were successfully obtained with both Span80 (HLB = 3) and the triblock copolymer surfactant Hypermer B246 (HLB = 5-6). However, it was expected that Hypermer B246 would provide better stability due to its polymeric and steric nature[1, 4-6, 17]. As can be seen in Figure 3.2, when Span80 was used as a surfactant, the resulting miniemulsion was only stable for a few hours before settling took place, whereas in the case of Hypermer B246 it remanid stable for much longer (~ 6 months). However, to stabilize an inverse miniemulsion with Span 80, a much larger concentration of surfactant is needed in comparison to when a polymeric surfactant is used[1]. As the stability of the nanocolorants based on a small amount of surfactant is desirable, only Hypermer B246 surfactant was considered in this study.

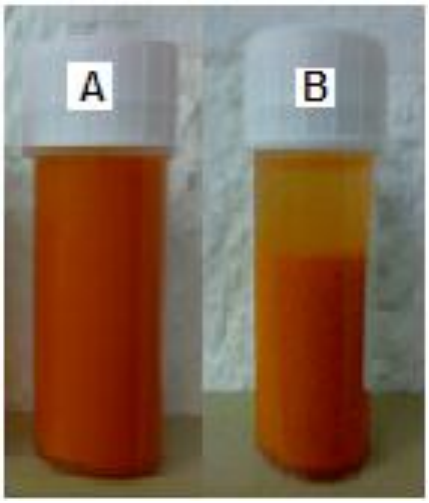

Figure 3.2: PAM/RhB nanocolorants stabilized with Hypermer B246 (A) and Span 80 (B).

3.3.2 Particle size and size distribution of nanocolorants

With the aid of DLS analysis, the particle size and size distribution of the nanocolorants could be measured. As shown in Table 3.2, the average particle size was in general around 200 nm, which is in the normal range for a miniemulsion system, with a monomodal size distribution and low polydispersity (≤ 0.1). Confirming reports in literature[6, 28], the particle size is dependent on variables such as the type of surfactant and the concentration of both lipophobe and surfactant. Therefore, it is expected, as it can be seen in Table 3.2, that increasing the amount of RhB dye, will increase the particle size of the nanocolorants. This also strongly suggests that RhB is completely encapsulated and located within the latexes particles.

Table 3.2: Average particle size of nanocolorants made with different RhB dye loadings.

nanocolorant	RhB loading	Z-avg (nm)	PDI
AM-2	0	184 ± 2	0.126
FAM-3	5	203 ± 2	0.108
FAM-4	10	229 ± 3	0.032
FAM-5	15	235 ± 3	0.063
FAM-6	20	240 ± 5	0.079
FAM-7	5	151 ± 2	0.148
FAM-8	10	175 ± 4	0.155
FAM-9	15	205 ± 3	0.138
FAM-10	20	212 ± 3	0.129
FAM-11	5	98.± 1	0.086
FAM-12	10	102 ± 3	0.092
FAM-13	15	139 ± 2	0.097

[a] Based on the monomer

3.3.3 Morphology of the nanocolorants

The architecture and morphology of the nanocolorants were investigated using SEM and TEM analyses. Two different types of particle morphologies were observed by TEM. PAAm/RhB based nanocolorants produced dark solid nanoparticles, whereas, both crosslinked-PAAm/RhB and poly(AAm-co-Sty)/RhB produced a core-shell type of nanoparticles.

- **SEM analysis of nanocolorants**

Typical SEM images of the PAAm/RhB, crosslinked-PAAm/RhB and poly(AAm-co-Sty)/RhB nanocolorants containing 10 wt % RhB (relative to monomer) are shown in Figure 3.3. The SEM images demonstrate that the nanocolorants are homogenous spherical particles.

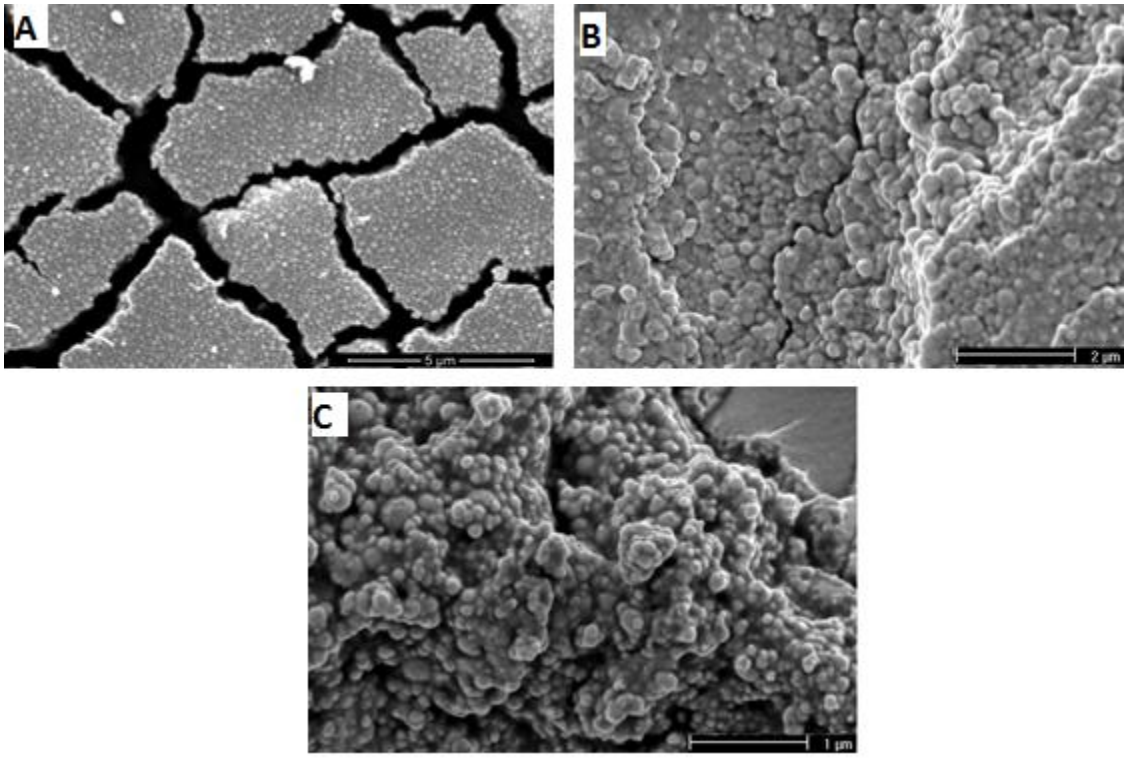

Figure 3.3: SEM images of (A) PAAm/RhB, (B) crosslinked-PAAm/RhB and (C) Poly(AAm-co-Sty)/RhB nanocolorants

- **TEM analysis of nanocolorants**

Figures 3.4, 3.5, and 3.6 represent TEM images of the PAAm/RhB, crosslinked-PAAm/RhB and poly(AAm-co-Sty/RhB nanocolorants respectively, all containing 10 wt% RhB. The images show that the average particle size is around 200 ± 50 nm, which is in the typical range of miniemulsion polymerization, and in a good

agreement with DLS results. A uniform particle size seems to indicate a narrow particle size distribution, and no RhB dye aggregates or clusters are observed. From the nanocolorants architecture, their uniform colour and the absence of dye aggregates/clusters we deduce that the RhB dye is completely incorporated into the polymeric matrix.

In Figure 3.4, TEM images of the PAAm/RhB nanocolorants are displayed. The images show uniform dark and solid PAAm particles, which suggests that the RhB dye is homogeneously distributed within the polymer matrix and that phase separation between RhB and PAAm did not take place during the course of polymerization.

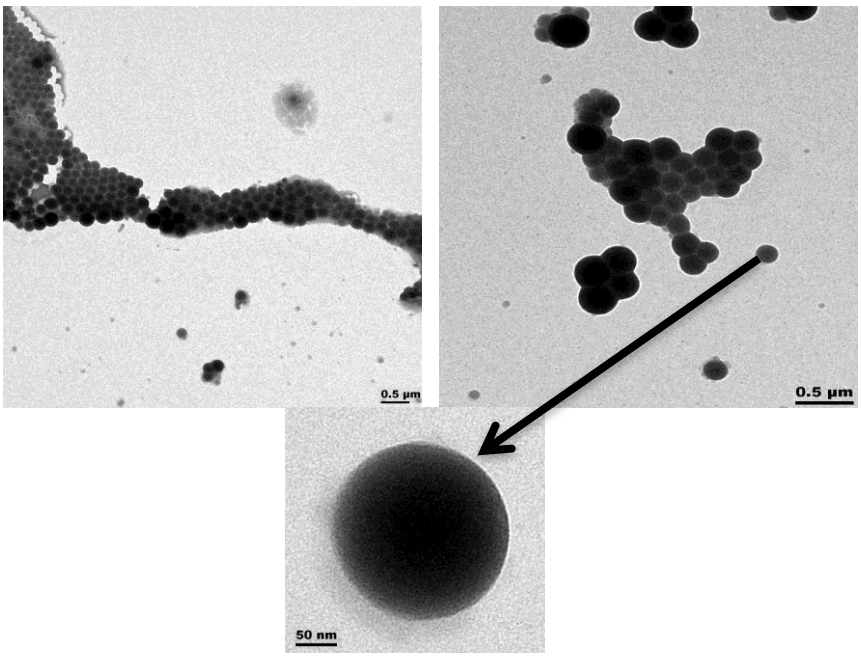

Figure 3.4: TEM images of PAAm/RhB nanocolorants with 10 wt% RhB.

According to some reports[29, 30], this morphology is expected when the polymer and the encapsulated material are fully miscible and soluble in the core liquid. Our

observation is in line with this, as RhB and PAAm are both hydrophilic and highly soluble in the aqueous core.

The morphologies of the crosslinked-PAAm/RhB and poly(AAm-*co*-Sty)/RhB nanocolorants as displayed by TEM images are shown in Figures 3.5 and 3.6. Contrary to the morphology observed for the PAAm/RhB nanocolorants, the crosslinked-PAAm/RhB and poly(AAm-co-Sty)/RhB nanocolorants revealed a core-shell type of morphology which is an indication that phase separation occurred during the polymerization. The presence of either the crosslinker MBA or the hydrophobic Sty monomer leads to the formation of a copolymer that is insoluble in the aqueous core, which in return results in a phase separation and formation of core-shell nanoparticles.

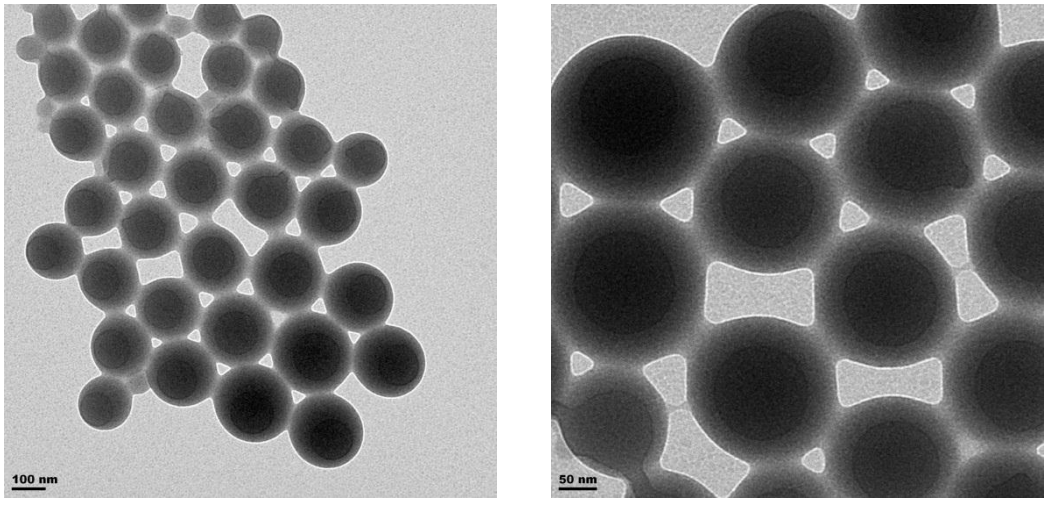

Figure 3.5: TEM images of crosslinked-PAAm/RhB nanocolorants with 10 wt % RhB.

The core-shell morphology shown in Figure 3.5 is the result of incorporating the crosslinker MBA in the formulation. The characteristic lighter outer shell

(representing the polymeric shell) and darker inner core (representing the embedded dye in the aqueous core) are clearly evident. As the polymerization proceeds, the cross-linked polymer becomes insoluble in the aqueous phase forming the polymeric shell (lighter ring), whereas the RhB dye stays soluble forming the core of the particle (darker domain).

Figure 3.6 shows nanocolorant particles of poly(AAm-*co*-Sty)/RhB, which also exhibit core-shell morphology. The phase separation occurred when interfacial polymerization proceeded to form a polymeric shell that is made of an amphiphilic copolymer of AAm and Sty. The darker domains represent the core of the particles comprising the RhB-containing aqueous phase.

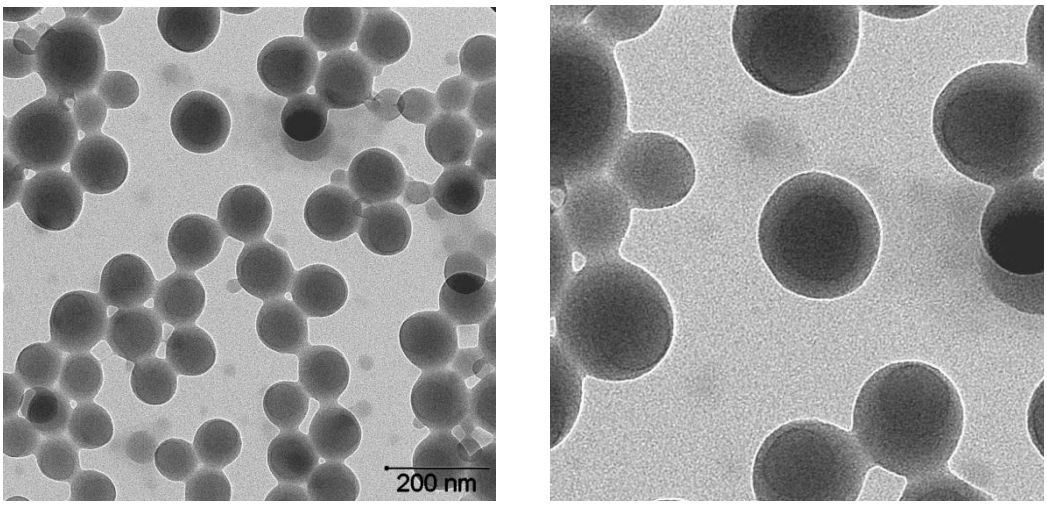

Figure 3.6: TEM images of poly(AAm-*co*-Sty)/RhB nanocolorants with 10 wt % RhB.

3.3.4 Colour and migration fastness of nanocolorants

UV-vis absorption was used to evaluate the colour strength of the nanocolorants as well as the migration fastness. RhB has a planar molecular structure and featured with main absorption peak appears at ~500-600 nm, which represents the transition moment of the main absorption band ($S_0 \rightarrow S_1$)[31, 32]. This absorption band is considered to be the maximum absorption wavelength (λ_{max}) of RhB dye and it was used as a reference band.

Figure 3.7 represents UV-vis absorption spectra of RhB dye, PAAm/RhB, crosslinked-PAAm/RhB and poly(AAm-*co*-Sty)/RhB nanocolorants (20 wt % RhB with respect to monomer).

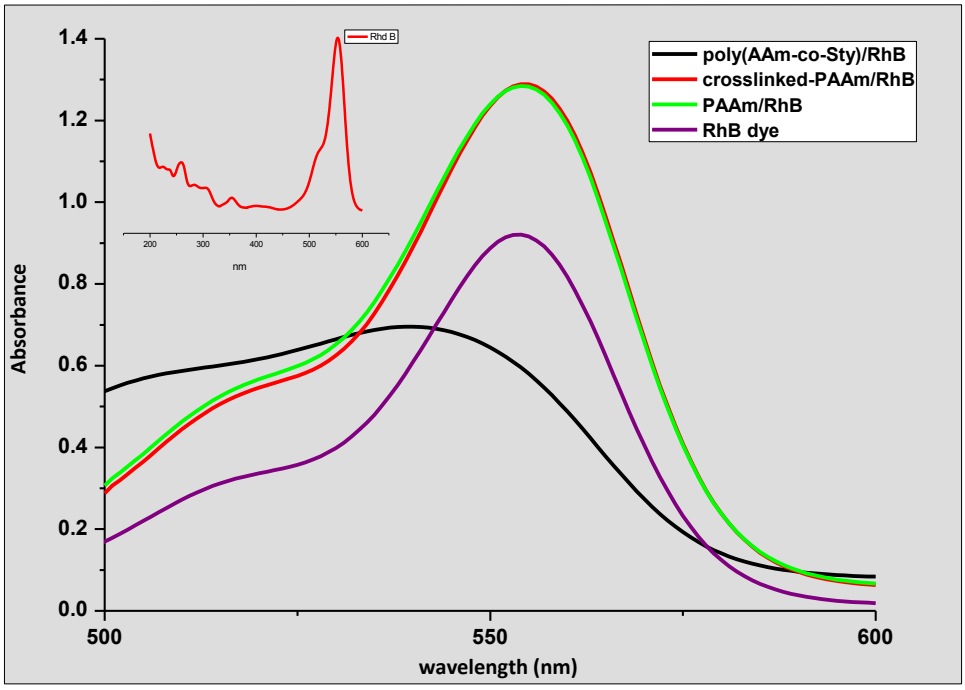

Figure 3.7: Absorption spectra of PAAm/RhB, crosslinked-PAAm/RhB and poly(AAm-co-Sty)/RhB nanocolorants loaded with 10 wt % RhB.

As can be seen in Figure 3.7, both PAAm/RhB and crosslinked-PAAm/RhB nanocolorants exhibit similar spectrum with λ_{max} appearing at 554 nm wavelength, which is identical to the RhB dye. Whereas, poly(AAm-co-Sty)/RhB nanocolorants showed a very broad absorption band with hypsochromic shift (λ_{max} is shifted towards shorter wavelength) at 540 nm. This suggests that, in the case of PAAm/RhB and crosslinked-PAAm/RhB, the encapsulation process had no effect on the dye chromophore and the nanocolorants retained the colour strength and properties of the RhB dye. On the other hand, the broad band and hypsochromic shift observed for poly(AAm-*co*-Sty)/RhB could be due to the interruption of the π-electron system of the dye chromophore by the redox initiation system. This assumption is based on the fact that the amino group substituents are part of the chromophore of RhB dye and the position of λ_{max} depends markedly on these substituents[31]. It was also observed that the colour of the miniemulsion faded a bit shortly after CHP was added to start the polymerization. This was an indication that RhB partially takes over the role of TEPA in the redox initiation with CHP to initiate the polymerization via its amino groups. Scheme 3.2 displays the chemical structure of RhB as well as the proposed mechanism of initiation by CHP/TEPA redox system.

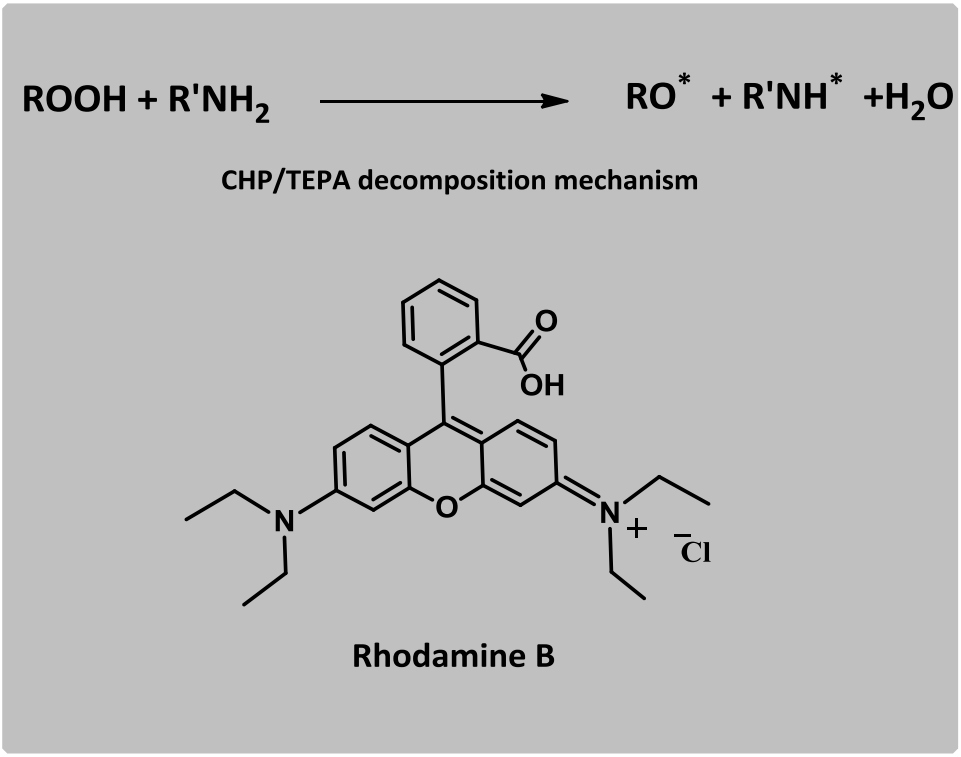

Scheme 3.2: The decomposition mechanism of CHP/TEPA and The chemical structure of Rhodamine B dye.

This speculation of the involvement of RhB dye in the initiation process can be explained by the decomposition mechanism of CHP/TEPA (Scheme 3.2)[33]. Thus, tertiary amino group of RhB can possibly compete with the amino group of TEPA in reacting with the hydroperoxy group of CHP. However, studies have shown that the mechanism displayed in Scheme 3.2 represents only a general formula of the actual mechanism steps. The reaction between amines and hydroperoxides can proceed in many different ways including the association via hydrogen bonding, formation of hydroxyl amines and nitroxide radicals[34-40]. Accordingly, RhB could possibly participate in the initiation process via the reaction of its amino groups with CHP. This assumption is supported by the observation of a coloured polymer precipitate during sample preparation for UV-vis analysis, suggesting that some of RhB was

chemically bonded to the polymer structure as a result of the initiation process. This becomes more evident when a comparison is made between the absorption spectra of poly(AAm-co-Sty)/RhB nanocolorants made with different dye concentrations. In Figure 3.8, the absorption spectra of poly(AAm-co-Sty)/RhB nanocolorants loaded with 10, 15 and 20 wt % (with regard to monomer) are displayed. The three absorption bands exhibit different λ_{max} values (λ_{max} 547 nm (20 wt %), λ_{max} 551 nm (15 wt %) and λ_{max} 540 nm (20 wt %)) absorbance values also decreased unexpectedly with increasing the concentration of the dye.

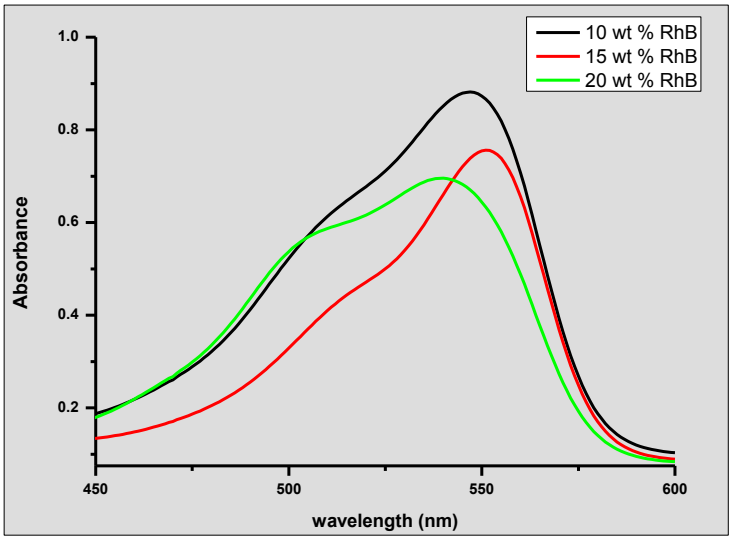

Figure 3.8: Absorption spectra of poly(AAm-co-Sty)/RhB nanocolorants loaded with 10, 15 and 20 wt % RhB.

We suspect that the decrease in absorption with increase in RhB concentration is related to the interaction between the amino groups of RhB and the hydroperoxy group of CHP, which becomes more frequent as the mount of RhB increases. According to some reports[40, 41], two types of complexes are formed as a result of the interaction between amines and hydroperoxides in solutions; 1) a hydrogen-bonded

complex (Scheme 3.3 A) and 2) a conjugated complex between the electrons at the nitrogen atom and the oxygen-oxygen bond of the hydroperoxy group (Scheme 3.3 B). When the concentration of the amine is high then complex B becomes the dominant complex formed. This could be the reason for increasing the interruption to the absorption of poly(AAm-co-Sty)/RhB nanocolorants as the amount of RhB dye increase.

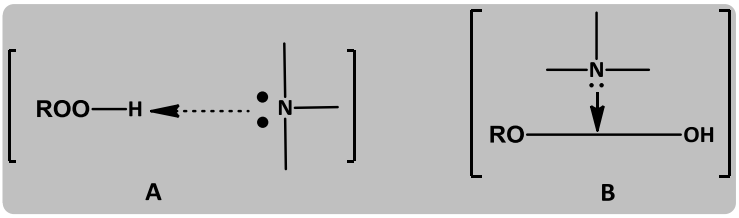

Scheme 3.3: Hydrogen-bonded and electron-conjugated complexes of amines and hydroperoxides.

It is a common issue that the encapsulated dye tends to migrate to the immiscible outside phase and precipitate as undesirable dyestuff aggregates[42-44]. Therefore, nanocolorants are required to have good dye preservation and prevent dye migration, especially, when a higher dye concentration and longer storage time are needed. In the current study, we attempted to improve the dye preservation by tuning the particle morphology. The dye migration was monitored over time using a UV-vis absorption method. However, based on the above discussion and conclusion regarding the influence of the initiation system on the absorption properties of poly(AAm-co-Sty)/RhdB nanocolorants, it is obvious that we cannot rely on the absorption measurements to evaluate dye migration in poly(AAm-co-Sty)/RhB nanocolorants. Therefore, only the migration properties of PAAm/RhB and crosslinked-PAAm/RhB nanocolorants will be discussed.

The evaluation of dye migration using UV-vis absorption measurements was carried out according to the following procedure[42, 43]. In order to obtain the real absorption value of dye content inside the nanocolorants particles at any storage time, all nanocolorants samples were filtered through 450 nm PTFE microfilters, immediately after the end of polymerization (storage time t=0 (t_0)) and at any given storage time (t). The filtration was necessary to exclude any dye clusters or aggregates might form during the polymerization (t_0), or with time due to dye migration (t), and also to insure that all samples are homogenous containing only the dye molecules entrapped inside the particles. The samples were then dried in a drying oven, dispersed in water and stirred over night until all the dye eluted in water (as PAAm is a water-soluble polymer, PAAm/RhB would dissolved completely). The concentration of nanocolorants samples was adjusted to 0.1 mg/mL to ensure that the dye concentration would be low enough to obey Beer's law. With this sample preparation one can measure the dye contents (wt %) inside the nanocolorants as a function of storage time. The relation between absorption at any given storage time (A_t) and residual dye content (dye %) can be expressed by the following equation[43] (Eq. 3.1).

$$Dye\ (\%) = (A_t/A_0)\ 100 \qquad (3.1)$$

Where A_0 is the absorbance at λ_{max} at storage time t=0 which was measured immediately after the polymerization stopped, and A_t is the absorbance at λ_{max} at storage time t.

Figure 3.9 shows the dye migration properties of PAAm/RhB and crosslinked-PAAm/RhB nanocolorants, both loaded with 5 and 15 % RhB.

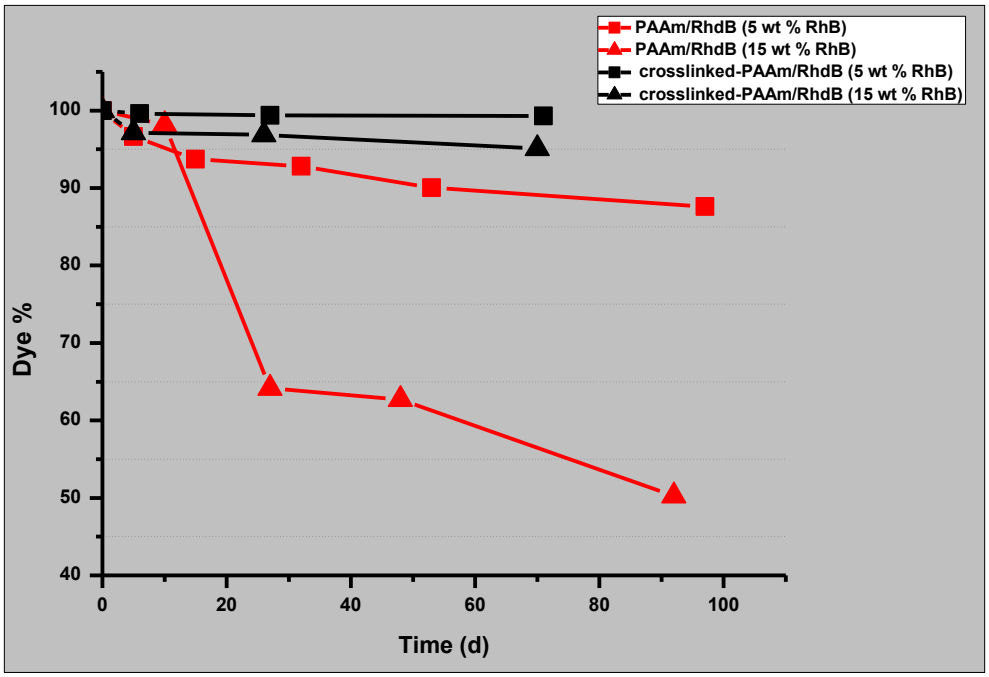

Figure 3.9: Dye migration properties of PAAm/RhB and crosslinked-PAAm/RhB nanocolorants loaded with 5 and 15 wt % RhB (with regard to monomer).

As it can be seen, the uncrosslinked PAAm/RhB nanocolorants show much higher rate of dye migration than the crosslinked-PAAm/RhB nanocolorant. Although all crosslinked-PAAm/RhB nanocolorants exhibited excellent dye retention over time, the dye migration rate in both cases increased with increasing the concentration of the dye. This can be strongly related to the morphology of the nanocolorants. The core-shell structure of the crosslinked-PAAm/RhB nanocolorants, as revealed by TEM images, plays a major role in restraining the dye migration. Besides the dye being confined to the interior of nanoparticles, the crosslinking of the polymeric outer shell reduces the free volume of the polymer and restricts the mobility of chains, which will prevent the dye molecules from passing through to the outside medium.

Whereas, in PAAm/RhB the RhB dye is homogenously distributed within the polymer matrix and can easily escape to the outside medium.

3.3.5 Thermal stability of nanocolorants

In order to use the nanocolorants in hot-melt ink applications, they are required to be thermally stable. TGA analysis was carried out to investigate the thermal behaviour and stability of the nanocolorants. The TGA thermograms of PAAm/RhB, crosslinked-PAAm/RhB and poly(AAm-co-Sty)/RhB nanocolorants prepared with 15 wt % RhB (relative to monomer) are shown in Figure 3.10. All the three thermograms show that the thermal stability of nanocolorants was improved, compared with neat PAAm as well as pure RhB. The onset temperature of degradation was shifted from about 300 °C and 350 °C for RhB and neat PAAm respectively, to 283, 287 and 308 °C for PAAm/RhB, crosslinked-PAAm/RhB and poly(AAm-co-Sty)/RhB, respectively. All three nanocolorants exhibit a degradation step at a lower temperature (100 °C), which could be attributed to the presence of water molecules. What can be also noted is the two-stage degradation process in the thermograms. The first stage, which is due to degradation of dye molecules, ranges from 260 to 400 °C. The second stage ranges roughly from 400 to 450 °C, which presents the degradation of the polymer. The increase in the degradation temperature could be due to a strong interaction between the embedded dye clusters and polymer chains at the interface. In this way the dye molecules cannot escape easily from the polymer interior and at the same time the polymer chains mobility become restricted and require more energy to degrade. Another reason that could explain the increased thermal stability of the nanocolorants is that the decomposition of the RhB dye before polymer

results in the formation of char on the surface of the polymer and, consequently, reduces the rate of decomposition[45, 46].

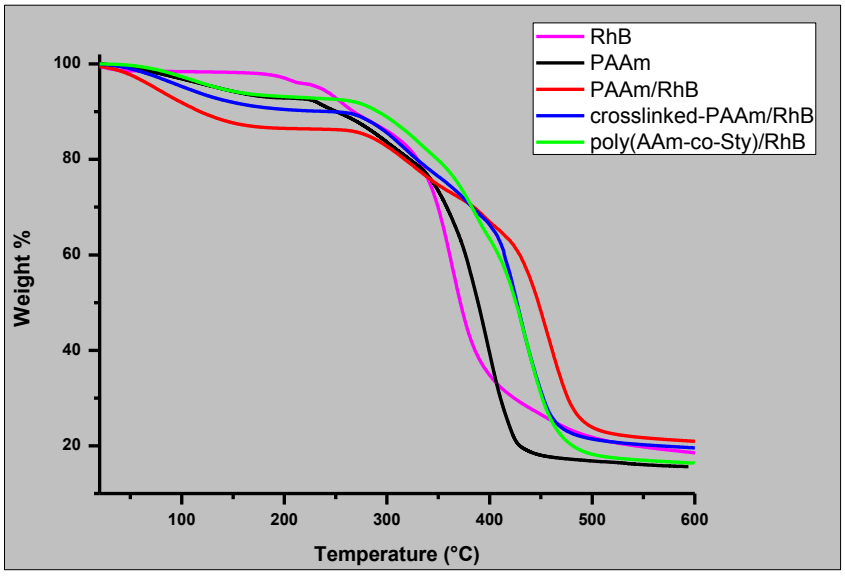

Figure 3.10: TGA thermograms of PAAm/RhB, crosslinked-PAAm/RhB and poly(AAm-co-Sty)/RhB nanocolorants prepared with 15 wt % RhB (relative to monomer).

Moreover, the increase in RhB content in the nanocolorants generally resulted in a slight increase in the thermal stability of the nanocolorants. For example, TGA thermograms in Figure 3.11 display the slight increase of thermal stability of the crosslinked-PAAm/RhB nanocolorants with increasing the dye content from 5 to 20 wt % (relative to monomer). It can be also noted in Figure 3.11 that the charred residue of the nanocolorants is increased significantly at increasing RhdB amount. This might contribute slightly towards the increase in thermal stability of the nanocolorants.

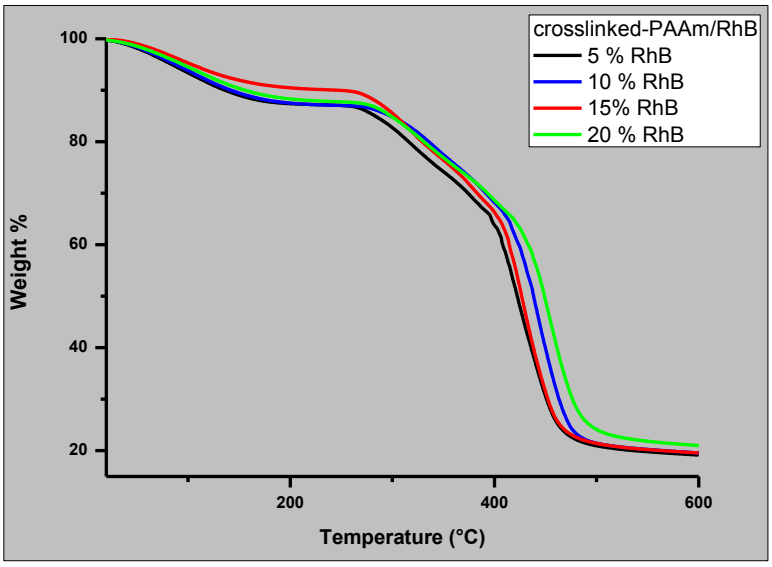

Figure 3.11: TGA thermograms of crosslinked-PAAm/RhB nanocolorants prepared with different amounts of RhB.

3.4 Conclusions

Three types of Rhodamine B-based nanocolorants, PAAm/RhB, crosslinked-PAAm/RhB and poly(AAm-co-Sty)/RhB, were successfully synthesized using a one-step encapsulation process via inverse miniemulsion polymerization. The obtained nanocolorants dispersions are highly stable (longer storage time) and possess excellent colouring properties. Stabilized nanocolorants were successfully obtained with both Span80 and the triblock copolymer surfactant Hypermer B246. However, Hypermer B246 provided excellent stability due to its polymeric and steric nature, therefore, it was chosen to use throughout the study. Based on the formulation of the inverse miniemulsion, three different types of nanocolorants were obtained. DLS results showed that the average particle size was in general around 200 nm, which is in the normal range for a miniemulsion system, with a monomodal size distribution and low polydispersity.

By varying the miniemulsion formulation, control over the nanocolorant morphology was achieved. SEM and TEM analyses confirmed the morphology and nanostructure of the nanocolorants as homogenous spherical nanoparticles with a uniform surface. Based on TEM analysis, the PAAm/RhB nanocolorants exhibited solid dark nanoparticles morphology, while crosslinked-PAAm/RhB and poly(AAm-co-Sty)/RhB showed a core-shell type of morphology. UV-vis absorption was used to evaluate the colour strength of the nanocolorants as well as the migration fastness. The nanocolorants showed improved dye migration properties, especially, nanocolorants with core-shell morphology. However, the colour and migration fastness of the Poly(AAm-co-Sty)/RhB could not be investigated as it seems that CHP/TEPA redox initiation system has an effect on the chromophore of the RhB dye. TGA analysis showed that the thermal stability of nanocolorants was improved compared with neat PAAm as well as pure RhB.

3.5 References

1. Landfester, K.; Willert, M.; Antonietti, M. *Macromolecules* **2000,** 33, 2370-2376.

2. Antonietti, M. B.-R., DE), Landfester, Katharina (Berlin, DE), Willert, Mirjam (Berlin, DE), Tiarks, Franca (Ludwigshafen, DE), Bechthold, Nina (Essen, DE), Polyreactions in non-aqueous miniemulsions. US 6,964,994 B1, 2005.

3. Jagielski, N.; Sharma, S.; Hombach, V.; Mailänder, V.; Rasche, V.; Landfester, K. *Macromol. Chem. Phys.* **2007,** 208, 2229-2241.

4. Qi, G.; Jones, C. W.; Schork, F. J. *Macromol. Rapid Commun.* **2007,** 28, 1010-1016.

5. Landfester, K.; Antonietti, M. *Top. Curr. Chem.* **2003,** 227, 75-123.

6. Antonietti, M.; Landfester, K. *Prog. Polym. Sci.* **2002,** 27, 689-757.

7. Anonymous, *The HLB System- A Time-Saving Guide to Emulsifier Selection*. ICI Americas Inc: Wilmington, Delaware 19897, USA, 1976; p 22.

8. Candau, F., Inverse Emulsion and Microemulsion Polymerization. In *Emulsion Polymerization and Emulsion Polymers*, Lovell, P.; El-Aasser, M., Eds. John Wiley & Sons Ltd: New York, 1997; pp 723-741.

9. Oh, J. K.; Bencherif, S. A.; Matyjaszewski, K. *Polymer* **2009,** 50, 4407-4423.

10. Siegwart, D. J.; Srinivasan, A.; Bencherif, S. A.; Karunanidhi, A.; Oh, J. K.; Vaidya, S.; Jin, R.; Hollinger, J. O.; Matyjaszewski, K. *Biomacromolecules* **2009,** 10, 2300-2309.

11. Oh, J. K.; Tang, C.; Gao, H.; Tsarevsky, N. V.; Matyjaszewski, K. *J. Am. Chem. Soc.* **2006,** 128, 5578-5584.

12. Oh, J. K.; Siegwart, D. J.; Matyjaszewski, K. *Biomacromolecules* **2007,** 8, 3326-3331.

13. Baker, A. S. EMULSIFYING AGENTS. 4509950, 1985.

14. Sudol, E.; El-Aasser, M., Miniemulsion Polymerization. In *Emulsion Polymerization and Emulsion Polymers*, Lovell, P.; El-Aasser, M., Eds. John Wiley & Sons Ltd: New York, 1997; pp 699-722.

15. Aston, M. S.; Herrington, T. M.; Tadros, T. F. *Colloids Surf.* **1989,** 40, 49-61.

16. Collins, I. R. Method For Inhibiting Hydrate Formation. US 7008466 B2, 2006.

17. Qi, G.; Eleazer, B.; Jones, C. W.; Schork, F. J. *Macromolecules* **2009,** 42, 3906-3916.

18. Wu, D.; Scott, C.; Ho, C.-C.; Co, C. C. *Macromolecules* **2006,** 39, 5848-5853.

19. Xu, Z. Z.; Wang, C. C.; Yang, W. L.; Deng, Y. H.; Fu, S. K. *J. Magn. Magn. Mater.* **2004,** 277, 136-143.

20. Oh, J. K.; Siegwart, D. J.; Lee, H.-i.; Sherwood, G.; Peteanu, L.; Hollinger, J. O.; Kataoka, K.; Matyjaszewski, K. *J. Am. Chem. Soc.* **2007,** 129, 5939-5945.

21. Crespy, D.; Stark, M.; Hoffmann-Richter, C.; Ziener, U.; Landfester, K. *Macromolecules* **2007,** 40, 3122-3135.

22. Paiphansiri, U.; Dausend, J.; Musyanovych, A.; Mailänder, V.; Landfester, K. *Macromol. Biosci.* **2009,** 9, 575-584.

23. Rosenbauer, E.-M.; Landfester, K.; Musyanovych, A. *Langmuir* **2009,** 25, 12084-12091.

24. Paiphansiri, U.; Tangboriboonrat, P.; Landfester, K. *Macromol. Symp.* **2007,** 251, 54-62.

25. Paiphansiri, U.; Tangboriboonrat, P.; Landfester, K. *Macromol. Biosci.* **2006,** 6, 33-40.

26. Crespy, D.; Landfester, K. *Polymer* **2009,** 50, 1616-1620.

27. Xu, Z. Z.; Wang, C.; Yang, W.; Fu, S. *J. Mater. Sci.* **2005,** 40, 4667-4669.

28. Landfester, K. *Annu. Rev. Mater. Res.* **2006,** 36, 231-279.

29. Torza, S.; Mason, S. G. *J. Colloid Interface Sci.* **1970,** 33, 67-83.

30. Weiss, C.; Landfester, K. *Adv Polym Sci* **2010,** 233, 185-236.

31. Drexhage, K., Structure and properties of laser dyes. In *Dye Lasers*, Schäfer, F., Ed. Springer Berlin Heidelberg: 1973; Vol. 1, pp 155-200.

32. Ishibashi, K.-i.; Sato, O.; Baba, R.; Tryk, D. A.; Hashimoto, K.; Fujishima, A. *J. Colloid Interface Sci.* **2001,** 233, 361-363.

33. Luo, Y.; Schork, F. J. *J. Polym. Sci., Part A: Polym. Chem.* **2001,** 39, 2696-2709.

34. Hoffmann, A. K.; Feldman, A. M.; Gelblum, E.; Hodgson, W. G. *J. Am. Chem. Soc.* **1964,** 86, 639-646.

35. Oswald, A. A.; Guertin, D. L. *J. Org. Chem.* **1963,** 28, 651-657.

36. Coppinger, G. M.; Swalen, J. D. *J. Am. Chem. Soc.* **1961,** 83, 4900-4902.

37. Mare, H. E. D. L.; Coppinger, G. M. *J. Org. Chem.* **1963,** 28, 1068-1070.

38. Yablonskii, O. P.; Belyaev, V. A.; Vinogradov, A. N. *Russ. Chem. Rev.* **1972,** 41, 565.

39. Harris, A.; Olcott, H. S. *J. Am. Oil Chem. Soc.* **1966,** 43, 11-14.

40. Grigoryan, S. K. *Russ. Chem. Rev.* **1983,** 52, 532.

41. Mare, H. E. D. L. *J. Org. Chem.* **1960,** 25, 2114-2126.

42. Takasu, M.; Kawaguchi, H. *Colloid. Polym. Sci.* **2005,** 283, 805-811.

43. Takasu, M.; Shiroya, T.; Takeshita, K.; Sakamoto, M.; Kawaguchi, H. *Colloid. Polym. Sci.* **2004,** 282, 740-746.

44. Liu, T.; Li, Z.; Wu, Q.; Ma, X. *Polym. Bull.* **2010,** 64, 511-521.

45. Ding, R.; Hu, Y.; Gui, Z.; Zong, R.; Chen, Z.; Fan, W. *Polym. Degrad. Stab.* **2003,** 81, 473-476.

46. Liu, T.; Li, Z.; Wu, Q.; Ma, X. *Polymer Bulletin* **2010,** 64, 511-521.

Chapter 4: Synthesis and characterization of modified acrylate-Rhodamine B-based nanocolorants.

Abstract

This chapter discusses the synthesis and characterization of a polymerizable Rhodamine B (RhB) dye as well as its use as a comonomer in inverse miniemulsion polymerization to prepare well-defined structured nanocolorants. RhB dye was first converted successfully to a polymerizable dye (RhB-acrylate) by introducing an acrylate group via esterification reaction using a DCC/DMAP coupling agents approach. NMR spectroscopy was used to confirm the chemical structure of the RhB-acrylate dye and UV-vis spectroscopy was used to investigate the colourfastness and properties of the dye. Highly stable nanocolorants of poly(PAAm-co-RhB) and crosslinked-poly(PAAm-co-RhB) with superior colour and migration fastness were synthesized successfully in a one-step inverse miniemulsion polymerization process. DLS, SEM and TEM analyses revealed that poly(PAAm-co-RhB) and crosslinked-poly(PAAm-co-RhB) nanocolorants have a homogenous and spherical structure with small particle size (below 200 nm) and uniform surface. TEM images showed that poly(PAAm-co-RhB) and crosslinked-poly(PAAm-co-RhB) nanocolorants have solid and core-shell morphology, respectively. A dialysis method was used to investigate the migration fastness of the nanocolorants and UV-vis to study the colour properties of the nanocolorants. The RhB-acrylate-based nanocolorants exhibited high T_g values and good thermal properties as well as high thermal stability as confirmed by DSC and TGA measurements.

4.1. Introduction

The coloured polymer latex industry has witnessed a rapid growth in the last few decades. Owing to their integrated properties of both dyes and pigments, *i.e*. excellent chromatic properties and good processibility of dyestuff and superior durability of organic pigments, coloured polymer latexes are seen as an excellent replacement for dyes and pigments, especially in applications such as inks[1-3], coating[4], and textile[5]. In medical and biomedical applications, coloured latexes are also more desirable than free dyes. They have been used as cell markers[6, 7], for enzyme immobilization[8], and as biochemical sensors[9, 10]. Their nanometre size provides easy access to the living cells, besides that the polymeric matrix protects the cellular environment from any dye toxicity or interference with bioprocesses.

However, dye migration and fading of colour are common problems associated with coloured latexes made of non-covalently bonded dyes to the polymer matrix. Although there has been some success in improving the light and migration fastness of the coloured latexes, *i.e*. by incorporating monomers of different polarities and crosslinkers, dye migration is still observed over longer period of time[11-14]. Reports have shown that the integration of dyes, covalently bonded to the polymer matrix can eliminate the dye migration out of the coloured particles[15]. Polymerizable dyes can be copolymerized with monomers to produce coloured latexes with superior light and migration fastness[16-18]. Polymerizable dyes based on 1,8-naphthalimide[17-20], benzothioxanthine[21-23], anthraquinone[16, 24] and xanthene[25-28] nucleus have been

copolymerized with various monomers to produce colored latexes for the use in various biomedical and polymer applications.

Rhodamine dyes are among the most known and extensively used dyes for making coloured particles. Owing to their high absorption coefficient, photostability, photophysical properties, and most importantly, the capability to preserve these properties upon functionalization, Rhodamine dyes have been widely used in applications that required covalent bonding of the dye with other molecules or surfaces[25, 29]. Rhodamine dyes have a general chemical structure shown in Figure 4.1 (A)[25]. As can be seen in Figure 4.1, there are three different sites of interest where modifications can take place, *i.e.* the amino groups at positions 3 and 6, the carboxyphenyl ring at positions 4' and 5' or the carboxylic acid group at position 2'. Modifications of the amino groups usually result in a complete change of photophysical properties, or even complete loss of fluorescence.

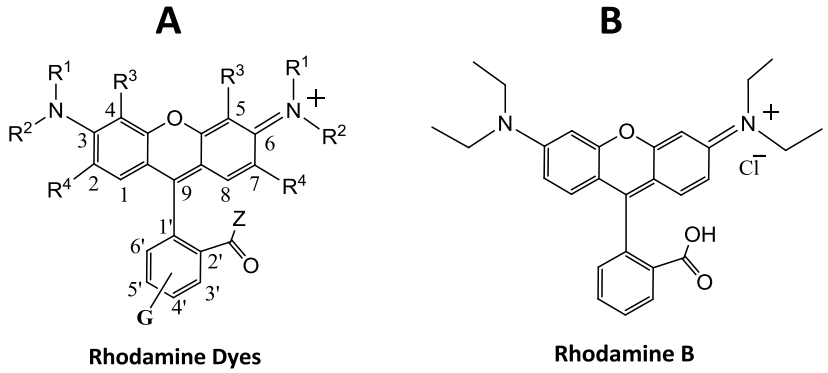

Figure 4.1: Molecular structures of Rhodamine dyes (A) and Rhodamine B dye (B)[25].

The modification of the carboxylic group at position 2' is considered to be the easiest, and more importantly does not affect the overall fluorescence properties of the dye[25]. In the current study, the functionalization of Rhodamine B dye (Figure 4.1

B) was carried out on the carboxylic group to introduce a polymerizable acrylate group. According to many reports the esterification of the carboxylic group at position 2' could be a strategic way for the introduction of an active functionality to Rhodamine dyes[30-32]. In one of the early studies on the functionalization of Rhodamine dyes, Grechishnikova *et al*.[33] reported the conjugation of bisteroid diol derivatives with Rhodamine 101 dye via an esterification reaction in the presence of DCC coupling agent. Ward and his colleagues[34] modified the Rhodamine B dye to include a polymerizable acrylate group and then copolymerized it with an acrylate monomer to produce a coloured hydrophilic copolymer. The polymerizable Rhodamine B acrylate is the ester of the Rhodamine B and 4-hydroxy butyl acrylate (HBA). The esterification reaction was carried out in the presence of DCC/DMAP coupling agents (Scheme 4.1).

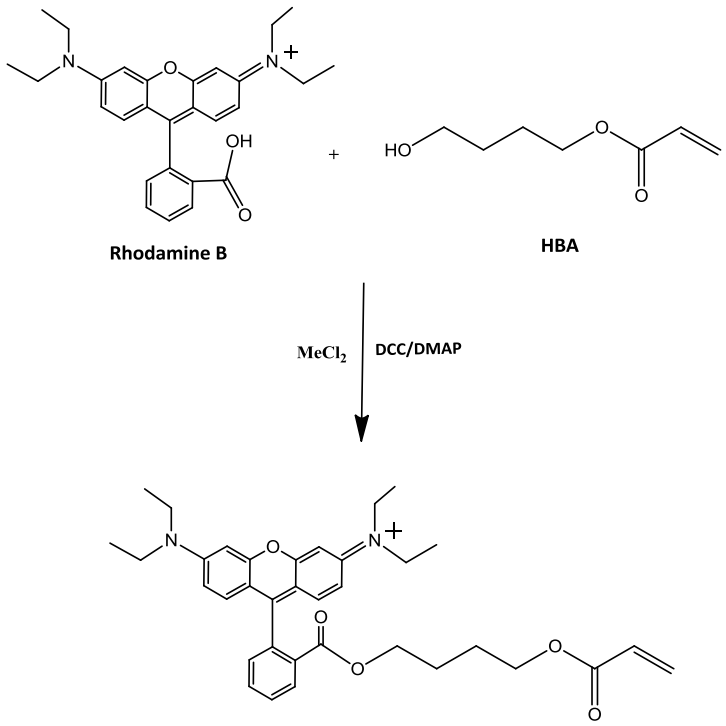

Scheme 4.1: Synthesis of a Rhodamine B acrylate derivative[34].

To the best of our knowledge, nanocolorants based on a polymerizable Rhodamine B derivative have never been reported before. Therefore, this approach was adopted in this study in order to obtain a polymerizable Rhodamine B that was implemented later in inverse miniemulsion polymerization to prepare nanocolorants. It is expected that by implementation of the Rhodamine B dye as a comonomer, the migration fastness of the nanocolorants would improve significantly, to a degree that no dye migration would be observed if complete conversion could be achieved.

4.2. Experimental

4.2.1 Materials

Acrylamide (AAm) (≥99%) and *N,N'*-methylenebisacrylamide (MBA) (≥99.5%,) were obtained from Fluka and used as received. The thermal initiator 2,2'-azo-bis(isobutyronitrile) (AIBN) (98%, Aldrich) was recrystallized from methanol. Rhodamine B (RhB) (dye content ~95 %) was obtained from Sigma. The polymeric surfactant Hypermer B246 was a gift from Croda. Cyclohexane (CH) (tech) was obtained from Sigma-Aldrich and used as received. 4-Hydroxybutyl acrylate (HBA) (90%, tech) was purchased from Sigma-Aldrich. Dichloromethane (99.8%) was obtained from LabChem. 1,3-dicyclohexyl carbodiimide (DCC) (99%, Aldrich) and 4-dimethylamino pyridine (DMAP) (98%, Aldrich) were all used as received.

4.2.2 Synthesis of Rhodamine B acrylate derivative.

The polymerizable Rhodamine B acrylate (RhB-acrylate) was synthesized according to a procedure described by Ward *et al*.[34], illustrated in Scheme 4.1. The obtained dark purple solid product (92% pure) was sticky, highly soluble in water and featured a potent staining colour.

4.2.2 Synthesis of poly(PAAm-*co*-RhB) and crosslinked-poly(PAAm-*co*-RhB) nanocolorants in inverse miniemulsion polymerization

The nanocolorants were prepared according to the following procedure. RhB-acrylate, AAm monomer and MBA crosslinker (where applicable) were dissolved in water and stirred until a homogenous aqueous solution was obtained. The aqueous solution then was added to the organic solution of cyclohexane containing Hypermer B246 surfactant and AIBN initiator, and the mixture was stirred at room temperature for 30 minutes. The resulting pre-emulsion was then emulsified by an ultrasonicator, Vibracell VCX 750, operated at 70% amplitude for 3 minutes under ice cooling to avoid polymerization due to heating. The resulting miniemulsion was then transferred to a three-neck 250 mL flask equipped with a nitrogen tube, a reflux condenser and magnetic stirrer. The system was purged with nitrogen while stirring for 30 minutes, then heated to 65 °C under nitrogen flow. Under stirring at 300 rpm, the polymerization was carried out for 6 hours.

4.2.3 Characterization and analytical techniques

The chemical structure of RhB-acrylate was confirmed by nuclear magnetic resonance (NMR) spectroscopy. For NMR analysis, the RhB-acrylate sample was dissolved in deuterated acetone $(CD_3)_2CO$ and ^1H NMR spectroscopy was performed at 20 °C using a Varian VXR-Unity 300 MHz instrument. The characterization of poly(PAAm-*co*-RhB) and crosslinked-poly(PAAm-*co*-RhB) nanocolorants was carried out the same way using the same instruments as described in Chapter 3. DLS, SEM and TEM techniques ware used to investigate the particle size and size distribution, nanostructure and morphology of the nanocolorants. The colour properties of both RhB-acrylate and its nanocolorants were also investigated using UV-vis spectrometry. The thermal stability and thermal properties were evaluated using TGA and Dynamic scanning calorimetry (DSC), respectively. DSC measurements were carried out using a TA Instruments Q100 system calibrated with indium metal. Samples were subjected to heating and cooling rates of 10 °C/min under a nitrogen atmosphere and the glass transition temperature (T_g) was determined from the second heating cycle.

4.3. Results and discussion

4.3.1 Characterization of RhB-acrylate

The transformation of the RhB dye to a polymerizable dye was done successfully by incorporation of a polymerizable acrylate group. A typical ^1H NMR spectrum shown in Figure 4.2 confirms the chemical structure of RhB-acrylate. All peaks are assigned

based on the expected structure. The small insert in Figure 4.2 demonstrates the characteristic peaks of the methylene groups (a and d) adjacent to the ester groups. The signals at 7 – 8.5 ppm are assigned to the aromatic protons. The peaks marked with asterisks are attributed to $(CD_3)_2CO$.

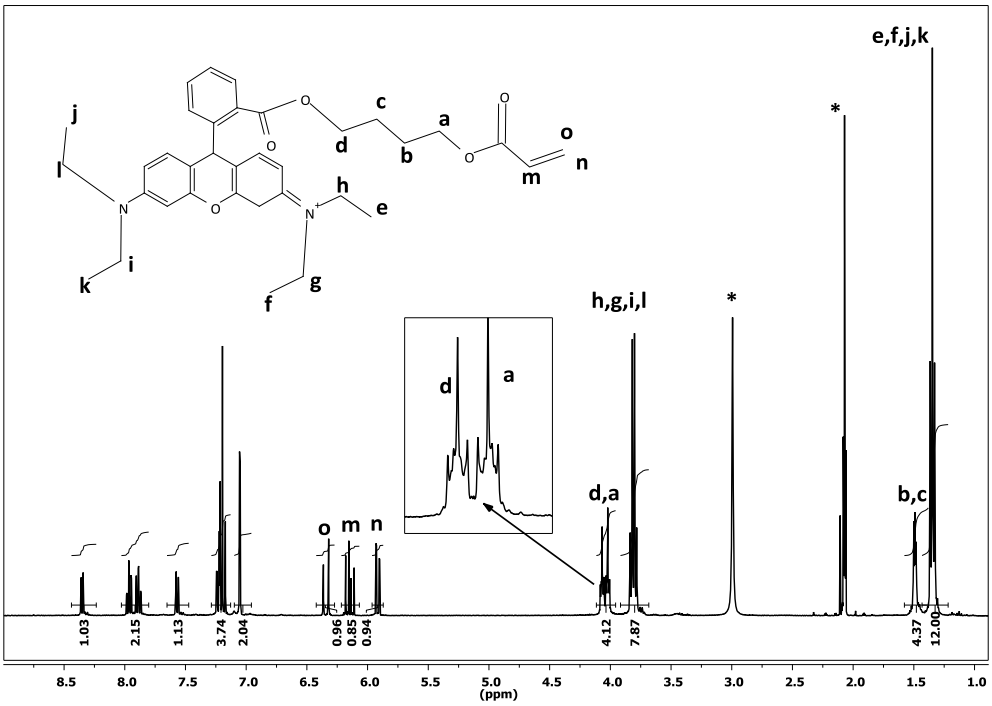

Figure 4.2: ^{1}H NMR spectrum of RhB-acrylate in $(CD_3)_2CO$.

The UV-vis absorption measurements of the RhB-acrylate dye have shown that the modified dye has a similar absorption spectrum as unmodified RhB, with the characteristic absorption peak appearing at 500-600 nm. However, a slight shift in λ_{max} is observed for the RhB-acrylate dye to λ_{max} at 560 nm. The comparison between RhB and RhB-acrylate dyes that is shown in Figure 4.3 suggests that the modification process had no effect on the dye chromophore, and the new polymerizable RhB-acrylate dye has reserved the colour strength and properties of RhB dye.

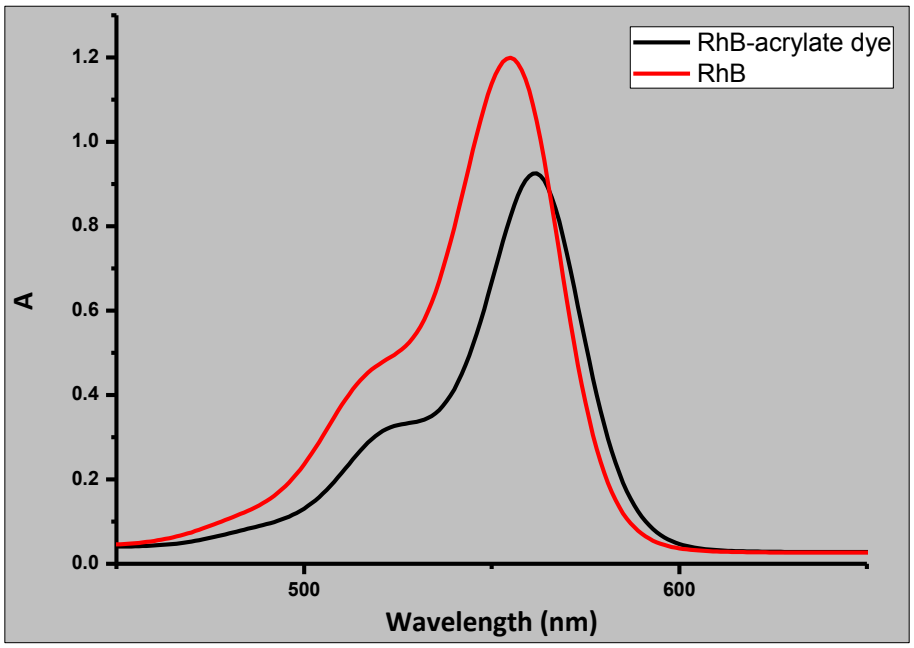

Figure 4.3: UV-vis absorption spectra of RhB and RhB-acrylate.

4.3.2 Characterization of poly(PAAm-*co*-RhB) and crosslinked-poly(PAAm-*co*-RhB) nanocolorants

The syntheses of RhB-acrylate-based nanocolorants were carried out successfully via an inverse miniemulsion polymerization process. The inverse miniemulsion formulations are presented in Table 4.1. The RhB-acrylate dye was completely soluble in the aqueous monomer phase and exhibited a very strong dark purple colour. The miniemulsion was very stable with no aggregates or precipitates observed during the polymerization, and the resulting latexes displayed a homogenous deep colour and were stable for more than six months.

Table 4.1: Formulations used in the inverse miniemulsion polymerizations for the preparation of poly(PAAm-*co*-RhB) and crosslinked-poly(PAAm-*co*-RhB) nanocolorants.

Nanocolorant	RhB-acrylate (g)	AAm (g)	MBA (g)	B246 (g)	AIBN (g)	H_2O (g)	CH (g)
poly(PAAm-*co*-RhB)	0.60	6.00	-	1.06	0.11	8.30	64.00
crosslinked-poly(PAAm-*co*-RhB)	1.00	5.08	0.62	1.04	0.10	9.00	64.03

4.3.2.1 Size distribution and morphology of the nanocolorants

DLS, SEM and TEM analyses were carried out to further evaluate the properties of the RhB-acrylate nanocolorants in terms of particle size, particle size distribution and morphology. As shown in Table 4.2, the average particle size of poly(PAAm-*co*-RhB) and crosslinked-poly(PAAm-*co*-RhB) as measured by DLS is in the normal range for a miniemulsion system, with a monomodal size distribution and low polydispersity (< 0.1).

Table 4.2: Average particle size of poly(PAAm-*co*-RhB) and crosslinked-poly(PAAm-*co*-RhB) nanocolorants.

Nanocolorant	Z-aveg (nm)	PDI
poly(PAAm-*co*-RhB)	160 ± 2	0.05
crosslinked-poly(PAAm-*co*-RhB)	181 ± 3	0.07

Typical SEM images of the poly(PAAm-*co*-RhB) and crosslinked-poly(PAAm-*co*-RhB) nanocolorants are shown in Figure 4.4. The SEM images demonstrate that the nanocolorants are spherical and have uniform surface.

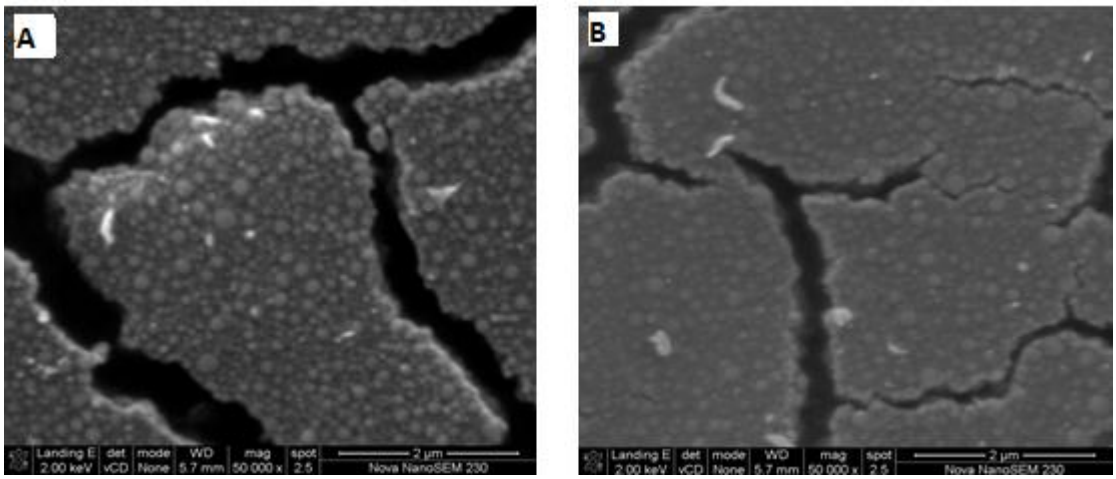

Figure 4.4: SEM images of (A) poly(PAAm-*co*-RhB) and (B) crosslinked-poly(PAAm-*co*-RhB) nanocolorants

Figures 4.5 and 4.6 represent TEM images of the poly(PAAm-*co*-RhB) and crosslinked-poly(PAAm-*co*-RhB) nanocolorants, respectively. The TEM images demonstrate that the morphologies of both poly(PAAm-*co*-RhB) and crosslinked-poly(PAAm-*co*-RhB) nanocolorants are characterized as homogeneous and spherical

nanoparticles. However, in Figure 4.5, particle deformation is observed for poly(PAAm-*co*-RhB) and it seems that it is due to film formation, which most probably occurred during sample preparation. There is also a strong possibility that this particle deformation is the result of melting of the polymer latex caused by the high energy electron beam of TEM[35, 36]. The nanoparticles of poly(PAAm-*co*-RhB) shown in Figure 4.5 appear as dark and solid particles, which suggest that there was no phase separation during the polymerization and the RhB-acrylate monomer completely copolymerized with AAm.

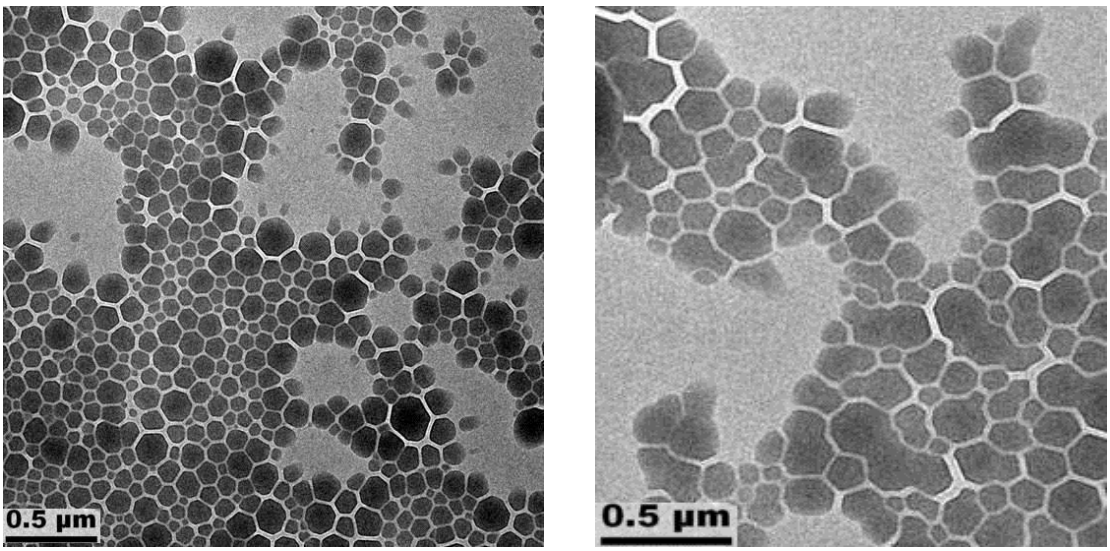

Figure 4.5: TEM images of poly(PAAm-*co*-RhB) nanocolorants

Contrary to that, the crosslinked-poly(PAAm-*co*-RhB) nanocolorants exhibited a core/shell morphology, which is an indication for phase separation that occurred during the copolymerization process. The presence of MBA crosslinker leads to the formation of a copolymer that is insoluble in the aqueous core, which in return results in phase separation and formation of core-shell nanoparticles.

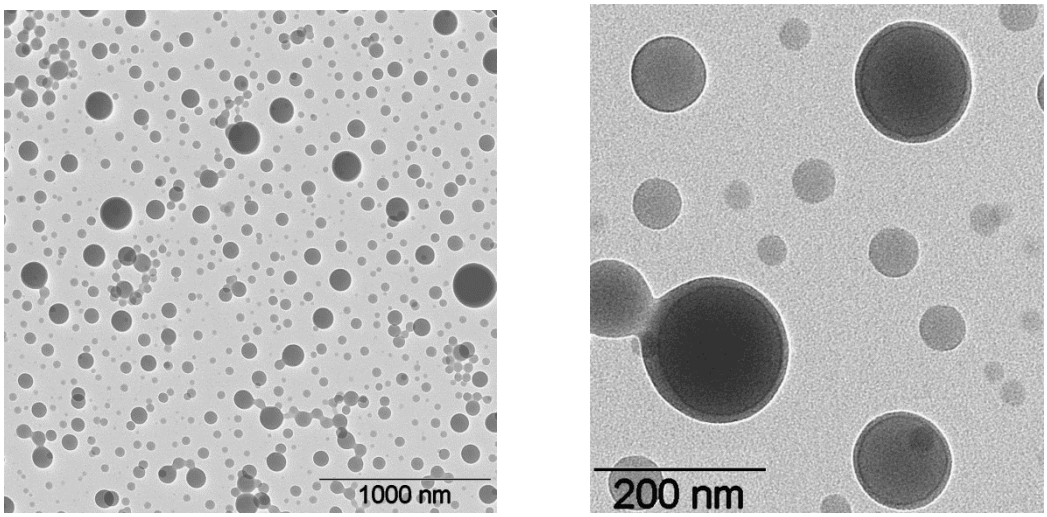

Figure 4.6: TEM images of crosslinked-poly(PAAm-*co*-RhB) nanocolorants.

4.3.2.2 Colour and migration fastness of the nanocolorants

UV-vis spectrometry was used to evaluate the colour strength of the nanocolorants with respect to the absorption of RhB-acrylate dye. Figure 4.7 represents a comparison between the UV-vis spectra of RhB-acrylate dye and both nanocolorants poly(PAAm-*co*-RhB) and crosslinked-poly(PAAm-*co*-RhB).

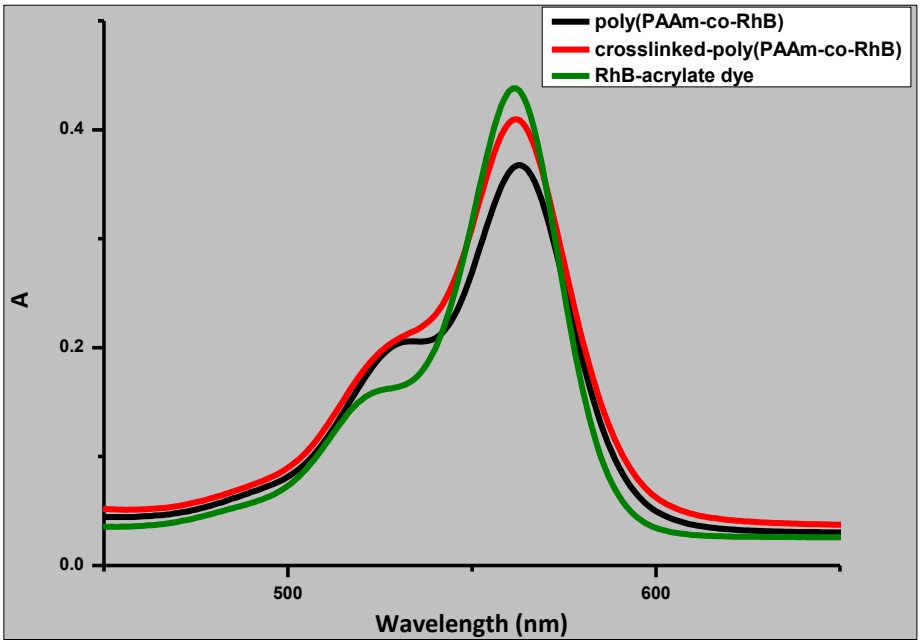

Figure 4.7: UV-vis absorption spectra of RhB-acrylate, poly(PAAm-*co*-RhB) and crosslinked-poly(PAAm-*co*-RhB).

As can be seen in Figure 4.7, both poly(PAAm-*co*-RhB) and crosslinked-poly(PAAm-*co*-RhB) nanocolorants exhibit similar spectra with λ_{max} appearing at 560 nm wavelength, which is identical to the RhB-acrylate dye. This suggests that the copolymerization process had no effect on the dye chromophore and that the nanocolorants retained the colour strength and properties of the RhB-acrylate dye.

In order to investigate the migration fastness of the nanocolorants, a dialysis method was implemented to monitor the diffusion of the dye. Dialysis is normally used for removing low molecular weight impurities by diffusion into an appropriate solvent through a dialysis membrane of a specific molecular weight cut-off (MWCO). The nanocolorants were placed in a 3500 MWCO dialysis membrane and dialyzed with D.I. water for two weeks. It is expected that poly(PAAm-*co*-RhB) nanocolorants would have a superior migration fastness because the RhB-acrylate dye, as a

comonomer, will be integrated into the polymer matrix, and therefore, no dye migration or leaching should be observed. Figure 4.8 displays a digital photograph of the dialysis experiment.

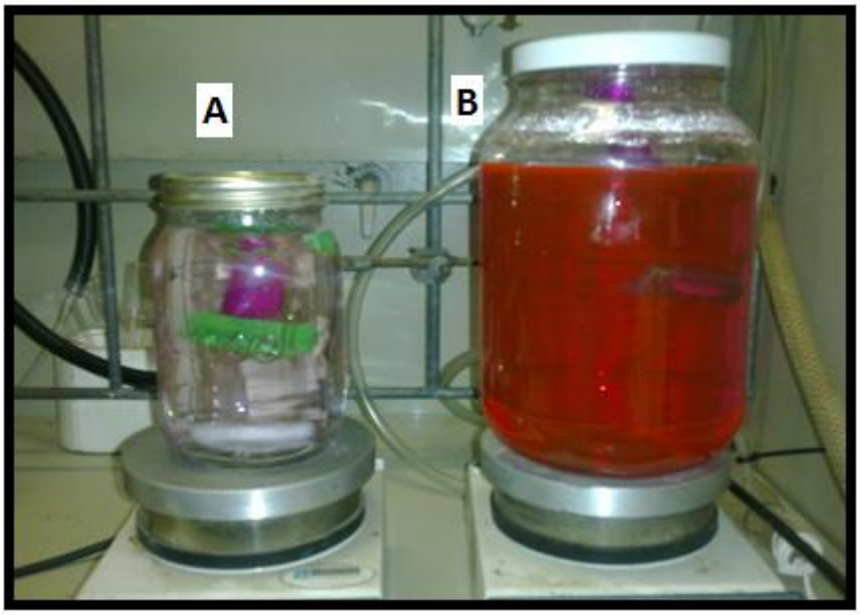

Figure 4.8: Dialysis of (A) poly(PAAm-*co*-RhB) nanocolorants and (B) PAAm/RhB nanocolorants.

The photograph in Figure 4.8 shows a comparison between two sets of dialysis experiments, (A) represents the dialysis process for poly(PAAm-*co*-RhB) nanocolorants and (B) the dialysis process for PAAm/RhB nanocolorants. It can be seen clearly that after two weeks, no colour change is observed for sample A, which is an indication that there were no dye molecules passing through the membrane. Nevertheless, sample B showed a high concentration of the RhB dye in the outside media. These observations prove that the integration of dyes covalently into the polymer matrix can eliminate dye migration out of the coloured particles. Indeed, the polymerizable dyes can be copolymerized with monomers to produce coloured latexes with superior light and migration fastness.

4.3.2.3 Thermal properties and stability of Poly(AAm-*co*-RhB) nanocolorants

4.3.2.3.1 Thermal properties and glass transition temperature of poly(AAm-*co*-RhB) nanocolorants as determined by DSC

The DSC second heating curves of poly(AAm-*co*-RhB) and crosslinked-poly(AAm-*co*-RhB) nanocolorants, PRhB, PAAm and the surfactant Hypermer B246 are shown in Figure 4.9. Only one single T_g is observed for both nanocolorants, which corresponds to the T_g of the PAAm made without RhB-acrylate monomer. This suggests that no homopolymerization occurred and all AAm and RhB-acrylate monomers are incorporated in the copolymer. The two melting peaks appear at -15 °C and 30 °C are ascribed to the melting peaks of the polymeric surfactant Hypermer B246. The T_g of the nanocolorants as well as the corresponding reference experiments are summarized in Table 4.3.

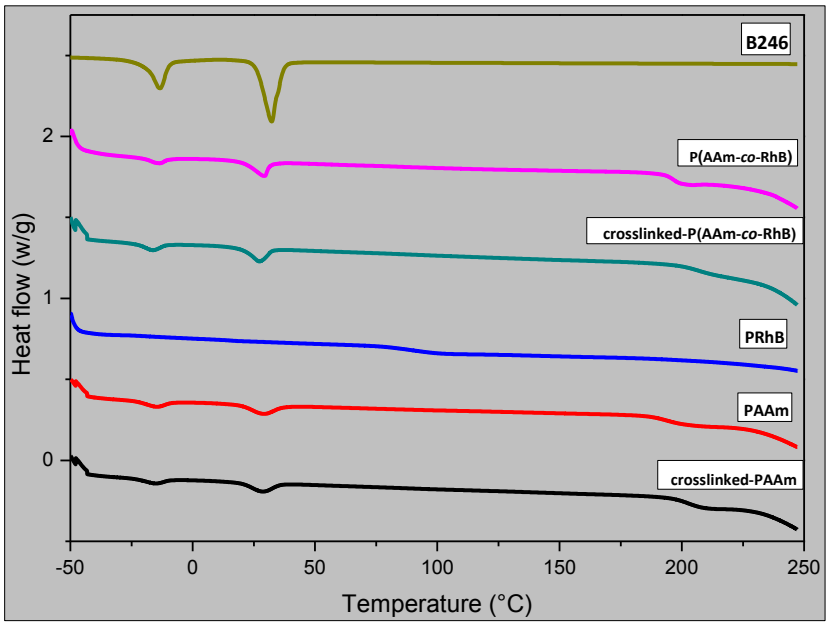

Figure 4.9: DSC thermograms of poly(AAm-*co*-RhB) and crosslinked-poly(AAm-*co*-RhB) nanocolorants and their corresponding reference experiments.

As can be seen in Table 4.3, the T_g value for crosslinked-PAAm is slightly higher than PAAm (about 10 °C), which is due to the crosslinking. Although, PRhB has a relatively low T_g at 88 °C, the incorporation of the polymeric RhB-acrylate dye had no significant effect on the T_g of neither poly(AAm-*co*-RhB) nor crosslinked-poly(AAm-*co*-RhB). This could be attributed to the polymeric RhB-acrylate being homogenously incorporated into the copolymer chains.

Table 4.3: T_g of poly(AAm-*co*-RhB) and crosslinked-poly(AAm-*co*-RhB) nanocolorants and their corresponding reference experiments.

Nanocolorant	T_g (°C)
Hypermer B246	-
PRhB	88.0
PAAm	194.0
Crosslinked-PAAm	203.0
Poly(AAm-*co*-RhB)	196.0
Crosslinked-Poly(AAm-*co*-RhB)	206.0

4.3.2.3.2 Thermal stability of RhB-acrylate and poly(AAm-*co*-RhB) nanocolorants as determined by TGA

Figure 4.10 displays the TGA weight loss curves of RhB and RhB-acrylate dyes. Although both dyes exhibit similar three stages degradation profiles, RhB-acrylate dye shows less thermal stability with regard to weight loss. In the first stage, which represents the dehydration of the dye, up to 200 °C RhB shows only 3% weight loss

while RhB-acrylate gives 33% weight loss. In the second stage between 200 °C and 400 °C, which is attributed to the degradation of the organic structure of the dye, RhB gives 62% weight loss while it is 44% for RhB-acrylate. In the third stage of degradation between 400 and 600 °C, which represents the degradation of oxygen-containing groups and other functional groups, RhB exhibits 14% weight loss while RhB-acrylate shows 15%. The overall weight loss for RhB and RhB-acrylate is found to be 79% and 92%, respectively. These results suggest that RhB-acrylate has less thermal stability than the parent RhB dye.

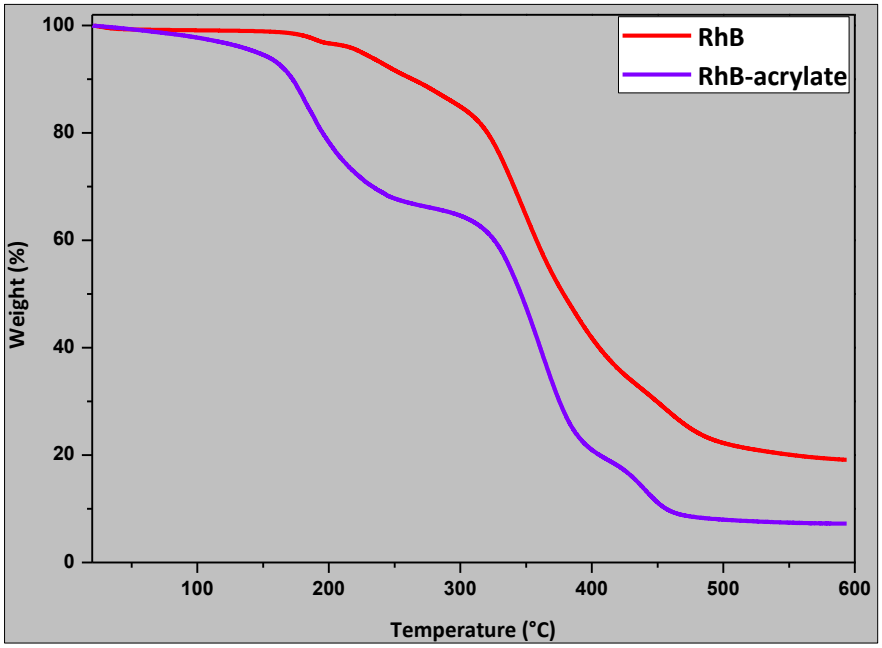

Figure 4.10: TGA thermograms of RhB and RhB-acrylate dyes.

Figure 4.11 displays the TGA weight loss curves of a neat PAAm, poly(AAm-*co*-RhB) and crosslinked-poly(AAm-*co*-RhB) nanocolorants. Both nanocolorants exhibit similar high thermal stability as the neat PAAm latex. However, the crosslinked-poly(AAm-*co*-RhB) nanocolorants shows less overall weight loss with a higher char residue.

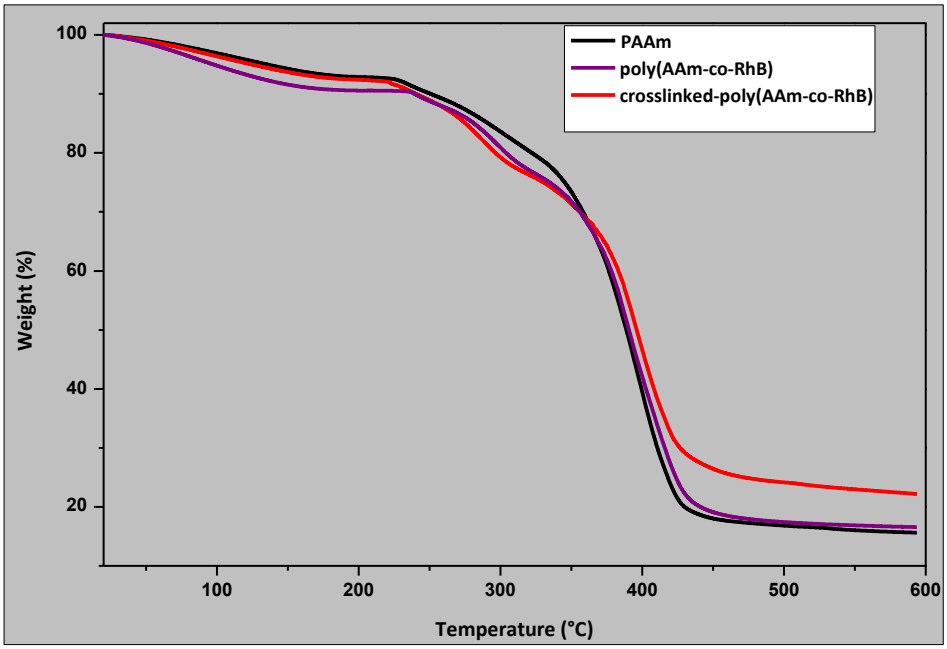

Figure 4.11: TGA thermograms of RhB-acrylate dye, PAAm and poly(AAm-co-RhB) and poly(PAAm-co-RhB) nanocolorants.

4.4 Conclusions

Poly(AAm-*co*-RhB) nanocolorants were successfully synthesized for the first time via inverse miniemulsion polymerization. RhB dye was first functionalized by esterification reaction to introduce an acrylate polymerizable group. The esterification reaction was carried out successfully between RhB dye molecules and 4-hydroxybutylacrylate using DCC/DMAP coupling agents. The chemical structure of the functionalized RhB-acrylate was confirmed by NMR analysis. RhB-acrylate exhibited features of a powerful dye with colour strength and properties almost identical to the RhB dye as confirmed by UV-vis spectroscopy.

The RhB-acrylate dye was copolymerized with AAm monomer in an inverse miniemulsion polymerization to produce nanocolorants with superior light and migration fastness. Poly(AAm-*co*-RhB) and crosslinked-poly(AAm-*co*-RhB) nanocolorants could be obtained based on the incorporation of the MBA crosslinker. DLS measurements confirmed that the size of the nanocolorants is in the normal range of miniemulsion particles. SEM and TEM images have shown that the nanocolorants are homogeneous and spherical nanoparticles with a uniform surface. Poly(AAm-*co*-RhB) and crosslinked-poly(AAm-*co*-RhB) nanocolorants exhibited a morphology of dark solid and core-shell particles, respectively, as determined by TEM. UV-vis absorption of poly(AAm-*co*-RhB) and crosslinked-poly(AAm-*co*-RhB) nanocolorants showed that both nanocolorants have absorption spectra identical to RhB-acrylate, which is an indication that the copolymerization process had no effect on the dye chromophore, and therefore, the nanocolorants retained the original colour strength and properties of the RhB-acrylate dye.

A dialysis experiment showed that RhB-acrylate dye had been completely integrated by copolymerization into the polymer matrix, and by that, the dye migration was completely supressed. The DSC and TGA analyses have shown that both poly(AAm-*co*-RhB) and crosslinked-poly(AAm-*co*-RhB) nanocolorants enjoy high thermal stability as well as high T_g values. These good thermal properties shown by the nanocolorants propose them as a good colouring agent for hot-melt ink application, where the high thermal stability is essential for a colouring agent.

4.5 References

1. Boehm, A. J.; Glaser, A.; Koch, O., Nanocolorants-more than colored nanoparticles. In *ANTEC 2003 Plastics: 61st Annual technical conference*, Society of Plastics Engineers: Nashville, USA, 2003; Vol. 2, pp 2419-2422.

2. Barashkov, N. N.; Liu, R., Fluorescent Nanocolorants Based on Dye-Packaging Technology for Ink Jet Application. In *IS&T NIP16: International Conference on Digital Printing Technologies*, Fort Lauderdale, Florida, 2001; pp 878-880.

3. Zhao, L.; Lei, Z.; Li, X.; Li, S.; Xu, J.; Peng, B.; Huang, W. *Chem. Phys. Lett.* **2006,** 420, 480-483.

4. Koskinen, M.; Wilén, C.-E. *J. Appl. Polym. Sci.* **2009,** 112, 1265-1270.

5. Wang, H.-H.; Tzai, G.-M.; Chang, C.-C. *J. Appl. Polym. Sci.* **2005,** 96, 2324-2335.

6. Holzapfel, V.; Musyanovych, A.; Landfester, K.; Lorenz, M. R.; Mailänder, V. *Macromol. Chem. Phys.* **2005,** 206, 2440-2449.

7. Verena, H.; Myriam, L.; Clemens Kilian, W.; Hubert, S.; Katharina, L.; Volker, M. *J. Phys.: Condens. Matter* **2006,** 18, S2581.

8. Pichot, C. *Curr. Opin. Colloid Interface Sci.* **2004,** 9, 213-221.

9. Waich, K.; Sandholzer, M.; Mayr, T.; Slugovc, C.; Klimant, I. *J. Nanopart. Res.* **2010,** 12, 1095-1100.

10. Kalogianni, D. P.; Litos, I. K.; Christopoulos, T. K.; Ioannou, P. C. *Biosensors Bioelectron.* **2009,** 24, 1811-1815.

11. Takasu, M.; Shiroya, T.; Takeshita, K.; Sakamoto, M.; Kawaguchi, H. *Colloid. Polym. Sci.* **2004,** 282, 740-746.

12. Takasu, M.; Kawaguchi, H. *Colloid. Polym. Sci.* **2005,** 283, 805-811.

13. Hu, Z.; Xue, M.; Zhang, Q.; Sheng, Q.; Liu, Y. *Dyes Pigm.* **2008,** 76, 173-178.

14. Liu, T.; Li, Z.; Wu, Q.; Ma, X. *Polym. Bull.* **2010,** 64, 511-521.

15. Mallakpour, S.; Rafiemanzelat, F.; Faghihi, K. *Dyes Pigm.* **2007,** 74, 713-722.

16. Meng, Q.; Huang, D.; Wei, S.; Chen, L. *J. Appl. Polym. Sci.* **2002,** 83, 1252-1257.

17. Grabchev, I.; Bojinov, V. *J. Photochem. Photobiol. A: Chem.* **2001,** 139, 157-160.

18. Grabchev, I.; Bojinov, V. *Polym. Degradation Stab.* **2000,** 70, 147-153.

19. Bardajee, G. R.; Vancaeyzeele, C.; Haley, J. C.; Li, A. Y.; Winnik, M. A. *Polymer* **2007,** 48, 5839-5849.

20. Bojinov, V.; Konstantinova, T. *Dyes Pigm.* **2002,** 54, 239-245.

21. Tronc, F.; Li, M.; Lu, J.; Winnik, M. A.; Kaul, B. L.; Graciet, J.-C. *J. Polym. Sci., Part A: Polym. Chem.* **2003,** 41, 766-778.

22. Tronc, F.; Winnik, M. A.; Kaul, B. L.; Graciet, J.-C. *J. Polym. Sci., Part A: Polym. Chem.* **2004,** 42, 1999-2009.

23. Song, J.-S.; Tronc, F.; Winnik, M. A. *Polymer* **2006,** 47, 817-825.

24. Li, B.; Shen, J.; Liang, R.; Ji, W.; Kan, C. *Colloid. Polym. Sci.* **2012,** 290, 1893-1900.

25. Beija, M.; Afonso, C. A. M.; Martinho, J. M. G. *Chem. Soc. Rev.* **2009,** 38, 2410-2433.

26. Zhu, M.; Zhou, C.; Zhao, Y.; Li, Y.; Liu, H.; Li, Y. *Macromol. Rapid Commun.* **2009,** 30, 1339-1344.

27. Pang, Y.; Kumar Sarvothaman, M.; Ritter, H. *J. Macromol. Sci. Part A Pure Appl. Chem.* **2005,** 42, 1013-1024.

28. Sun, H.; Scharff-Poulsen, A. M.; Gu, H.; Almdal, K. *Chem. Mater.* **2006,** 18, 3381-3384.

29. Gonçalves, M. S. T. *Chem. Rev.* **2008,** 109, 190-212.

30. Baranovsky, V.; Petrova, T.; Rashkov, I. *Eur. Polym. J.* **1991,** 27, 1045-1048.

31. Zettl, H.; Häfner, W.; Böker, A.; Schmalz, H.; Lanzendörfer, M.; Müller, A. H. E.; Krausch, G. *Macromolecules* **2004,** 37, 1917-1920.

32. Kim, H. N.; Lee, M. H.; Kim, H. J.; Kim, J. S.; Yoon, J. *Chem. Soc. Rev.* **2008,** 37, 1465-1472.

33. Grechishnikova, I. V.; Johansson, L. B. Å.; Molotkovsky, J. G. *Chem. Phys. Lipids* **1996,** 81, 87-98.

34. William J. Ward, G. E. I. L.; Jeffrey R. Cramm, W. I. L.; Peter E. Reed, P. I. L.; Brian S. Johnson, N. I. L. Derivatized rhodamine dye and its copolymers. US 5772894, 1998.

35. Chen, Y. C.; Dimonie, V.; El-Aasser, M. S. *Macromolecules* **1991,** 24, 3779-3787.

36. Tiarks, F.; Landfester, K.; Antonietti, M. *Langmuir* **2001,** 17, 908-918.

Chapter 5: Synthesis and characterization of PAAm/RhB nanocolorants-based solid inks

Abstract

The focus in this chapter will be on discussing the applicability of the PAAm/RhB's nanocolorants as a colorant for solid inks. Crosslinked-PAAm/RhB and crosslinked-Poly(AAm-*co*-RhB) nanocolorants were successfully utilized in making paraffin wax-based solid inks. The synthesis of the crosslinked-PAAm/RhB nanocolorants-based solid ink was carried out via *in situ* inverse miniemulsion where the paraffin wax was employed as the organic continuous phase. The synthesis of crosslinked-Poly(AAm-*co*-RhB) nanocolorants-based solid ink was carried out by the mixing of the readymade nanocolorants miniemulsion (in cyclohexane) with melted paraffin wax until all the cyclohexane evaporated leaving the nanocolorants suspended in the wax. SEM and TEM images confirmed the nanostructure of the nanocolorants as homogenous and spherical structure with small particle size (below 200 nm) and uniform surface. Fluorescence microscopy was used to visualize the fluorescent nanoparticles dispersed in the wax. DSC results showed that the obtained solid inks possess the essential thermal properties required for a solid ink.

5.1 Introduction

Solid ink, also known as phase change ink as well as hot-melt ink, is a fairly new generation of inks that have been developed in ink-jet printing technology over the past 2 decades. It was first developed successfully and employed in colour ink jet printers in 1991 by Tektronix. Since then, solid inks have gained so much attention, in terms of the huge number of patents found in the patent literature, due to its environmental friendliness and low cost. Solid inks are solid at ambient temperature but they are transferred to the molten liquid state at the moment of printing. The melted ink is jetted out by the printer onto the printed surface, on which it solidifies immediately to give the final print[1-4]. Figure 5.1 gives a simple illustration of the printing process using a solid ink[5].

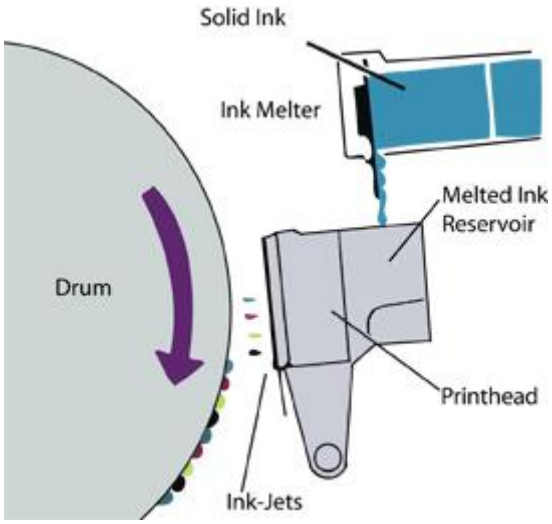

Figure 5.1: Printing process using solid ink printer with offset printing[5].

Conventional solid inks mainly consist of an ink carrier, chemical additives and a colouring agent. The ink carrier is usually a semicrystalline vehicle composed of waxes and resins as the main components. Any natural or synthetic waxes and

resins, with a melting point in the range of 50-90 °C, can be used. Chemical additives such as tackifiers, adhesion promoter, antioxidants, etc., are added to improve the performance and properties of the ink. The colour in solid ink is promoted mainly by one of three different types of colouring agents, pigments, dyes and polymeric coloured particles[1, 2].

The choice of colorant is not limited or restricted to a certain type of colorants provided that the colorant is fully dispersible and compatible with the ink composition. Therefore, the colorant can be any dye or pigment, combination of dyes or pigments or coloured polymer particles[2, 6-11]. Modified dyes and pigments as well as polymeric dyes and pigments have been also reported[12-15]. However, the colorant selected for solid ink application must be thermally stable, otherwise, it will thermally degrade forming aggregates that could block the printhead and lead to an ink with poor quality[2]. It has been debated whether it is better to use dyes or pigments as the suitable colorant for inkjet printing inks, as they both have many advantages and disadvantages. On one hand, dyes are totally soluble and well distributed in the ink medium, which would allow smooth and reliable ink jetting. They also offer the ink excellent colour properties and wide colour gamut. However, due to their high solubility and molecular nature, dyes tend to undergo undesirable interactions that affect the ink quality and print performance. Issues like poor light fastness due to photooxidation, poor image quality due to dye diffusion from the ink into the recording surface and poor water and solvent fastness due to the tendency of the dye to leach out from the ink into another solvent. On the other hand, pigments enjoy higher thermal stability and better light fastness compare to dyes.

Nevertheless, pigments tend to agglomerate due to their large particle size and size distribution. This can become a serious issue and concern as it may lead to the formation of phase-segregated ink and cause blockage to the inject nozzles of the printing device[2, 6].

The input of many researches and studies has shown that coloured nanoparticles (nanocolorants) could be the ideal replacement for dyes and pigments, especially in applications such as inks and toners. The integration of dyes into polymer matrices, especially by emulsion/miniemulsion polymerization, result in developing nanocolorants that embrace the best properties of both dyes and pigments[16-25]. It is only required that the dye is soluble in the monomer phase and compatible with the end polymer. Indeed, there has been a great success in improving the ink quality and performance by employing nanocolorants instead of dyes and pigments. However, migration of the dye from the particles to the outside medium is still observed, especially over longer period of time[17, 20, 26, 27]. All the reported nanocolorants used in solid inks are based on hydrophobic dyes, therefore, it is most likely that this would encourage the dye migration to the like hydrophobic ink vehicle.

To the best of our knowledge, the application of hydrophilic nanocolorants based on the hydrophilic Rhodamine B dye and its derivative as a colorant for solid inks have never been investigated before. As it has been discussed throughout this study, the PAAm/RhB-based nanocolorants prepared via inverse miniemulsion polymerization exhibit superior light and migration fastness as well as excellent thermal stability. It

is expected that the RhB-based nanocolorants will improve the colour properties of solid inks significantly, especially where the dye migration is concerned. The hydrophilic nature of the RhB dye will reduce the chances of the dye migration to the unlike hydrophobic ink medium. However, due to the lack of equipment and facilities as well as the necessary experience to work with solid inks, we have only conducted preliminary investigations such as the morphology and fluorescence analyses, hoping to carry out the investigations further in more details when the opportunity allows it. While it was in the liquid state, the prepared ink was poured into a commercial ink container to give it the final shape.

5.2. Experimental

5.2.1 Materials

Acrylamide (AAm) (≥99%) and *N,N'*-methylenebisacrylamide (MBA) (≥99.5%,) were obtained from Fluka and used as received. The thermal initiator 2,2'-azo-bis(isobutyronitrile) (AIBN) (98%, Aldrich) was recrystallized from methanol. Rhodamine B (RhB) (dye content ~95 %) was obtained from Sigma. The polymeric surfactant Hypermer B246 was a gift from Croda. Cyclohexane (CH) (tech) was obtained from Sigma-Aldrich and used as received. FR Paraffin wax (m.p. 58-60 °C) was purchased from PAC-CHEM cc.

5.2.2 Synthesis of (PAAm/RhB) and Poly(AAm-*co*-RhB) nanocolorants-based solid inks in inverse miniemulsion polymerization

Two approaches were adapted to carry out the synthesis of PAAm/RhB-based solid inks. First approach was to prepare the solid ink following the same procedure described in Chapters 3 (3.2.2) and 4 (4.2.2) except that the cyclohexane was replaced by paraffin wax. This implicated that the wax must be in the molten state, which required working at temperature above the melting point of the wax (80 °C) throughout the procedure, including the pre-emulsion preparation and the sonication processes to avoid the solidification of the wax at room temperature. The second approach involved the mixing of the readymade nanocolorants with a melted wax at 70-80 °C until all cyclohexane evaporated and the nanocolorants became homogenously dispersed in the wax. The wax was heated in a reactor equipped with an overhead mechanical stirrer until it melted. The nanocolorant miniemulsion dispersion was then added and the mixture stirred at high speed until all the cyclohexane was evaporated.

5.2.3 Characterization and analytical techniques

SEM, TEM and DSC techniques were used for the characterization of (PAAm/RhB) and Poly(AAm-*co*-RhB) nanocolorants-based solid inks using the same instruments described in Chapter 3 and 4.

SEM and TEM techniques were used to investigate the nanostructure and morphology of the ink. Ink samples were mounted on top of the SEM stub and then

coated with a thin layer of gold. For TEM analysis, the ink samples were first diluted with wax (100×) before they were ultra-microtomed with a diamond knife on a Reichert Ultracut S ultramicrotome to produce sections of approximately 100 nm thickness. The microtoming was carried out at -60 °C under liquid nitrogen environment using a special holder. The sections were then collected on a water surface and transferred to 300-mesh copper grids for the final analysis.

Based on the fluorescence emission of the RhB dye, fluorescence microscopy was used to visualize the nanocolorants particles dispersed in the ink. Fluorescent Image acquisition was performed on an Olympus Cell® system attached to an IX 81 inverted fluorescence microscope equipped with an F-view-II cooled CCD camera (Soft Imaging Systems). Using a Xenon-Arc burner (Olympus Biosystems GMBH) as light source, images were acquired using the 360 nm, 472 nm or 572 nm excitation filter. Emission was collected using a UBG triple-bandpass emission filter cube (Chroma). For the z-stack image frame acquisition, a step width of 0.5 µM, an Olympus Plan Apo N 60x/1.4 Oil objective and the Cell® imaging software have been used. Images were processed and background-subtracted using the Cell® software. Sections of ultra-microtomed samples were placed on a glass cover slide prior to imaging.

5.3 Results and discussion

A successful synthesis of (PAAm/RhB) and Poly(AAm-*co*-RhB) nanocolorants-based solid inks was carried out via either *in situ* inverse miniemulsion polymerization or direct mixing of readymade PAAm/RhB-based nanocolorants with paraffin wax. Since

crosslinked-AAm/RhB and crosslinked-poly(AAm-*co*-RhB) nanocolorants exhibited the highest migration fastness and thermal stability (with regard to the other nanocolorants) as it was discussed somewhere else in this study, thus these two nanocolorants were used to make solid inks. The crosslinked-AAm/RhB nanocolorants formulation was applied for making solid ink via *in situ* inverse miniemulsion, while readymade crosslinked-Poly(AAm-*co*-RhB) nanocolorants were applied for making solid ink via mixing process. Table 5.1 represents the formulations used for *in situ* inverse miniemulsion of crosslinked-PAAm/RhB and -based solid inks.

Table 5.1: Formulations used in the *in situ* inverse miniemulsion polymerizations for the preparation of crosslinked-PAAm/RhB and crosslinked-Poly(AAm-*co*-RhB) nanocolorants-based inks.

Ink	RhB (g)	RhB-acrylate (g)	AAm (g)	MBA (g)	B246 (g)	AIBN (g)	H_2O (g)	CH (g)	Wax (g)
K-1	1.17	-	6.00	0.60	1.06	0.11	8.30	-	64.00
K-2	-	1.20	5.08	0.62	1.04	0.10	9.00	64.00	64.03

Neither aggregates nor coloured precipitates were observed during the polymerization or mixing processes. The prepared wax in both cases exhibited solid homogenous waxy material with deep bright colour reflecting that the nanocolorants were well dispersed in the wax. Figure 5.2 displays digital photographs of moulded crosslinked-PAAm/RhB and crosslinked-(PAAm-*co*-RhB) nanocolorants-based solid inks and commercially available solid inks used in Xerox

Phaser®.8400 colour printers. As it can be seen in Figure 5.2, the synthesized ink in picture (a) resembles very much the commercial inks shown in picture (b) in shape and structure. However, the variation of colour is of course due to the use of different colorants. The pink block of ink shown in picture (a) is related to the crosslinked-PAAm/RhB nanocolorants-based solid ink, while the dark purple block belongs to the crosslinked-Poly(AAm-*co*-RhB) nanocolorants-based solid ink.

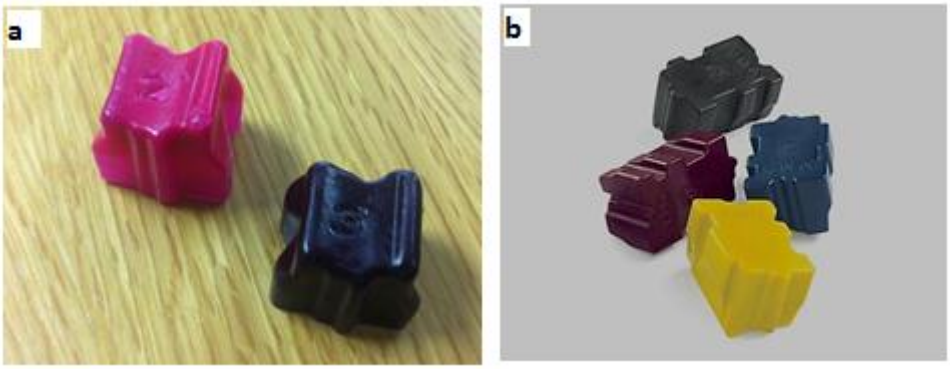

Figure 5.2: (a) the synthesized crosslinked-PAAm/RhB and crosslinked-Poly(AAm-*co*-RhB) nanocolorants-based solid inks and (b) commercial solid inks.

5.3.1 Size distribution and morphology of the solid ink

The SEM images presented in Figure 5.3 reveal the nanostructure of the crosslinked-AAm/RhB and crosslinked-Poly(AAm-*co*-RhB) nanocolorants-based solid ink as spherical nanoparticles with uniform surface. This suggests that neither the polymerization at high temperature nor the mixing process had any impact on the particles nanostructure.

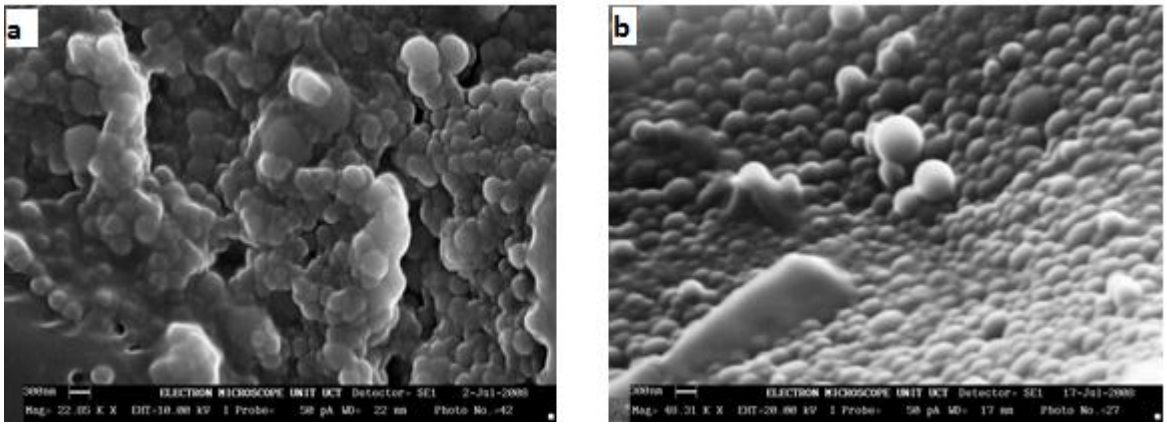

Figure 5.3: SEM images of (a) the crosslinked-PAAm/RhB nanocolorants-based solid ink and (b) the crosslinked-Poly(AAm-*co*-RhB) nanocolorants-based solid ink.

Figures 5.4 represents TEM images of the crosslinked-PAAm/RhB and crosslinked-Poly(AAm-*co*-RhB) nanocolorants-based solid inks. The average particle size of the crosslinked-PAAm/RhB and crosslinked-Poly(AAm-*co*-RhB) nanocolorants-based solid ink was 161 nm and 116 nm respectively, as calculated manually by ImageJ computer software. The average particle size is in the normal range of a miniemulsion, but the particle size distribution of the crosslinked-PAAm/RhB nanocolorants-based solid ink is broader than that of the crosslinked-Poly(AAm-*co*-RhB) nanocolorants-based solid ink. This relatively broad particles size distribution could be a result of insufficient sonication. Because sonication had to be done at high temperature while the wax in its liquid state which entailed some difficulties controlling the temperature and viscosity of the miniemulsion.

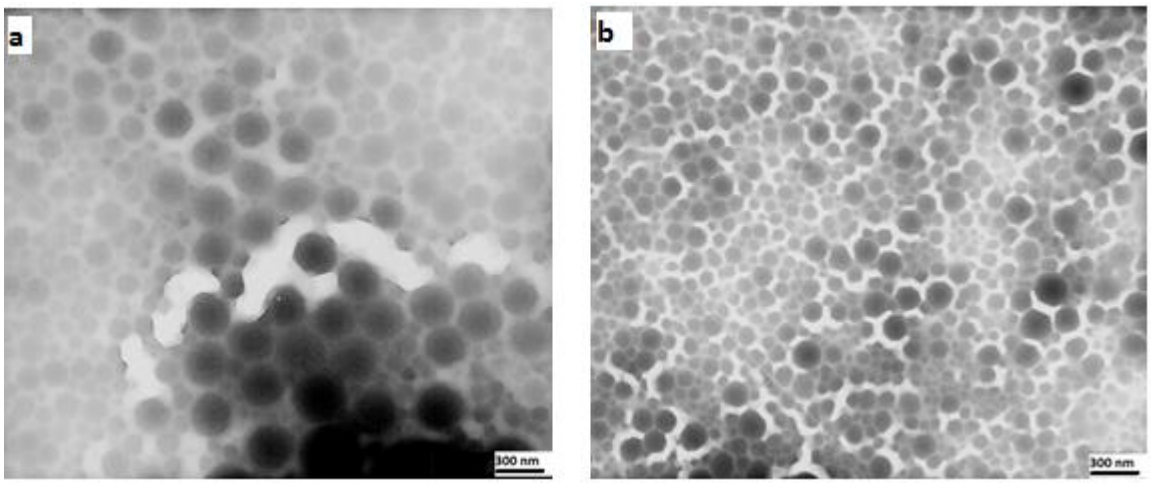

Figure 5.4: TEM images of (a) the crosslinked-PAAm/RhB nanocolorants-based solid ink and (b) the crosslinked-Poly(AAm-*co*-RhB) nanocolorants-based solid ink.

5.3.2 Fluorescence microscopy

Figure 5.5 shows images obtained from the fluorescence microscope for highly diluted microtomed samples of the crosslinked-PAAm/RhB and crosslinked-Poly(AAm-*co*-RhB) nanocolorants-based solid inks. These images are just an addition to the SEM and TEM images (Figures 5.3 and 5.4) that already indicated that the nanocolorants particles are homogenously dispersed within the wax medium.

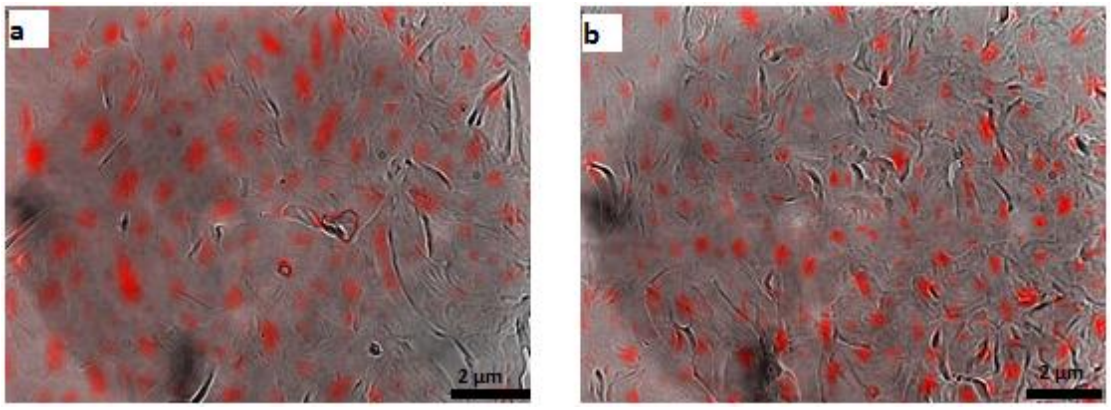

Figure 5.5: Fluorescence microscope images of (a) the crosslinked-PAAm/RhB nanocolorants-based solid ink and (b) the crosslinked-Poly(AAm-*co*-RhB) nanocolorants-based solid ink (The scale bar in the images represents 2 µm).

5.3.3 Thermal properties of the crosslinked-PAAm/RhB and crosslinked-Poly(AAm-*co*-RhB) nanocolorants-based solid inks as determined by DSC

The DSC second heating curves of the nanocolorants-based solid inks are displayed in Figure 5.6. In comparison with the DSC thermograms of the crosslinked-PAAm/RhB and crosslinked-Poly(AAm-*co*-RhB) nanocolorants displayed in Figure 4.9 Chapter 4, the T_g values correspond to crosslinked-PAAm/RhB and crosslinked-Poly(AAm-*co*-RhB) as well as the melting peaks related to the surfactant could not be detected due probably to the very low concentration of the nanocolorants relative to the wax. The DSC thermograms in Figure 5.6 are characterized with one sharp melting peak related to the paraffin wax appears at about 60 °C.

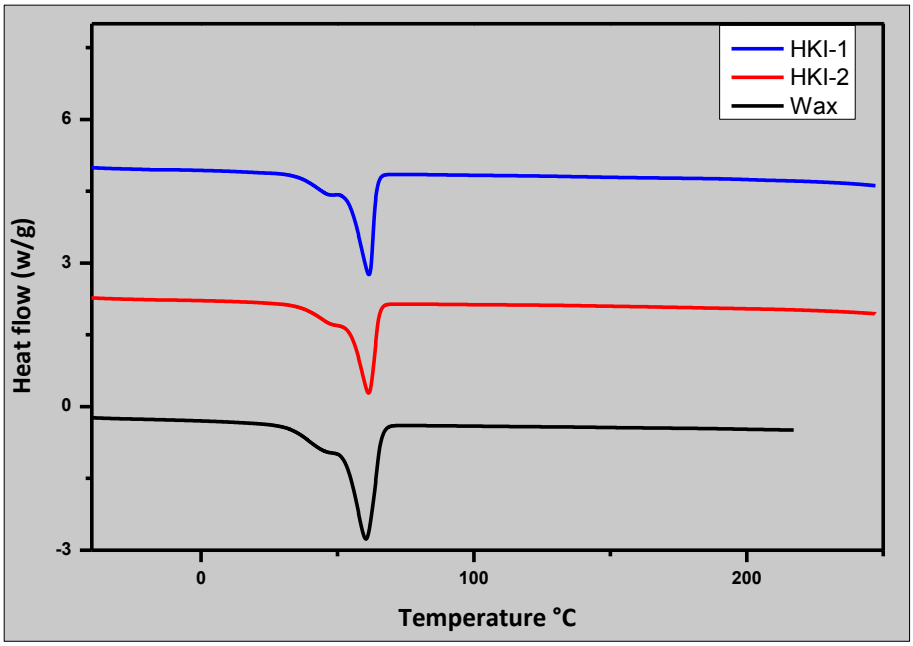

Figure 5.6: DSC thermograms of the crosslinked-PAAm/RhB and crosslinked-Poly(AAm-co-RhB) nanocolorants-based solid inks.

It is one of the most important properties of conventional solid inks vehicles is to have sharp melting transitions[2, 4]. Waxes with sharp melting peaks usually form small spherulitic structures, which is desirable as this lead to high quality prints. Therefore, the presence of the sharp melting peak in the DSC thermograms displayed in Figure 5.6 could be a good indication for the reliability of the PAAm/RhB nanocolorants for hot-melt ink application. Since it means that the nanocolorants did not interfere with the thermal properties of the ink carrier, which is the paraffin wax in this case, and most importantly, did not interfere with the formation of the spherulitic structure of the wax.

5.4 Conclusions

The syntheses of PAAm/RhB nanocolorants-based solid inks were carried out successfully via inverse miniemulsion polymerization. An *in situ* inverse miniemulsion

polymerization, with the paraffin wax as the organic phase, was utilized successfully in making a crosslinked-PAAm/RhB nanocolorants-based solid ink. A crosslinked-Poly(AAm-*co*-RhB) nanocolorants-based solid ink was prepared by the direct mixing of the readymade crosslinked-PAAm/RhB nanocolorants (suspended in cyclohexane) with paraffin wax at temperature above the melting temperature of the wax until all the cyclohexane evaporated. The obtained solid inks exhibited solid homogenous waxy material with deep bright colour reflecting that the nanocolorants were well dispersed in the wax. SEM and TEM analyses confirmed the morphology of the solid inks as homogenous spherical nanoparticles with uniform surface. The particle size and size distribution was in the normal range of miniemulsion. The fluorescence emission of the nanocolorants containing RhB dye observed by the fluorescence microscope further confirmed the well dispersion of the nanocolorants particles within the wax. DSC thermograms showed that the solid inks have one sharp melting transition indicating the applicability of our nanocolorants for hot-melt ink applications.

5.5 References

1. Bhide, H., Hot-Melt Inks for Rotogravure. *GRAVURE* 2002, pp 38-47.

2. Pekarovicova, A.; Bhide, H.; Paul D, F.; Pekarovic, J. *J. Coating. Technol.* **2003,** 75, 65-72.

3. Le, H. P. *J. Imaging Sci. Technol.* **1998,** 42, 49-62.

4. Chovancova-Lovel, V.; Pekarovicova, A.; Fleming, P. D. *J. Imaging Sci. Technol.* **2006,** 50, 550-555.

5. Jaeger, C. W. Color Solid Ink Printing. http://www.imaging.org/ist/resources/tutorials/solid_ink.cfm

6. Birau, M. M. M.; Iftime, G. M.; Vanbesien, D. W. B.; Wosnick, J. H. T.; Wagner, C. A. E.; Allen, C. G. W. FLUORESCENT SOLID INK MADE WITH FLUORESCENT NANOPARTICLES. US 2010/0086683 A1, 2010.

7. Raymond W. Wong, M.; Marcel P. Breton, M.; Shadi L. Malhotra, M. Phase change ink compositions. US 6319310, 2001.

8. Turek, C. M. H.; Breton, M. P. M.; Odell, P. G. M. Solid ink set incorporating naturally derived materials and processes thereof. US 7677713, 2010.

9. Masahiro Nishizaki, N.; Naomichi Kobayashi, N. Hot-melt solid ink composition. US 6022910, 2000.

10. Hidemasa Sawada, G. Hot-melt type ink-jet recording ink composition and process for preparation of the same. US 5788751, 1998.

11. Vasudevan, S. C. O. R. Polymeric colorants having pigment and dye components and corresponding ink compositions. US 2006/0089421 A1, 2006.

12. Banning, J. H. H. O. R.; Meinhardt, M. B. S. O. R.; Titterington, D. R. T. O. R.; King, C. R. S. O. R. Phase change ink formulations, colorant formulations, and methods of forming colorants. US 7985865, 2011.

13. Benjamin J. Brown, K. N. H. Pigmented hot melt inks. US 6702884, 2004.

14. Banning, J. H. H. O. R.; Meinhardt, M. B. S. O. R.; Titterington, D. R. N. O. R.; King, C. R. H. N. C. PHASE CHANGE INK FORMULATIONS, COLORANT FORMULATIONS, AND METHODS OF FORMING COLORANTS. US 2008/0091037 A1, 2008.

15. C. Wayne Jaeger, B. O. R.; Loc V. Bui, P. O. R.; Donald R. Titterington, T. O. R.; Clifford R. King, S. O. R. Use of polymeric dyes in hot melt ink jet inks. US 5621022, 1997.

16. Barashkov, N. N.; Liu, R. In *Fluorescent Nanocolorants Based on Dye-Packaging Technology for Ink Jet Application*, IS&T NIP16: International Conference on Digital Printing Technologies, Fort Lauderdale, Florida, 2001; Fort Lauderdale, Florida, 2001; pp 878-880.

17. Takasu, M.; Kawaguchi, H. *Colloid. Polym. Sci.* **2005,** 283, 805-811.

18. Boehm, A. J.; Glaser, A.; Koch, O., Nanocolorants-more than colored nanoparticles. In *ANTEC 2003 Plastics: 61st Annual technical conference*, Society of Plastics Engineers: Nashville, USA, 2003; Vol. 2, pp 2419-2422.

19. Hu, Z. K.; Xue, M. Z.; Zhang, Q.; Sheng, Q. R.; Liu, Y. G. *J. Appl. Polym. Sci.* **2007,** 104, 3036-3041.

20. Hu, Z.; Xue, M.; Zhang, Q.; Sheng, Q.; Liu, Y. *Dyes Pigm.* **2008,** 76, 173-178.

21. Qing, Z., Nanocolorants. In *Handbook of Nanophysics*, CRC Press: 2010; pp 1-16.

22. Wang, X. R. N. Y.; Chen, H. D. W. N. Y.; Reczek, J. A. R. N. Y. Ink jet ink composition and printing method. US 7317042, 2008.

23. Wang, X. R. N. Y.; Chen, H. D. W. N. Y.; Williams, K. W. R. N. Y.; Madaras, M. L. R. N. Y. Ink jet ink composition and printing method. US 2003/0119938 A1, 2003.

24. Wang, X. W. N. Y.; Erdtmann, D. R. N. Y.; Wang, Y. W. N. Y.; Klingman, K. J. P. N. Y.; Decker, D. E. R. N. Y. Composite colorant particles. US 2004/0127639 A1, 2004.

25. Xiaoru Wang, R. N. Y.; Huijuan D. Chen, W. N. Y. Polymer dye particles and process for making polymer dye particles. US 6867251, 2005.

26. Takasu, M.; Shiroya, T.; Takeshita, K.; Sakamoto, M.; Kawaguchi, H. *Colloid. Polym. Sci.* **2004,** 282, 740-746.

27. Liu, T.; Li, Z.; Wu, Q.; Ma, X. *Polym. Bull.* **2010,** 64, 511-521.

Chapter 6: Summary and recommendations

As the main driving force behind carrying out this study was the need for a new class of nanocolorants to improve some properties and the printing quality of the commercially available solid inks, the results presented in this dissertation describe the potential application of the PAAm/RhB-based nanocolorants as a novel colorant for solid inks. In this chapter, the obtained results of the study are summarized and some recommendations are given.

6.1 Summary

Three types of Rhodamine B-based nanocolorants, PAAm/RhB, crosslinked-PAAm/RhB and poly(AAm-co-Sty)/RhB, were successfully synthesized using a one-step encapsulation process via inverse miniemulsion polymerization. The obtained nanocolorants dispersions were highly stable (longer storage time) and possessed excellent colouring properties. DLS results showed that the average particle size was in general around 200 nm, which is in the normal range for a miniemulsion system, with a monomodal size distribution and low polydispersity. SEM and TEM analyses confirmed the morphology and nanostructure of the nanocolorants as homogenous spherical nanoparticles with a uniform surface. Based on TEM analysis, the PAAm/RhB nanocolorants exhibited solid dark nanoparticles morphology, while crosslinked-PAAm/RhB and poly(AAm-co-Sty)/RhB showed a core-shell type of morphology. These nanocolorants showed improved dye migration properties, especially, nanocolorants with core-shell morphology. However, the colour and

migration fastness of the Poly(AAm-*co*-Sty)/RhB could not be investigated as it seems that CHP/TEPA redox initiation system has an effect on the chromophore of the RhB dye. TGA analysis showed that the thermal stability of nanocolorants was improved compared with neat PAAm as well as pure RhB.

Poly(AAm-*co*-RhB) nanocolorants were successfully synthesized for the first time via inverse miniemulsion polymerization. RhB dye was first functionalized by esterification reaction to introduce an acrylate polymerizable group. The RhB-acrylate dye was copolymerized with AAm monomer in an inverse miniemulsion polymerization to produce nanocolorants with superior light and migration fastness. The size of the nanocolorants was in the normal range of miniemulsion particles. The nanocolorants were homogeneous and spherical nanoparticles with a uniform surface. Poly(AAm-*co*-RhB) and crosslinked-poly(AAm-*co*-RhB) nanocolorants exhibited a morphology of dark solid and core-shell particles, respectively. UV-vis analysis showed that the copolymerization process had no effect on the dye chromophore, and therefore, the nanocolorants retained the original colour strength and properties of the RhB-acrylate dye. A dialysis experiment showed that RhB-acrylate dye had been completely integrated by copolymerization into the polymer matrix, and by that, the dye migration was completely supressed. The DSC and TGA showed that both poly(AAm-*co*-RhB) and crosslinked-poly(AAm-*co*-RhB) nanocolorants enjoy high thermal stability as well as high T_g values.

The syntheses of PAAm/RhB nanocolorants-based solid inks were carried out successfully via inverse miniemulsion polymerization. An *in situ* inverse miniemulsion

polymerization, with the paraffin wax as the organic phase, was utilized successfully in making a crosslinked-PAAm/RhB nanocolorants-based solid ink. A crosslinked-Poly(AAm-*co*-RhB) nanocolorants-based solid ink was prepared by the direct mixing of the readymade crosslinked-PAAm/RhB nanocolorants (suspended in cyclohexane) with paraffin wax at temperature above the melting temperature of the wax until all the cyclohexane evaporated. The obtained solid inks exhibited solid homogenous waxy material with deep bright colour reflecting that the nanocolorants were well dispersed in the wax. SEM and TEM analyses confirmed the morphology of the solid inks as homogenous spherical nanoparticles with uniform surface. The particle size and size distribution was in the normal range of miniemulsion. The fluorescence emission of the nanocolorants containing RhB dye observed by the fluorescence microscope further confirmed the adequate dispersion of the nanocolorants particles within the wax. DSC thermograms showed that the solid inks have one sharp melting transition indicating the applicability of our nanocolorants for hot-melt ink applications.

6.2 Recommendations

This study has shown that there is a great potential for the PAAm/RhB-based nanocolorants to replace the colorants that have been used in solid ink applications. However, the behaviour of the nanocolorants still needs to be tested in a printable solid ink formulation. In a future work the nanocolorants should be incorporated in commercially available solid inks and tested in a printing device.